Response Vindication of Effects of Corner Configuration and Interference on Tall Buildings under Wind Loads using CFD Modelling

A PROJECT REPORT

SUBMITTED IN PARTIAL FULFILMENT OF THE

REQUIREMENTS

FOR THE AWARD OF THE DEGREE OF

MASTER OF TECHNOLOGY

IN

STRUCTURAL ENGINEERING

Submitted by:

NIKHIL GAUR

(2K18/STE/18)

Under the supervision of

Dr. Ritu Raj (Assistant Professor)

DEPARTMENT OF CIVIL ENGINEERING

DELHI TECHNOLOGICAL UNIVERSITY

(Formerly Delhi College of Engineering)

Bawana Road, Delhi-110042

CANDIDATE'S DECLARATION

I, **Nikhil Gaur, 2K18/STE/18** of M.Tech. (Structural Engineering), hereby declare that the project report titled "**Response Vindication of Effects of Corner Configuration and Interference on Tall Buildings under Wind Loads using CFD Modelling**" which is submitted by me to the **Department of Civil Engineering**, Delhi Technological University, Delhi in partial fulfilment of the requirements for the award of the degree of Master of Technology, is original and not copied from any source without citation. This work has not previously formed the basis for the award of the Degree, Diploma, Fellowship or other similar title or recognition.

Place: DELHI **NIKHIL GAUR**

Date: 31-08-2020 **(2K18/STE/18)**

CERTIFICATE

I hereby certify that the Project Report titled **"Response Vindication of Effects of Corner Configuration and Interference on Tall Buildings under Wind Loads using CFD Modelling"** which is submitted by **Nikhil Gaur (2K18/STE/18)**, **Department of Civil Engineering**, Delhi Technological University, Delhi in partial fulfillment of the requirement for the award of the degree of Master of Technology, is a record of the project work carried out by the student under my supervision. To the best of my knowledge this work has not been submitted in part or full for any Degree or Diploma to this University or elsewhere.

Place: Delhi **Dr. RITU RAJ**

Date: 31-08-2020 **SUPERVISOR**

ABSTRACT

This study explores a recent application of the computational fluid dynamics technique “CFD” for wind analysis and its comparisons with the conventional wind tunnel experimentations. This study is centered on the wind response of square and corner cut-shaped building models and its optimization caused by the variation of the wind incidence angle. Extensive rigid model experiments of two building models of length scale 1:100 have been performed in the boundary layer wind tunnel. The numerical analysis has been carried out with the standard k-ε turbulence model to evaluate the force coefficients, base moments, power spectra, external surface pressure coefficients, and flow field characteristics of the models with variable wind angles of incidence. The comparisons between experimental results and CFD analysis suggest the computational approach’s viability in wind analysis of tall structures efficiently and accurately. A case study of aerodynamic mitigation by corner cut suggests minor modification techniques performance, efficiency, and limitations. Wind induced interference plays a vital role in the design of tall structures. However, the complex features of structure design and shape require a detailed wind tunnel/CFD (Computational Fluid Dynamics) study as codal provisions don’t suffice for such scattered parameters.

The current study focuses on the effects of height ratio, orientation, and blockage configuration of interfering structure on interference effects. Interference factor (IF), transient pressure, and force spectra are used to account for the interference effects at major probe points to understand the dynamic wind response. To study these effects among complex arrangements, a numerical simulation for a CFD analysis on a corner configured principal building model and a single upstream interfering building model having identical geometry has been performed. The configuration included six kinds of heights ratio ($H_r=H_{principal}/H_{interfering}$). Furthermore, force coefficients, base moments, and external surface pressure coefficients both in the along and across wind direction are determined and listed for wind incidence angle of attack of 0° to 90° at an interval of 15°. Interference effects among full, half, and no blockage conditions were investigated. The data is presented in terms of the interference factor relating wind load responses of the isolated principal building to interference configuration. The results indicate that in close proximity of structure, the shielding effect suppresses the interference effects on the principal building, but across wind responses have been investigated in close vicinity configurations too. This study also suggests the interfering model's orientation contributes to great measures to the wind response under interference.

ACKNOWLEDGEMENT

I, **Nikhil Gaur** wish to express my profound gratitude and indebtedness to **Dr. Ritu Raj,** Department of Civil Engineering, Delhi Technological University, Delhi for introducing the present topic and for his inspiring guidance, constructive criticism and valuable suggestion throughout the project work. And my sincere thanks to my friends and family who have patiently extended all sorts of help for accomplishing this undertaking.

Nikhil Gaur (2K18/STE/18)

Department of Civil Engineering,

Delhi Technological University, Delhi-110042

TABLE OF CONTENTS

LIST OF TABLES

LIST OF FIGURES

NOMENCLATURE

C_{fy}	Lift force coefficient
C_p	Pressure coefficient
$C_{1\epsilon}$, $C_{2\epsilon}$	Turbulence model constants
μ	Viscosity coefficient
ρ	Air density
K_1	Risk coefficient
K_2	Terrain category
K_3	Topography factor
K_4	Importance factor
Vz	Design wind speed in m/s at height Z.
ω	Specific (per unit k) turbulence dissipation rate
P	Buoyant production term
fc	Correction function of eddy viscosity
f	Re-distributed function in the turbulence model
k	Energy of turbulent fluctuations
μ_{eff}	Effective viscosity
μ_t	Turbulence viscosity
P_k	Turbulence due to shear

$\sigma\varepsilon$	Turbulent Schmidt number
Re	Reynolds number
P’	Modified pressure
S_M	Sum of body forces
Tu	Turbulence intensity
U, V	Undisturbed flow velocity
υ^2	Fluctuation energy of velocity components normal to the wall
ε	Dissipation rate of turbulence kinetic energy
$\varepsilon_{22}, \varphi_{22}$	Dissipation rate and re-distributed term of Reynolds stress tensor components
IF	Interference factor
PM	Principal Model
IM	Interfering Model
FB	Full blockage
NB	No blockage
HB	Half blockage
S(n)	PSD for lift coefficient
n	Frequency
σ_{Cfy}	Standard deviation of lift coefficient variation at time t

Chapter 1 INTRODUCTION

Multi-story tall buildings are a key requirement in major metro cities in India due to the gradual increase in population and the necessary land for a living. It is required to assemble high rise structure to survive where a smaller amount of property is presented. A high-rise structure presents many structural troubles, such as lateral load effect, lateral displacement, and stiffness, etc. In general, for high rise structure wind and earthquake load effects are prevailing. Therefore, for a high rise structure, it is mandatory to analyze these loads and their effect on the structure. The revolutionary scientific, commercial development, and advancement of construction techniques, high strength materials, and innovation in architectural approach have led to the construction of super-tall structures. Contemporary tall buildings are remarkably much more slender, flexible, and lighter than their former precedents. We have moved on from conventional and symmetrical cross-sections to more complex and non-uniform shapes of tall buildings. The shape of the structure plays an important role in the structure's resistance against the wind-induced load and response. The modern age tall buildings are extremely susceptible to dynamic wind loads that severely affect serviceability. These super tall structures are man-made bluff-bodies. The wind-induced excitations due to the bluffness of the building shapes cannot be neglected for a bluff body. For a typical tall building as the height and slenderness increase, the building suffers from increased flexibility, which has negative effects on wind loading. Flexible structures are affected by vibration under the action of wind, which leads to building motion and plays a prominent role in the structural designs. The lateral wind load is more prominent than the earthquake load in some cases. The importance of wind load over earthquake load depends on the place and zone factor distinct by codes.

The modern age tall buildings are extremely susceptible to dynamic wind loads that severely affect serviceability. These super tall structures are man-made bluff-bodies. The wind-induced excitations due to bluffness of the building shapes cannot be neglected for a bluff body. For a typical tall building as the height and slenderness increase, the building suffers from increased flexibility, which has negative effects on wind loading. Flexible structures are affected by vibration under the action of wind, which leads to building motion and plays a prominent role in the structural designs.

As tall structures move onward the envelope to higher heights, designers are not only faced with difficulty in choosing a structural element to take the lateral load such as wind load and earthquake load but also ensuring the design criteria that meet reliability and serviceability requirement under challenging wind environment. Wind load acts as along and across wind components on a tall building. The wind load for the tall buildings cannot be generalized due to the wide variability in shapes and surroundings for a building. These advancements in heights and shapes are accompanied by a lack of sufficient damping and low natural frequency of the structures. Such undesired conditions cause excessive vibration, bad serviceability, and occupant discomfort under the action of wind. This increment of wind load with heights imparts problems related to vortex shedding excitations and wind-induced dynamic response in the range of wind gust. This oscillatory motion generated by dynamic motion is perceived by the occupants and can produce discomfort or a nuisance. Therefore, the wind-induced building motions are also within the performance design scope, such as comfort level for building occupancy. It must satisfy the serviceability requirements as an occupant's discomfort feeling arises from the building’s lateral motion.

The sharp corners of buildings can produce wind flow separation resulting in strong wind-structure interaction induced loads. The bluff structures are more prone to excessive wind loads. Due to flow separation and reattachment around bluff bodies, external shape affects wind interaction with tall buildings. To ensure the

functional performance of tall flexible structures and control the wind-induced motion various types of aerodynamic modifications to the shape and geometry of the buildings are possible. Some aerodynamic modifications in architectural design are effective in reducing the effects of the lateral wind forces significantly. These aerodynamic modifications in building shape change the flow pattern around the building, thus moderating the wind responses.

Corner modification of building planes such as chamfer, recession, roundness, and slotting are common approaches in this category. In fact, horizontal corner modifications of building shapes have been proven to reduce wind effects on tall buildings effectively. These changes may improve the structural design, but structural measures or damping devices may still be required to serve the objective of wind restraint design in many cases.

These improvements turn more beneficial as the corners are progressively rounded [6]. These methods alter the characteristics of the separated shear layers, thus reducing the drag and lift forces and the wake size of the vortex [31]. A corner modification strategy can only be valid for a certain type and size of the plan [11] and wind direction[33]. Slotted and chamfered corners disturb the vortex shedding, whereas Recessed Corners make smaller separation zones and narrower wakes than a traditional square shape. Virote Boonyapinyo et al. [34] suggested chamfering and recession may produce reductions in the base moment up to the extent of 25%. Contrary to benefits, these modifications may have an adverse effect on structural stability too [19]. The models with corners recessed and chamfered effectively reduce wind loads than corner rounded models [27],[24].

Many studies have been performed to investigate the effect of corner modifications and their impact on the aerodynamic forces, including rounded corners (Carassale et al.[5]), chamfered corners (Gu and Quan [11]), recessed corners (Kawai[16], Tse et al.[33]), and finned corners (Kwok and Bailey[17], Kwok et al.[18]). K. C. S. Kwok [18] measured the static and dynamic along-wind displacement responses and the standard deviation cross-wind displacement response at the top of the building model. In chamfered corners, the reductions were more than

the slotted corners i.e. up to a 40% reduction in response than the plain building shape. These changes mean a suppressed vortex shedding process, hence a significant reduction in cross-wind response. In chamfered corners, the excitation processes were altered, both in frequency and in magnitude. Jamieson et al.[14] conducted a study to investigate the effect of the different corner configurations on the magnitude and distribution of the peak pressure coefficient. Bevelling the corners weakened peak suctions that occur at the trailing edges of the side faces, and the peak suctions on the side faces move forward to the leading edges.

The aqua tower in Chicago, Taipei 101 skyscraper in Taiwan and Yokohama Building in Japan are prime examples of tall buildings to adopt corner modifications as aerodynamic mitigation. These modifications have led to a 25% decrement in the base moment in Taipei 101 skyscraper. The aqua tower in Chicago has applied rounded corner modification to disrupt the wind flow around the tower. Ping, an International Finance Centre is tapered first as building shrinks with the elevation. Then each corner of the building is bevelled to create a rounded octagonal-shaped floor, effectively controlling the crosswind effect. A reduction of 35% in wind loads and 32% in the overturning moment was observed [7].

It was evident from past research work that the conventional methods of wind analysis, both codal provisions as well as wind tunnel experiments have their shortcomings in terms of application and finances. Wind codes are restricted with height and conventional geometry provisions. The wind tunnel experiments are too expensive. Therefore, the sophisticated computational methods for numerical simulation have been introduced in wind analysis of buildings, but the reliability of such simulations is yet to be verified.

A series of works have been carried out in the area of wind engineering based on wind tunnel test and Computational Fluid Dynamics (CFD) technique earlier. Ahmed Elshaer et al. [8] studied the application of Computational Fluid Dynamics "CFD" modeling for aerodynamic modification performance assessment. The comparison between the low dimensional CFD based methods and results of wind tunnel experiments were produced. The k-epsilon turbulence model was used to

simulate turbulence. Higher values for the drag coefficient were produced as the bluffer body induced a larger wake size. The problem considered by Vikram C. K. et al. [12] was the flow past a single square cylinder, and two square cylinders of the pitch to perimeter ratios of 2, 4, and 6 with and with-out corner modifications carried out numerically by using a commercial CFD code fluent. A square cylinder had more lift coefficient but lowers strouhal number when compared to chamfered and rounded corner. The lift and drag coefficient was lower for corner modified models because of the large tangential velocity of the square cylinder, which made the width of the wake behind the corner modified model small.

This study aims at utilizing computational fluid dynamics to study aerodynamic mitigation by corner modification, after verifying its reliability with respect to wind tunnel experiment data. Validation of the experimental and numerical data is necessary to justify the simulations for unconventional and irregular geometries. Comparison between force and moment coefficients of CFX simulation with wind tunnel results has been made for three corner modified sections in this study to validate CFD simulation technique. Thereafter, the same CFX setup is used to study predetermined building corner modifications for a square section. Moreover, results obtained from this study can preliminarily offer an insight into other projects in case the geometrical properties of the models match since the tests provide some normalized parameters. Wind response of an isolated building modifies in the presence of interfering structure in near vicinities. The interfering structure produces turbulence, which may increase or decrease wind load on the principal structure. This study is based on previous research work on corner-cut configured structures. Interference refers to the increased or decreased effect that nearby buildings may have upon the wind behavior of one another. Within an urban environment, this arrangement is very common with significant effects on the structures; thus it is necessary to consider the context that independent structures cannot be treated in isolation. Along with the large research fields of bluff bodies and computational wind engineering, interference is also a significant area of study. The geometry, configuration, wind incidence angle, and upstream exposure of interfering structure are vital factors deciding wind loads on a building.

Table 1.1 A comparison of previous research on corner modifications

Reference	**Approach**	**Mitigation**	**Results**
Tamura and Miyagi [31]	HFFB [wind tunnel]	Chamfering, rounded corners	Along-wind forces and drag are reduced. Variation in fluctuating lift coefficient is observed
Gu and Quan [11]	HFFB [wind tunnel]	Chamfering, recession	Formulation for power spectra of the across-wind dynamic forces, base moment coefficient, and shear forces are derived, aerodynamic damping effects discussed
Tse et al. [33]	HFFB [wind tunnel]	Chamfering, recession	The effects of the aspect ratio of recessed corners are sounder compared to chamfered corners. Round corners reduce drag the most.
Carassale et al. [33]	Aeroelastic [wind tunnel]	Rounded corners with varying modification length.	Critical angle of incidence decreases with the increase in the modification length
Kwok and Bailey [17]	Aeroelastic [wind tunnel]	Square sections with vertical and vented fins, corner slots	Fins are efficient for acrosswind response only while corner slot works in both alongwind and acrosswind directions.
Kawai [16]	Aeroelastic [wind tunnel]	Rounded, chamfered and recessed corners	Rounding corners are most effective.
Kwok [18], Kwok et al. [19]	Aeroelastic [wind tunnel]	Chamfering, corner slots, horizontal slots	Significant effect on along-wind and across-wind excitation and responses.
N.J. Jamieson et al. [14]	Aeroelastic [wind tunnel]	Rounded, recessed and bevelled slots	Peak suction coefficients and location observed.
Yi Li et al. [23]	Aeroelastic [wind tunnel]	Bevelled, chamfered and recessed corners and Corner cut at 10% rate	Recessed and chamfered corners were found more effective in reducing wind loads than a rounded corner.
Elshaer et al. [8]	CFD	Chamfering, recession for 2D flow	For optimal shape, mean along-wind and fluctuating across-wind force coefficients could be reduced considerably. Drag coefficient could be reduced by up to 40 % by rounding the corners.

The variables responsible for such prediction involve topographical and meteorological elements too; thus codal provisions for interference effects are not too accurate and extensive. Stathopoulos [30] suggested that wind load can be over and under predicted by 525% and 46% respectively, for simple prismatic structures.

In case of a standalone structure, a positive pressure is developed on windward side of a building due to direct impact of wind. The other faces and wall develop negative pressure due to edge separation. The sharp corners of buildings can produce wind flow separation resulting in a strong wind-structure interaction induced loads. Some aerodynamic modifications in architectural design are effective in reducing the effects of the lateral wind forces significantly. These aerodynamic modifications in building shape change the flow pattern around the building, thus moderating the wind responses. In fact, horizontal corner modifications of building shapes have been proved to be effective for the reduction of wind effects on tall buildings. A similar study has been performed beforehand on the numerical simulations and wind tunnel results to study aerodynamic mitigation by minor modification in terms of corner cutting. The optimum aerodynamically efficient corner configured model section of that case study with most force and moment reductions has been taken as test PM (Principal Model) and IM (Interfering Model) in this study. There are various parameters that alter the manner in which one building affects the forces on other buildings in its vicinity. A series of works have been carried out in the area of wind engineering to analyze the effect of position configuration, orientation, and aspect ratio on interference effects. Agrawal et al. [1], Zhang and Gu [40], Gu and Xie [11], Xie and Gu [36], and Zhang et al. [39] has worked on the same research aspects in their studies.

The study by Pallab and Sujit, 2015 [15] is based on the directionality effects of interfering structures. They suggested interference effect alters the projections based on the geometry of the primary building and the surrounding topography, terrain, and directionality conditions. The paper suggested wind pressure response variation dependence on the arrangement of adjacent structures and the wind flow direction. Interference excitation for torsional and translational structure response was investigated by Tang and Kwok (2004) [32] in a wind tunnel setup. Xie

and Gu [36] explained channeling and shielding effect of interfering building configurations and interference factor variations through a series of wind tunnel tests. Lam et al. [20] studied the interference effects on closely spaced structures and suggested that the vortex shedding dilutes in case of a closely spaced configuration compared to an isolated configuration.

Abhay gupta et al. [10] suggested that interfering building models with heights less than half the height of principal model do not affect principal building response significantly, and corners of vertical wall cladding must be examined for wind response. Lee et al. studied surface pressure distribution on rectangular structures with varying aspect ratios and side ratios. The current study focuses on the effects of height ratio, orientation, and blockage configuration on interference effects. The pressure and force coefficients of isolated and interfering cases are plotted and duly compared. The dynamic behavior of wind is also incorporated in the study by calculating local peak pressure coefficients and plotting power spectral density curves.

Chapter 2 WIND TUNNEL EXPERIMENT

The synchronous multi-pressure scanning system (SM-PSS) to measure pressure, high frequency base balance (HFBB) test to measure base force components, and aeroelastic model which takes account of stiffness and damping properties of structure are major three experiments performed to analyse wind structure interaction in a wind tunnel. In this study, Wind tunnel experimental data has been taken from the base force component studies of Dr. Ritu Raj et al. [2] work on wind loads on cross shaped tall buildings.

2.1 Measurement technique

The base shear, base moments, and twisting moments acting on rigid models for several angles of attack of wind incidence varying from 0° to 180° at an interval of 15° are measured by a five-component load cell. Average output has been recorded for 60-second observations at intervals of 1 second by the specialized data acquisition system.

2.2 Model description

Rigid models of plywood at a scale of 1:100 are used to model prototype buildings of cross section 400 m^2 and height 60 m (Fig. 2.3). Three sections, one square (A) and two with corner cuts (B and C), have been modeled with the same height of 600 mm and a cross-sectional area of 40,000 mm^2 (Fig. 2.1 and Fig. 2.2). The models B and C have corner cuts of 50 mm and 100 mm respectively

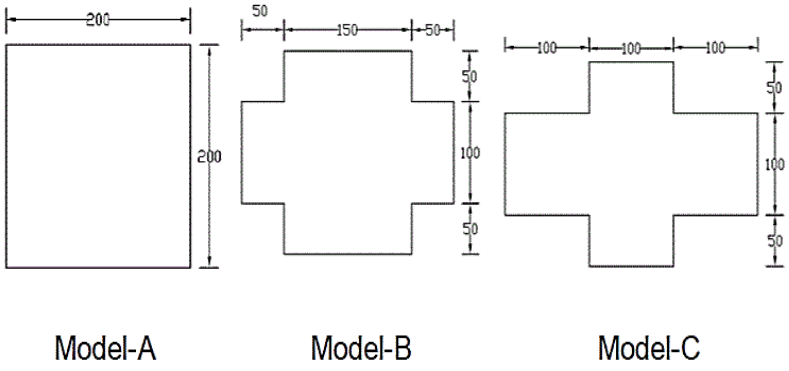

Figure 2.1 Model cross-sectional shapes

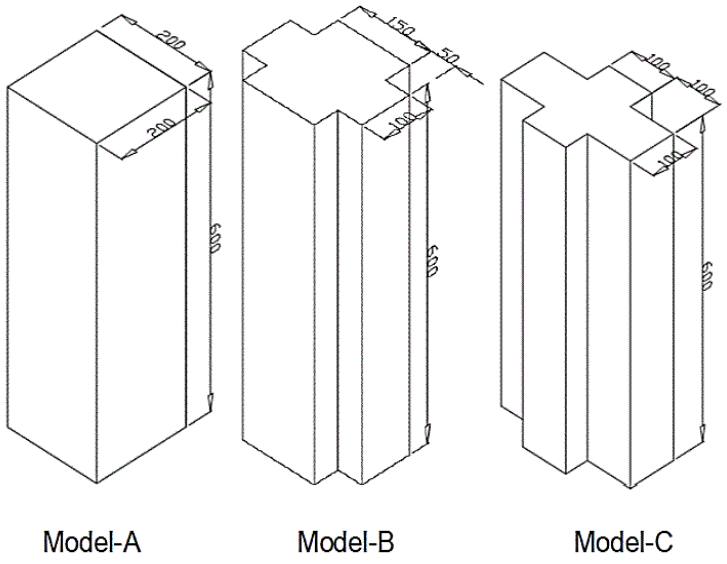

Figure 2.2 ***Dimensions of rigid models***

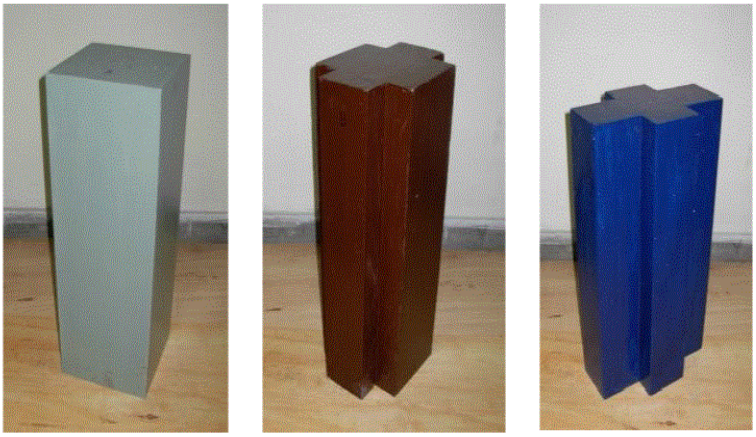

Figure 2.3 Wooden models test sections

2.3 Flow characteristics

In this study, the experiments have been performed in open circuit boundary layer wind tunnel at the Department of Civil Engineering, IIT Roorkee, India. The wind tunnel has a cross-section of 2 m (width) x 2 m (height) and a 15 m long test section (Fig. 2.4). 99 cm vortex generators, 16 cm barrier wall, and 70 mm, 50 mm, 38 mm cubical blocks (Fig. 2.5) were set up at upstream test length to produce terrain category-II as per IS 875 (Part 3)-1987 [13]. The models placed on load balance at 10.1 m distance from the upstream test section have been exposed to wind velocity 9.78 m/s. Atmospheric boundary layer with turbulence intensity 12 % was formed in the wind tunnel.

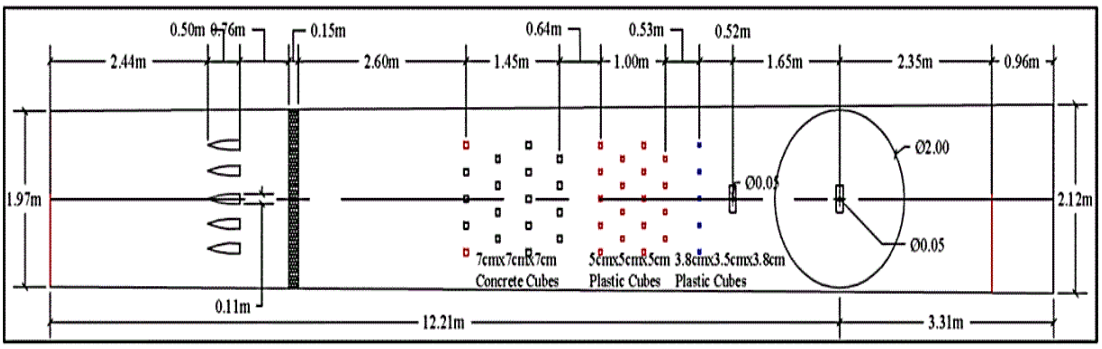

Figure 2.4 Flow profile of wind tunnel

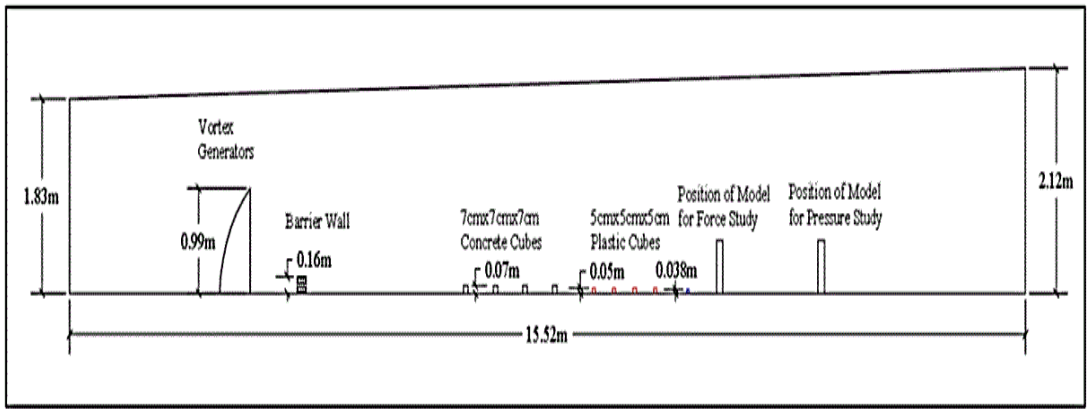

Figure 2.5 Elevation view of the tunnel section

2.4 Evaluation of wind load as per IS:875

IS: 875 (Part 3) is the code that provides guidance for the design of wind load in the Indian context. To calculate design wind pressure on a structure over an area, first we collect information about the basic wind speed (V_b) over the area from the Code. Design wind speed depends upon some factors, i.e, the topography of the area, architectural features and probability of wind occurrence. The basic wind speed is multiplied by the influencing factors K_1, K_2, K_3 and K_4.

2.4.1 Design Wind Speed (Vz)

$$Vz = K_1 * K_2 * K_3 * V_b \quad (2.1)$$

where V_b = Basic wind speed based on peak gust velocity averaged over a short time interval of about 3 seconds and corresponding to mean height (height 10 m) above ground level in open terrain (Category 2). Basic wind speeds given in IS: 875 (Part 3) have been worked out for a 50-year return period.

2.4.2 Design Wind Pressure (Pz)

Bernoulli's equation for streamline flow can be used to determine the local pressure at the stagnation point as a column of airstrikes (90°) an immovable body Thus

$$Pz = 0.5*\rho*(Vz)\text{^}2 \quad (2.2)$$

For the calculation of wind load on individual structural elements such as roofs, walls, and individual cladding units and their fittings, it is essential to take account of the pressure difference between opposite faces of such elements. For clad structures, external and internal pressures have to be found out first. Wind load (F) acting in a direction normal to the individual structural element or cladding is:

$$F = (Cpe-Cpi)*A*Pz \quad (2.3)$$

Cpe = External pressure coefficient [Clause 6.2.2 of IS: 875 (Part 3)].

Cpi = Internal pressure coefficient [Clause 6.2.3 of IS: 875 (Part 3)].

Chapter 3 NUMERICAL STUDY

Transient analysis of the three blockage configurations has been performed in the CFX package of commercial CFD software Workbench 19.1 (ANSYS). A steady-state Reynolds-Averaged Navier-Stokes (RANS) equation-based k-ε turbulence model has been used to predict the time series of wind loadings and pressure on the building models. The structural responses are explored with the help of the Fourier transformation function on major pressure probe points. The flow chart of the process adopted has been depicted in Fig. 3.1. Total of 8 monitors were created to observe the transient variations. A Perl script (Appendix 1) was written to automate the post-processing result file for graphical outputs.

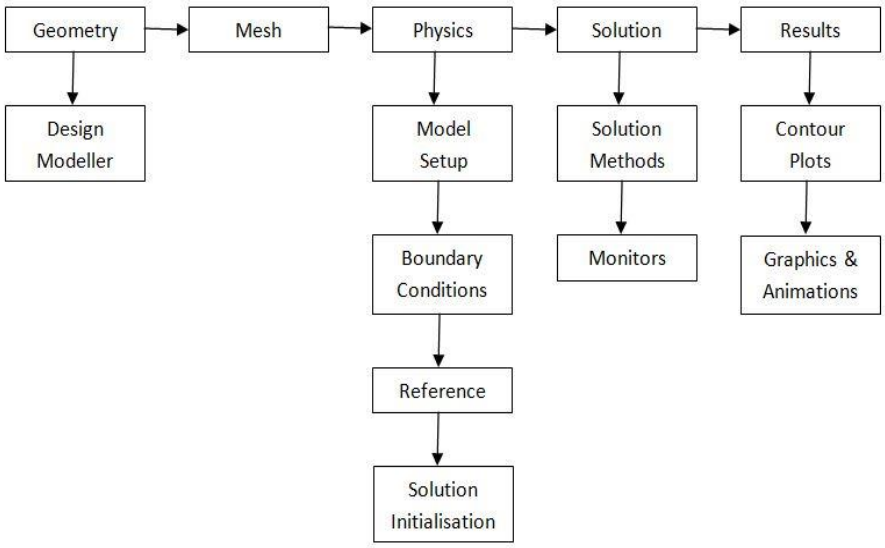

Figure 3.1 Flow chart of simulation run

3.1 Turbulence model

The CFD software package of ansys provides multiple turbulence models. However, only a proper turbulence model flow profile generates accurate results as compared to wind tunnel experiments. The accuracy mainly depends upon the computational grids and discretization method incorporated. All the above factors are considered in this study. Numerical predictions are verified by their comparison to the results of a wind tunnel special experiment. The standard k-ε turbulence model has been producing the fastest and accurate results except non-isotropic k-ε turbulence simulations [38]. In comparison with the RNG k-ε model and SST model it was evident that the standard k-ε turbulence model has produced more convergent results.

The k-ε model relates the Reynolds stresses to the mean velocity gradients and turbulent viscosity, where 'k' is turbulence kinetic energy i.e., the variance of fluctuations in velocity and 'ε' is the turbulence eddy dissipation. The three components of velocity momentum equations and turbulence kinetic energy and dissipation of turbulent kinetic energy equations are solved by the CFX solver. Bhattacharyya and Dalui [4] have also used two equations k-ε turbulence model for wind force and pressure coefficients study on the surfaces of an unsymmetrical E-shaped building using CFD. The RNG k-ε produces adequate results too but fails in back wall result convergence.

The k-ε turbulence is also limited to the fully developed turbulent and non-separated flows. To negate these limitations turbulence coefficients have been modified according to *k-ε* models developed by Mohammadreza Shirzadi [29]. This modified model produces a less viscous flow, hence more realistic flow features with the complex geometry. Therefore, two equation k-ε turbulence model was introduced for better accuracy and less numerical effort.

Generally, laminar and turbulent flows are represented by Navier-stokes equations for different turbulent length and time scales as mentioned below. In CFD,

turbulence models alter the unsteady Navier-stokes equations by introducing averaged and fluctuating quantities to produce the Reynolds Averaged Navier-Stokes (RANS) equations thus producing statistical turbulence models.

$$\frac{\partial \rho}{\partial t} + \frac{\partial \rho}{\partial x_j}(\rho U_j) = 0 \tag{3.1}$$

$$\frac{\partial \rho U_j}{\partial t} + \frac{\partial (\rho U_j)}{\partial t} = -\frac{\partial P\prime}{\partial x_i} + \frac{\partial}{\partial x_j}[\mu_{eff}(\frac{\partial U_i}{\partial x_j} + \frac{\partial U_j}{\partial x_j})] + S_M \tag{3.2}$$

The k-ε model, is based on the eddy viscosity concept, so that

$$\mu_{eff} = \mu + \mu_t \tag{3.3}$$

The turbulence viscosity is related to turbulence kinetic energy and dissipation such that

$$\mu_t = C_\mu \rho \frac{k^2}{\varepsilon} \tag{3.4}$$

Therefore, differential transport equations for the turbulence kinetic energy and turbulence dissipation rate as per differential transport equations [26] are

$$\frac{\partial (\rho k u_j)}{\partial x_j} = \frac{\partial}{\partial x_j}[(\mu + \frac{\mu_t}{\sigma_k})\frac{\partial k}{\partial x_j}] + P_k - \rho\varepsilon + P_{kb} \tag{3.5}$$

$$\frac{\partial (\rho \varepsilon u_j)}{\partial x_j} = \frac{\partial}{\partial x_j}[(\mu + \frac{\mu_t}{\sigma_\varepsilon})\frac{\partial \varepsilon}{\partial x_j}] + \frac{\varepsilon}{k}(C_{\varepsilon 1}P_k - C_{\varepsilon 2}\rho\varepsilon + C_{\varepsilon 1}P_{\varepsilon b}) \tag{3.6}$$

The standard and modified k-ε model constants are given below in Table 3.1

Table 3.1 Turbulence model k-ε model constants

	$C\varepsilon 1$	$C\varepsilon 2$	$\sigma\varepsilon$	$C\mu$
Standard Value	1.44	1.92	1.3	0.09
Modified Value	1.489	2.801	0.373	0.146

3.2 Domain and Meshing

The domain size has been introduced as per suggestions by Franke et al. [9]. The upstream, side, and top clearance from model faces of model height H has been taken as 5H. The downstream clearance has been provided with length 15H so that vortex and back flow on the leeward side can be curbed (Fig. 3.2). The meshing is produced with physics preference CFD and solver CFX. Tetrahedral meshing with inflation control has been formed to generate uniform flow around the model. The size function for the mesh is set as curvature to maintain the shape of the model. Skewness and orthogonality controls have been used to check the mesh quality. The ANSYS (CFX) uses the finite volume method to discretize the region of interest into the finite number of cells. The discretization square model is shown in Fig. 3.3.

Face sizing: An unstructured tetrahedral element size of 0.01m has been provided to the model walls. A 20 layered inflation is also provided to form uniform flow. Further refinement is conducted on the bottom boundary near the model domain for accuracy of the model results. Mesh characteristics are listed in Table 3.2.

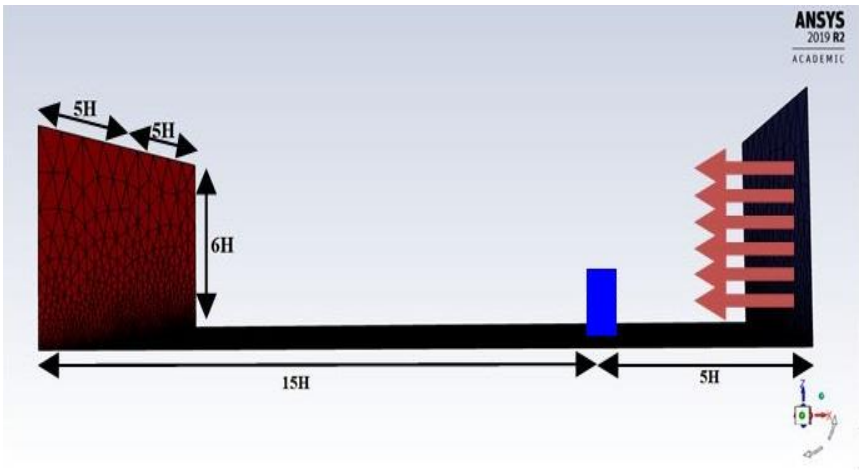

Figure 3.2 Domain mesh and size

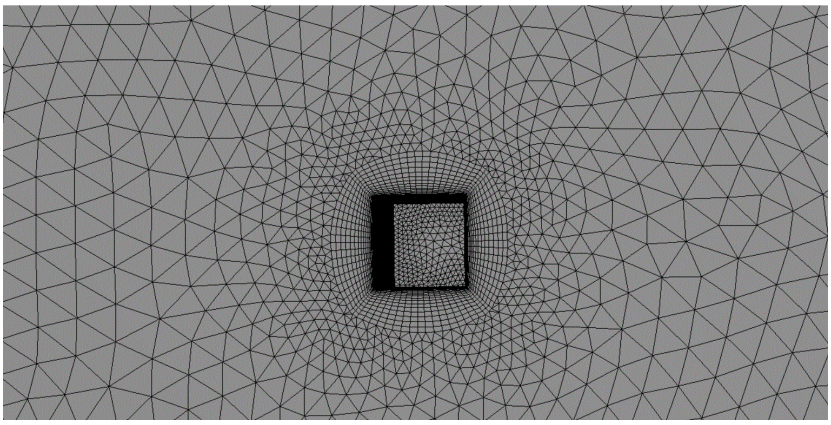

Figure 3.3: Structured domain and meshing

Table 3.2: Mesh characteristics

Criteria	Value
Body sizing	0.03 m
Face sizing	0.12 m
Edge sizing	0.01 m
Inflation layer	40
Growth rate	1

3.3 Boundary Conditions

The wind tunnel experiment boundary conditions have been introduced so that numerical and experimental results can converge. Boundary layer wind flow is generated by incorporating inlet velocity with power law at inlet boundary. The gauge pressure at the outlet has been considered as 0 Pa. The ground surface and model surface are provided with no slip condition with ground roughness 0.0024 m. The side walls and top wall of tunnel domain have free slip condition so that no force generates there. The boundary wall conditions are mentioned Table 3.3. A power law expression (Eq. 3.7) has been incorporated to introduce boundary layer wind flow at the inlet with reference speed (URef) 4.781 m/s at a reference height (ZRef) of 0.005 m. The value of power exponent (α) has been taken as 0.144 for the numerical simulation to generate a velocity profile.

$$U/\,URef = (Z/\,ZRef)^{\alpha} \tag{3.7}$$

Table 3.3: Boundary conditions and settings

Boundaries	
Boundary - inlet	**Setting**
Type	INLET
Location	inlet 2
Settings	
Flow Regime	Subsonic
Mass and Momentum	Normal Speed
Normal Speed	power
Turbulence	Intensity and Auto Compute Length
Fractional Intensity	1.20E-01
Boundary - outlet	
Type	OUTLET
Location	outlet 2
Settings	
Flow Regime	Subsonic
Mass and Momentum	Average Static Pressure

Pressure Profile Blend	5.00E-02
Relative Pressure	0.0000e+0 [Pa]
Pressure Averaging	Average Over Whole Outlet
Boundary - bottom	
Type	WALL
Location	wall solid 2
Settings	
Mass and Momentum	No Slip Wall
Wall Roughness	Rough Wall
Sand Grain Roughness Height	2.4000e-3 [m]
Boundary - model	
Type	WALL
Location	model
Settings	
Mass and Momentum	No Slip Wall
Wall Roughness	Rough Wall
Sand Grain Roughness Height	3.0000e-3 [m]
Boundary - walls	
Type	WALL
Location	walls
Settings	
Mass and Momentum	Free Slip Wall

3.4 Model Description for interference study

Two corner-configured models of cross-sectional dimensions 200*200 mm with corner cuts of 25 mm in each direction have been taken as IM and PM in this study. The PM remains at 600 mm height throughout the simulation, whereas the IM height is varied for H_r values 1 to 6. Three blockage conditions have been produced in the virtual wind tunnel named half blockage (HB), full blockage (FB), and no blockage (NB) according to their blockage dimension of PM by half breadth, full breadth, and zero breadth respectively as shown in Figs. 3.4, 3.5, and 3.6. The interference spacing (S) has been maintained 120 mm throughout the experiment.

One centreline on each face and one horizontal polyline at 0.9H have been created as data points to monitor pressure coefficients on PM. Six pressure probe points have also been created at height 0.9H and 20 mm distance from front and side faces monitoring transient pressure variations during the simulation. The tapping points are depicted in Fig. 3.7.

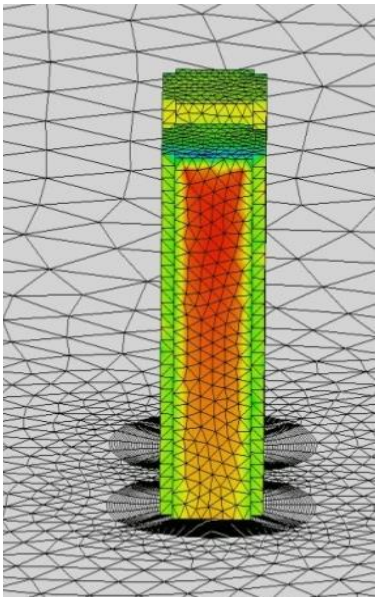

Figure 3.4 No blockage

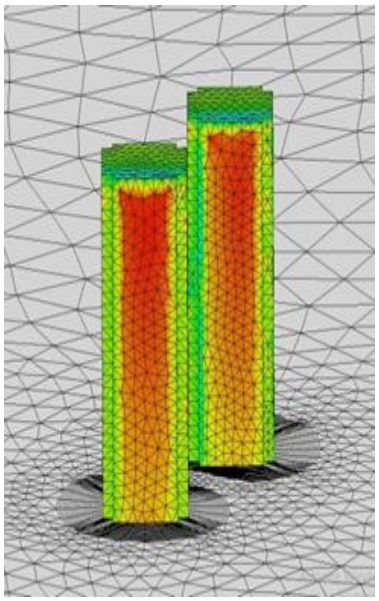

Figure 3.5 Full blockage

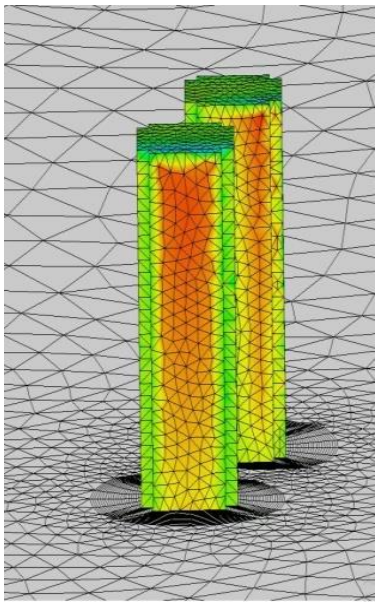

Figure 3.6 Half blockage

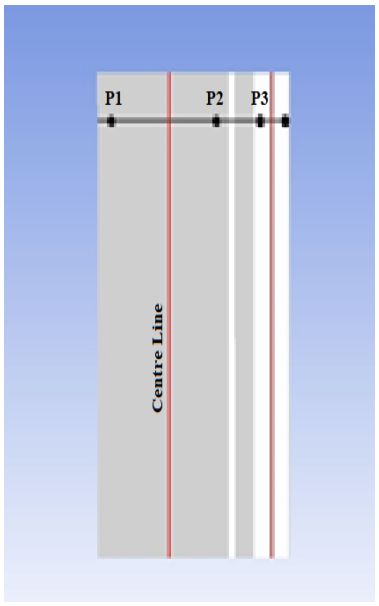

Figure 3.7 Tapping points

3.5 Grid independence study

Unstructured grids are incapable of condensing mesh nodes, thus providing less accurate computational results. About 0.4 million grid cells are introduced in the domain, out of which 0.16 million are on the tunnel floor. The cell height of the grid is also allotted according to y+ study. Grid independent studies are performed to generate grid independent numerical solutions. The mesh must be divided into higher orders to reduce vortex sizes in wake regions and achieve accuracy in CFD simulation. It is observed that simulations with a higher number of nodes produce better accuracy. However, a higher number of nodes will increase simulation time proportionally. The results of convergence study for finer base sizing with constant face sizing and inflation suggest that mesh and results are better converged in case of finer sizing.

Chapter 4 RESULTS

4.1 Corner study

4.1.1 Comparative Study

A comparative study between numerical simulations and the wind tunnel experiment results has been carried out. It was observed that the CFD simulations were at par with the tunnel results. Force coefficient (drag) and moment in Y direction have been compared for this analysis. The convergence appears to decrease with corner cut models because of the complexity of meshing. Orthogonality and skewness in corner cut models also affected the results. A finer face and mesh sizing in the corner cut models resulted in more converged results. Interpolation has been adopted for major discrepancies in results. The comparative graphs for force coefficient and moments have been presented in the Fig. 4.1- 4.6.

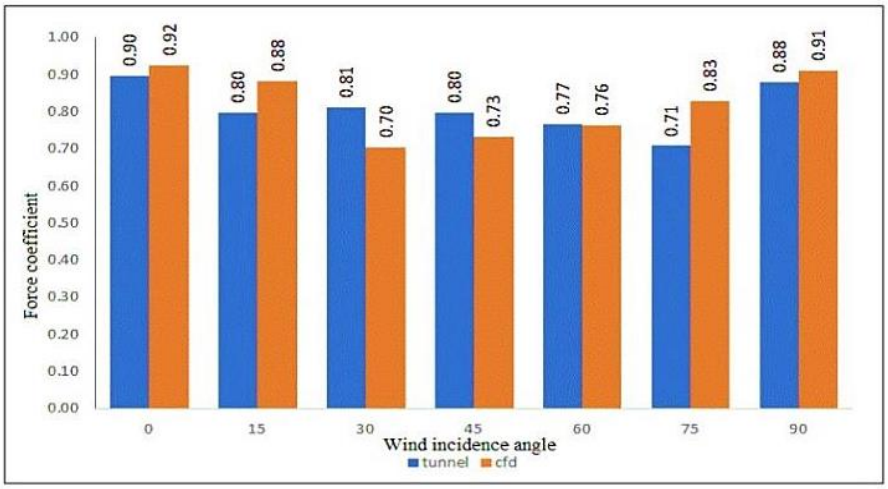

Figure 4.1: Force coefficients C_d for model

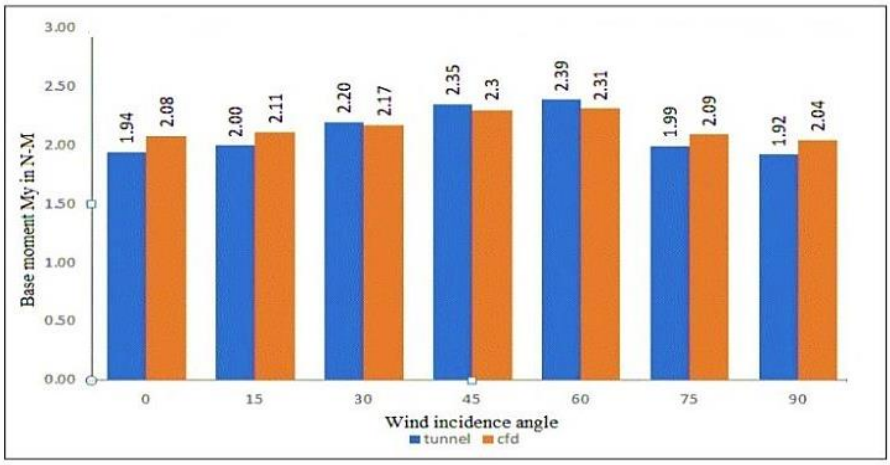

Figure 4.2: Moment My values for model A

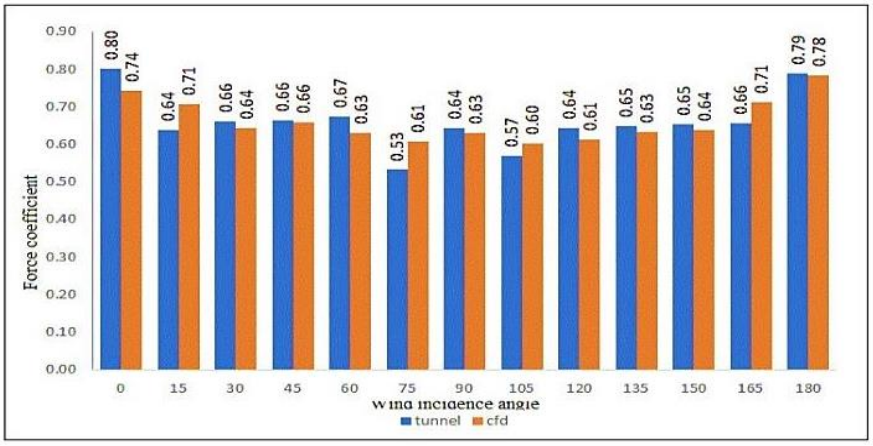

Figure 4.3: Force coefficients C_d for model B

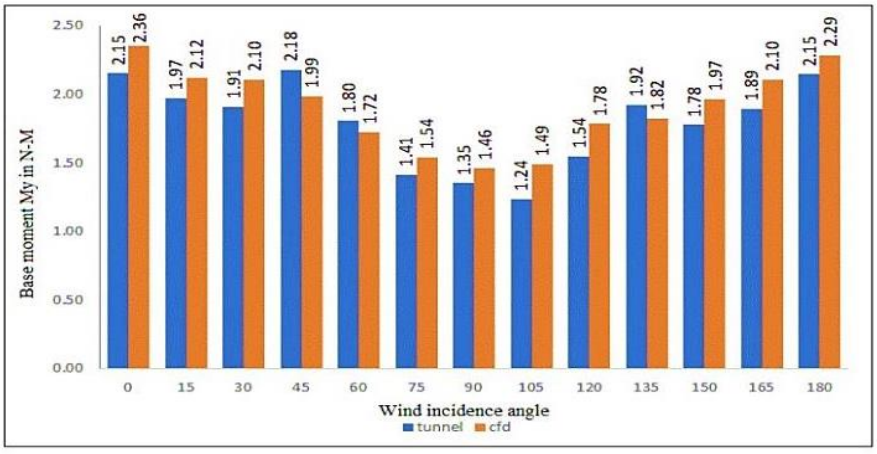

Figure 4.4: Moment My values for model B

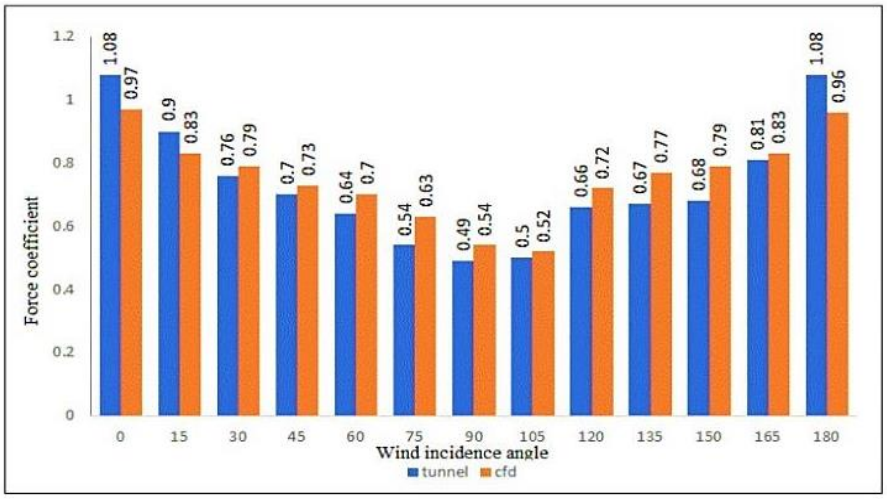

Figure 4.5: Force coefficient C_d for model C

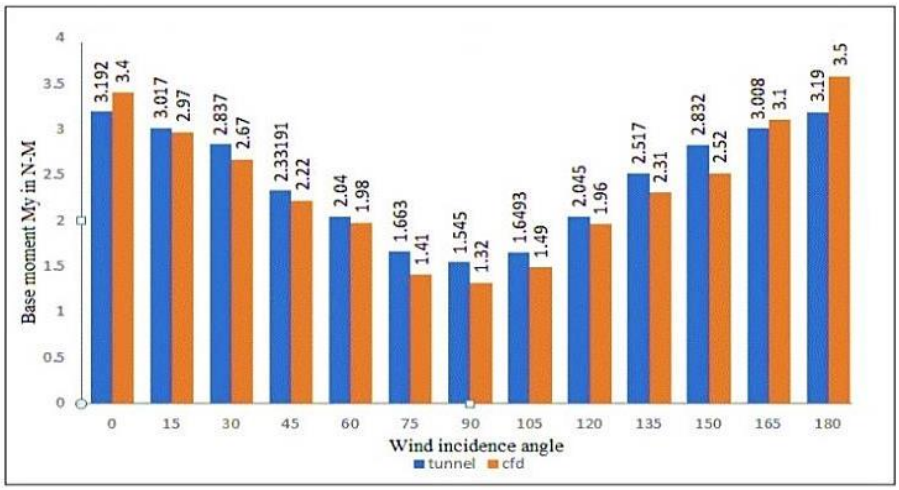

Figure 4.6: Moment My values for model C

4.1.2 Error analysis

A statistical error analysis has been performed to obtain the convergence accuracy in computational simulation and wind study. The Pearson's correlation coefficient (R), mean absolute error (MAE), mean absolute percentage error (MAPE), root mean standard deviation (RMSD) values have been calculated to compare the results. The force coefficient and moment coefficients have been shown in Table 4.1.1 and 4.2 respectively. The RMSD values suggest better convergence for the rectangular model than the corner cut model. The results indicate the accuracy

of CFD simulation in more complex geometries may vary but are within acceptable limits. Therefore, this modeling can be trusted with future simulations.

Table 4.1: Error analysis of drag force response

Model	R	MAE	MAPE	RMSD
A	0.493	0.063	8	0.075
B	0.809	0.033	5.2	0.041
C	0.953	0.067	9.2	0.075

Table 4.2: Error analysis of moment response

Model	R	MAE	MAPE	RMSD
A	0.986	0.09	4.4	0.097
B	0.893	0.168	9.8	0.176
C	0.977	0.178	7.7	0.203

4.2 Case Study

In present work, implications of corner configuration and performance of computational fluid dynamics in study of wind interactions has been performed. A case study has been performed based on the results of the numerical simulations to study aerodynamic mitigation by minor modification in terms of corner cutting. The same flow, domain and boundary conditions have been applied to new models with better face and edge meshing to compare corner modification effects on structures. A square section of dimension 200 mm has been taken for this study. The height of the section has been taken as 600 mm. A corner cut at the 6.25 mm rate on all sides has been applied in the square model and force, moment and pressure variations in the CFX solver have been observed. The results listed in Table 4.3 suggest significant force and moment deductions for 12.5 mm, 18.75 mm and 25 mm corner cut cases. These results are further explored in subsections.

Table 4.3: Force and moment observations of test models

Model	Corner cut [mm]	Drag force [N]	Lift force [N]	Moment [N-M]
A	0	5.70	0.010	1.92
B	6.25	5.20	-0.058	1.72
C	12.5	4.22	0.006	1.46
D	18.75	4.44	-0.019	1.52
E	25	4.88	0.025	1.56
F	31.25	5.34	-0.011	1.80
G	37.5	5.50	-0.003	1.84
H	43.75	5.72	-0.023	1.90
I	50	5.84	-0.021	1.95

4.2.1 Power Spectral Density

This section explores the power spectral density function for a more nuanced study of the across wind response. The power spectra are used for a better understanding of across wind responses of test models of smaller magnitudes. The hannings FFT model is used to plot power spectral density of lift coefficient ($nS(n)/\sigma_{Cfy}$) versus strouhal number (nD/H).

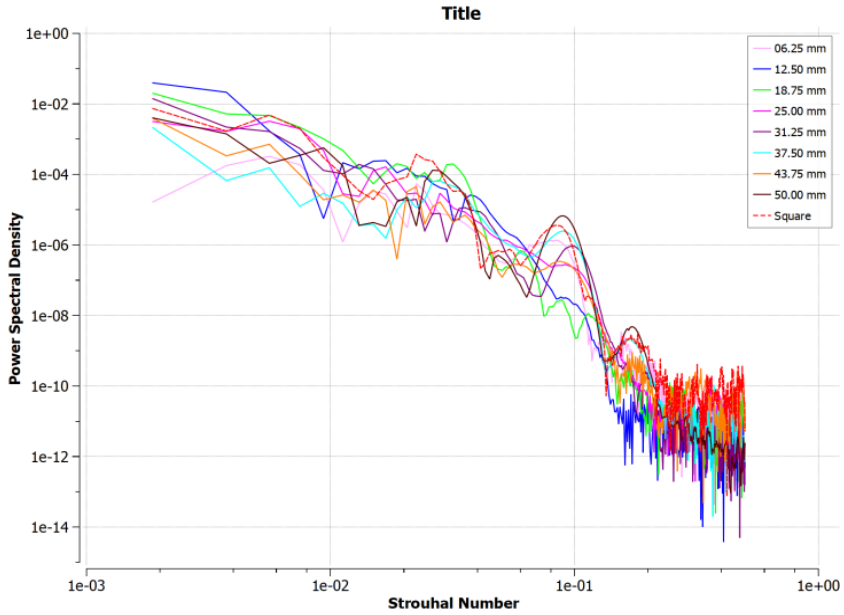

Figure 4.7: PSD for across wind response

It is evident from the PSD plot (Fig. 4.7) for across wind response that the spectra of all corner cut cases flow under the square model spectra, thus producing smaller magnitudes of force across wind direction than the square model. However, the 50 mm corner cut spectra flows over the square model's spectra, thus producing greater magnitudes of wind response. The gap between PSD responses is least for 6.25 mm corner cut and square model thus, magnitudes of the force were in closer proximities. The most docile PSD curves was observed for 12.5 mm and 18.75 mm corner cut cases.

4.2.2 Horizontal pressure coefficient

The pressure coefficient variation due to different corner cut dimensions has been discussed in this section. A perimeter is placed at 0.9H height i.e. 540 mm from the base on the model in the form of a polyline to measure the external pressure coefficient. A series of four probe points are also placed on this pressure belt to monitor the transient pressure variations. It is evident from the C_p plot (Fig. 4.8) that for corner cuts of 12.5 mm and 18.75 mm the front face cp values turn negative, which is responsible for the reduction in drag force in these cases. The transient pressure study on the front face later suggested suction points on the model's front face. In 12.5 mm corner cut condition, windward projections for front and side faces reverse in magnitudes as corner cut disturbs the flow profile around the model. The maximum variation in cp values is observed for 12.5 mm and 50 mm corner cut case. The increment in positive cp in the case of 50 mm cut is observed 24.8%, thus producing higher drag values. The increment is responsible for more turbulence in the wake regions of the model. The maximum negative cp value doubles in the case of a 12.5 mm corner cut.

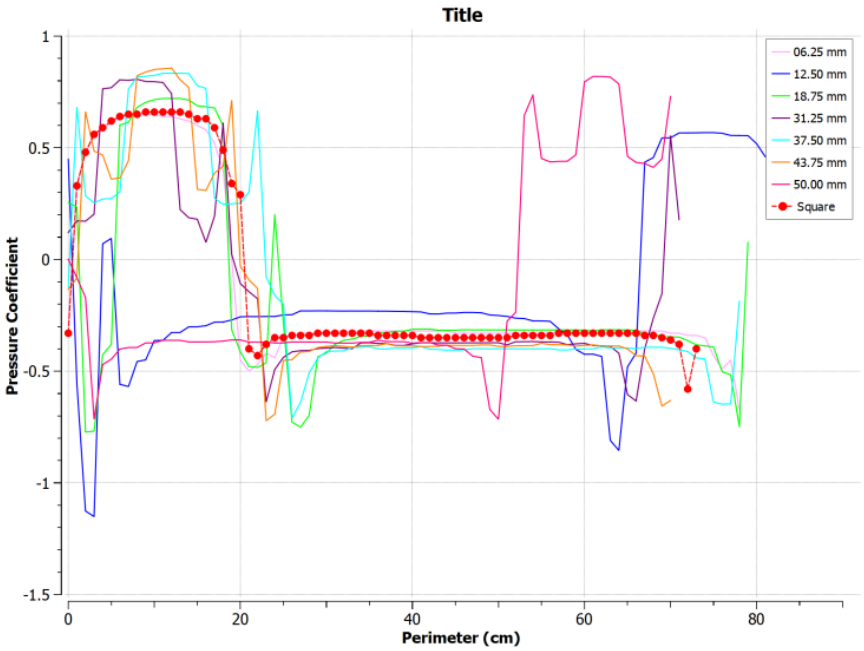

Figure 4.8: Pressure coefficient curve for polyline at 540 mm

4.2.3 Kinetic energy fluctuations and Turbulence

On monitoring probability density function, many subsequent peaks were observed. These subsequent peaks may suggest vortex shedding and reattachment of the separated turbulent flow. These flow conditions produce turbulence in the wake regions. The vortex shedding and turbulence majorly contribute to the kinetic energy (KE) in the wake region. A section plane was created at the top of the model to analyze the pattern of wake region employing kinetic energy fluctuations and compared them with the square model (Fig. 4.9- 4.17). The kinetic energy plot of the square model suggests flow separation at model corners. The corner cuts help to reattach this separated flow. The reattachment of flow is observed in the wake region in these cases. In the case of 12.5 mm and 18.75 mm corner cuts, the reattached flow was the most stable, and prolonged wake religion was observed. This reattachment helps stabilising the wake turbulence, and suction is developed on the model face which was evident from the C_p plots on the polyline.

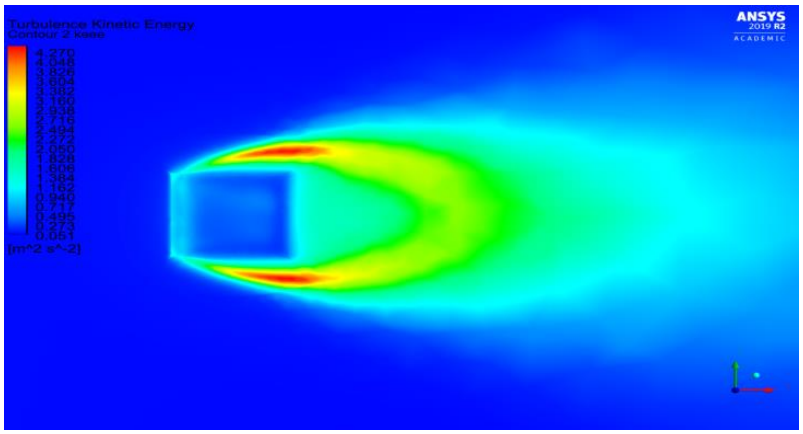

Figure 4.9: Kinetic energy spectrum for square model

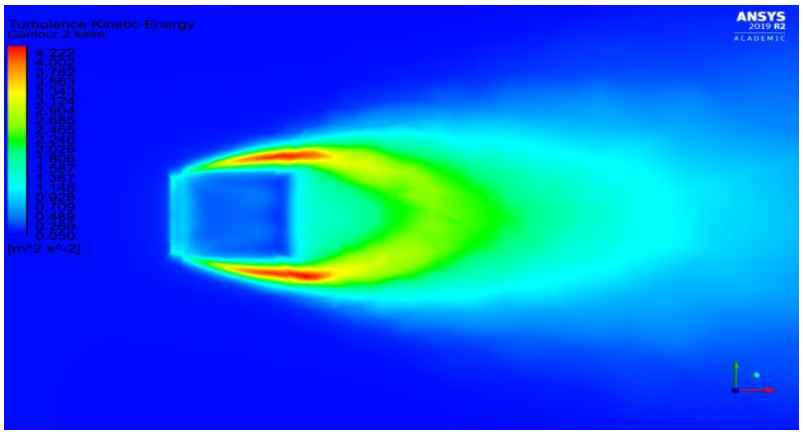

Figure 4.10: Kinetic energy spectrum for 6.25 mm cut section

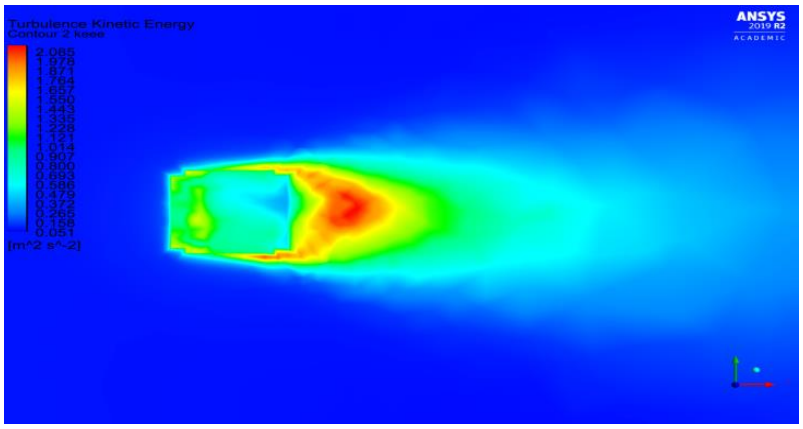

Figure 4.11: Kinetic energy spectrum for 12.5 mm cut section

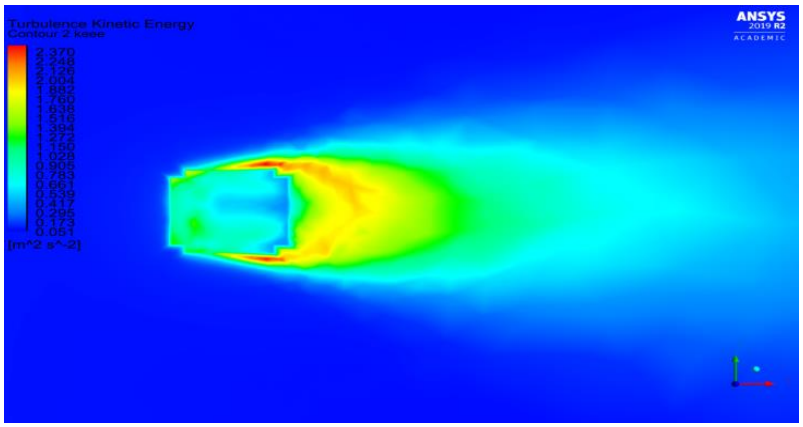

Figure 4.12: Kinetic energy spectrum for 18.75 mm cut section

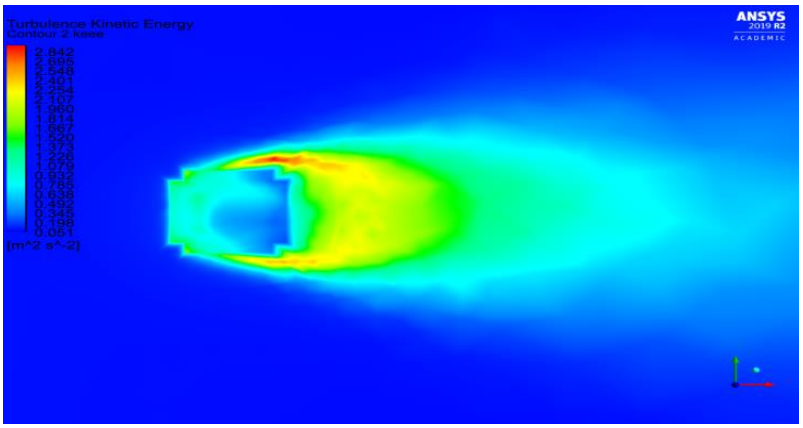

Figure 4.13: Kinetic energy spectrum for 25 mm cut section

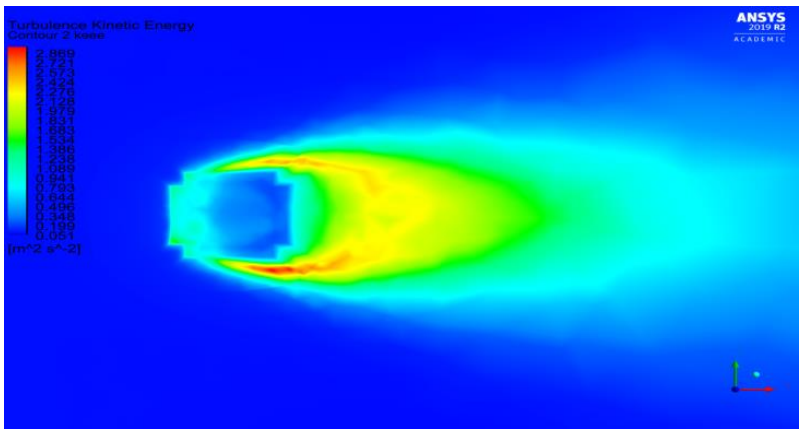

Figure 4.14: Kinetic energy spectrum for 31.25 mm cut section

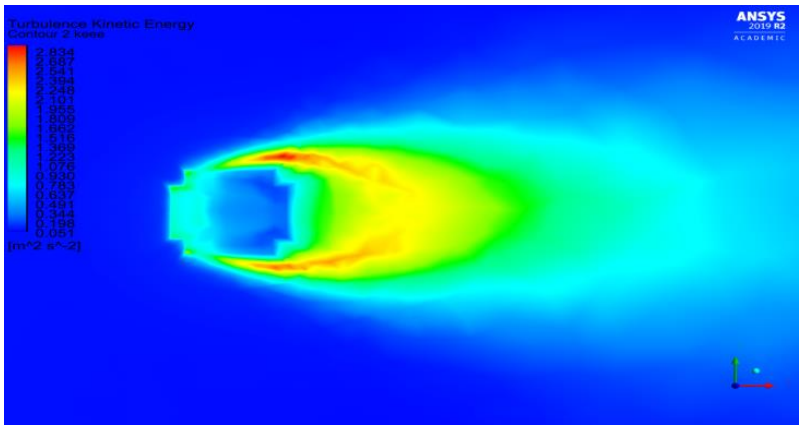

Figure 4.15: Kinetic energy spectrum for 37.5 mm cut section

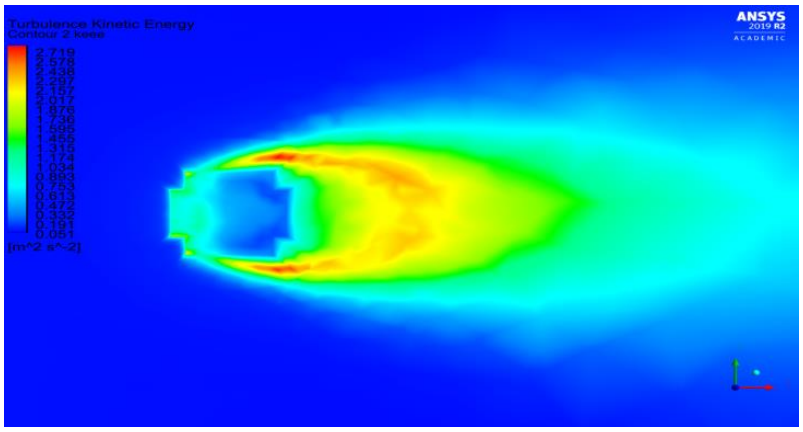

Figure 4.16: Kinetic energy spectrum for 43.75 mm cut section

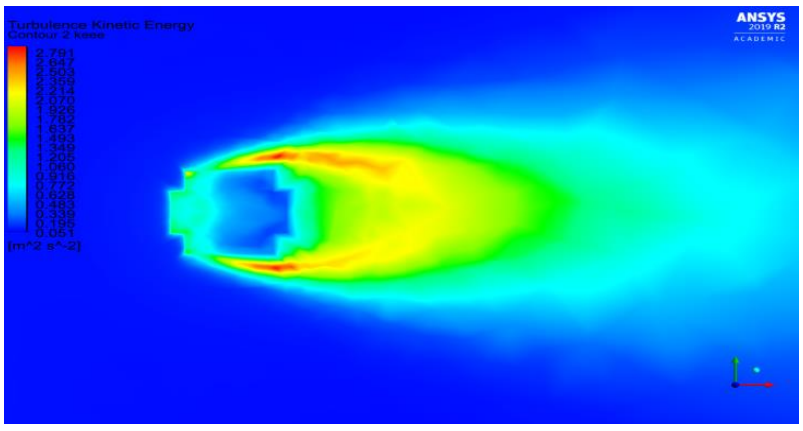

Figure 4.17: Kinetic energy spectrum for 50 mm cut section

Furthermore, these responses showed prolonged and wider wake religions as magnitudes of corner cuts increase. A higher magnitude of turbulence with a larger wake in kinetic energy plot was observed for 50 mm case. A reduction of 50% in wake region kinetic energy magnitude was observed for all cases except 6.25 mm corner cut. The corner cuts of the principal model may be responsible for this across wind wake regions.

4.2.4 Pressure Contours

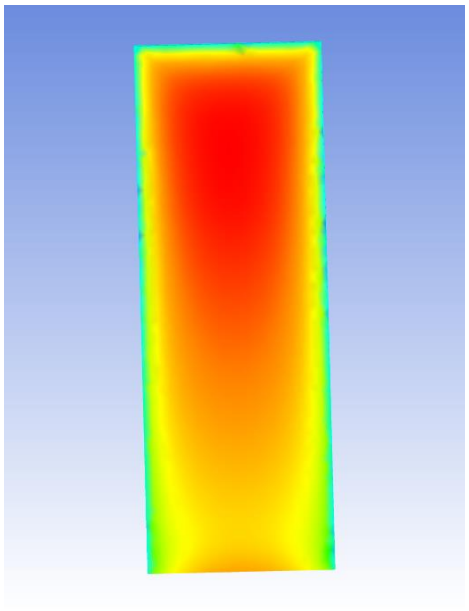

Figure 4.18 Front face square model

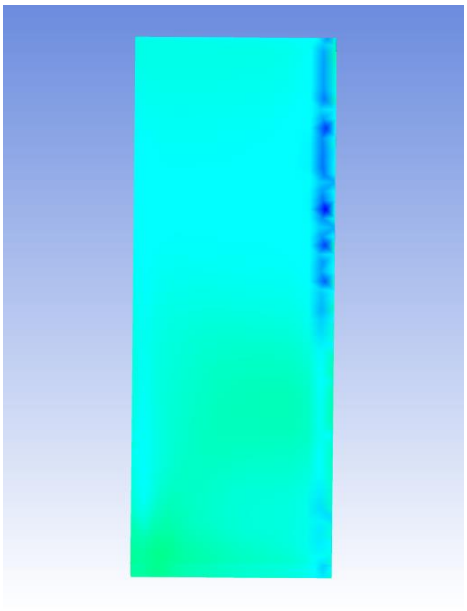

Figure 4.19 Side face square model

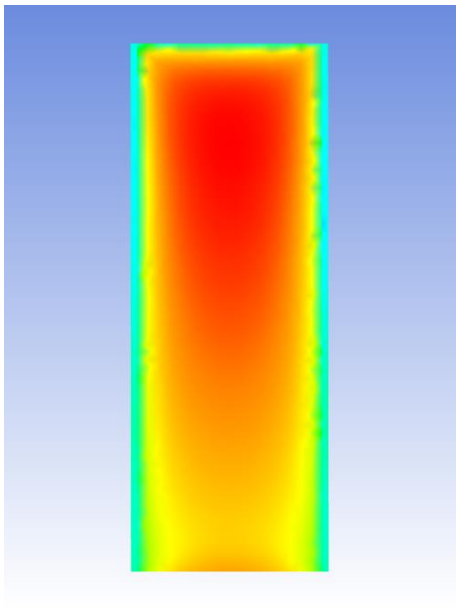

Figure 4.20 Front face 6.25 mm corner cut

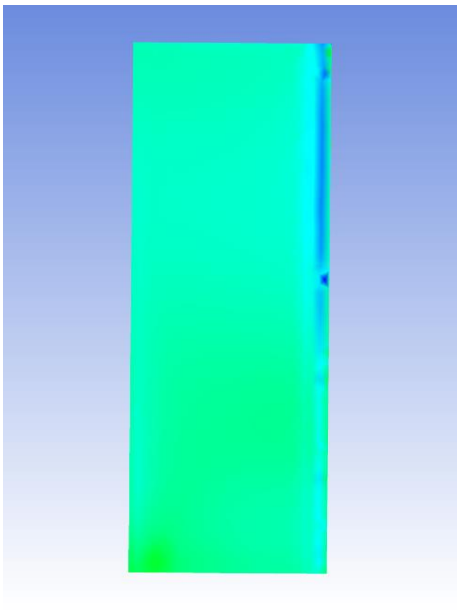

Figure 4.21 Side face 6.25 mm corner cut

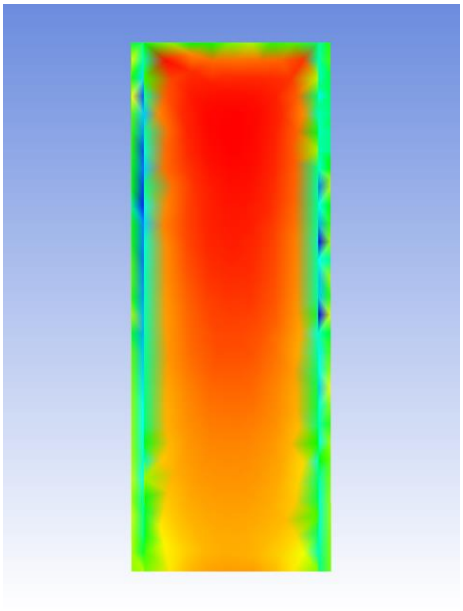

Figure 4.22 Front face 12.5 mm corner cut

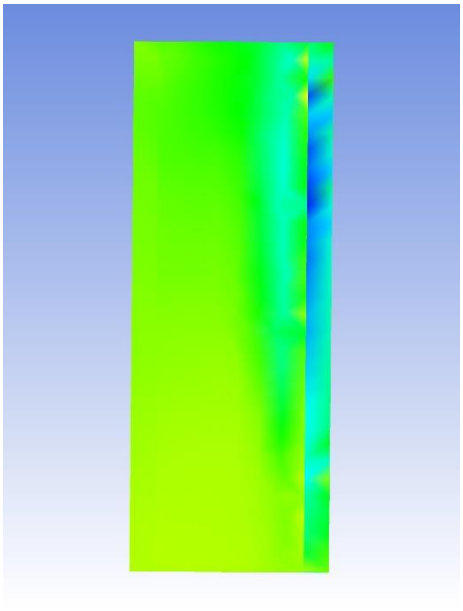

Figure 4.23 Side face 12.5 mm corner cut

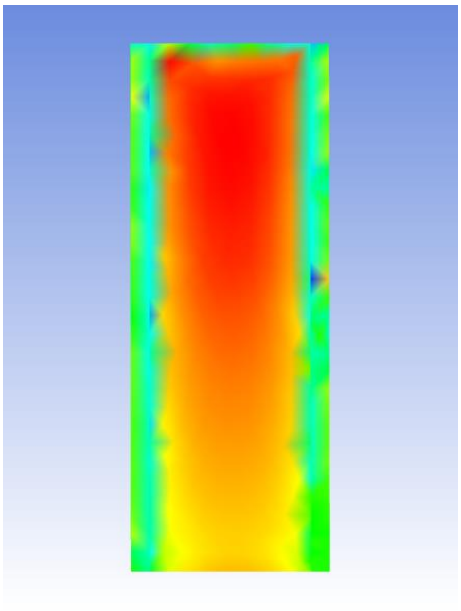

Figure 4.24 Front face 18.75 mm corner cut

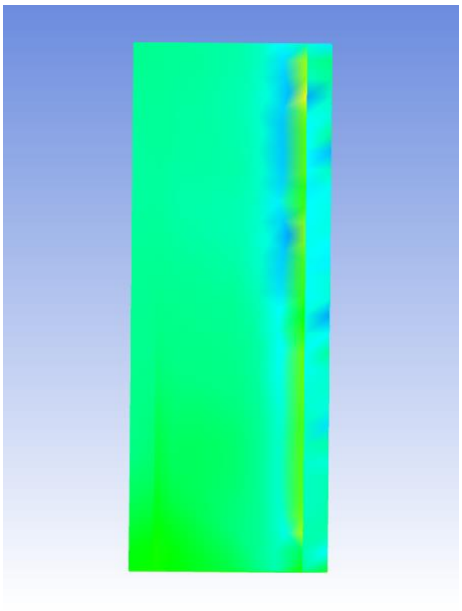

Figure 4.25 Side face 18.75 mm corner cut

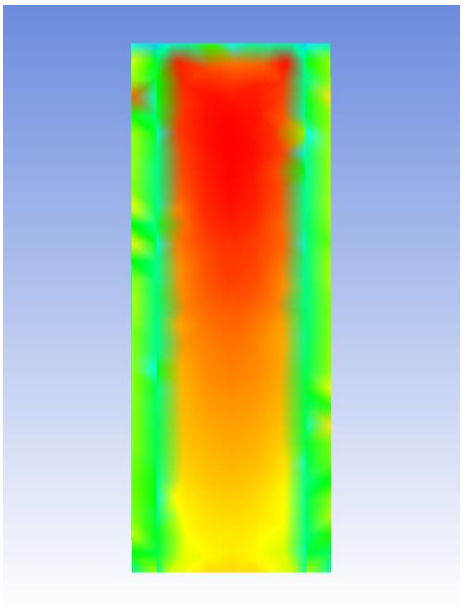

Figure 4.26 Front face 25 mm corner cut

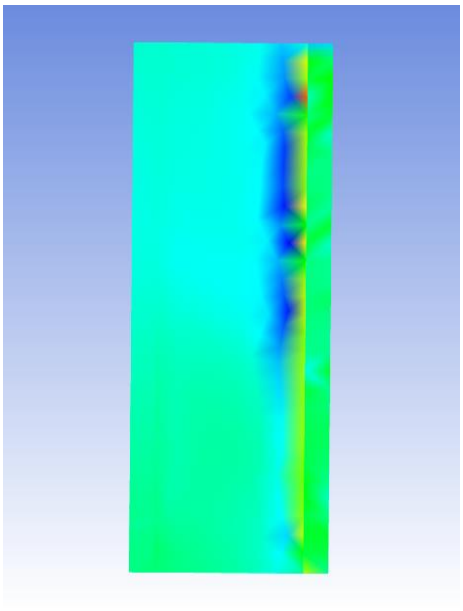

Figure 4.27 Side face 25 mm corner cut

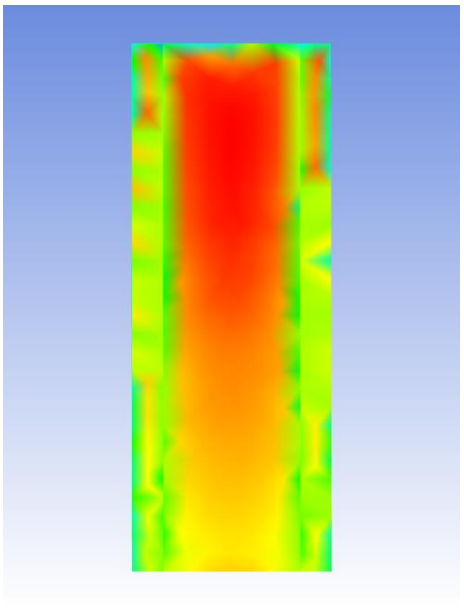

Figure 4.28 Front face 31.25 mm corner cut

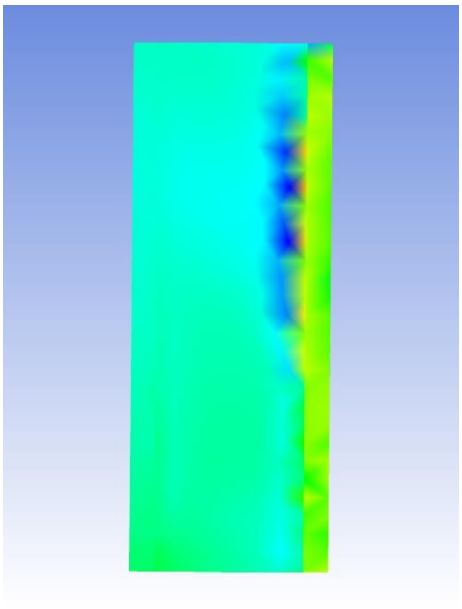

Figure 4.29 Side face 31.25 mm corner cut

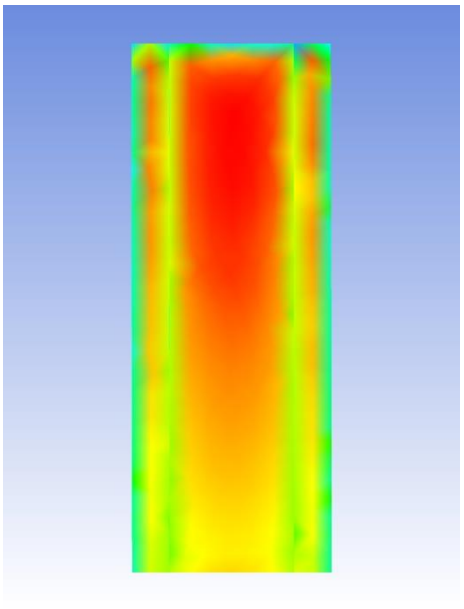

Figure 4.30 Front face 37.5 mm corner cut

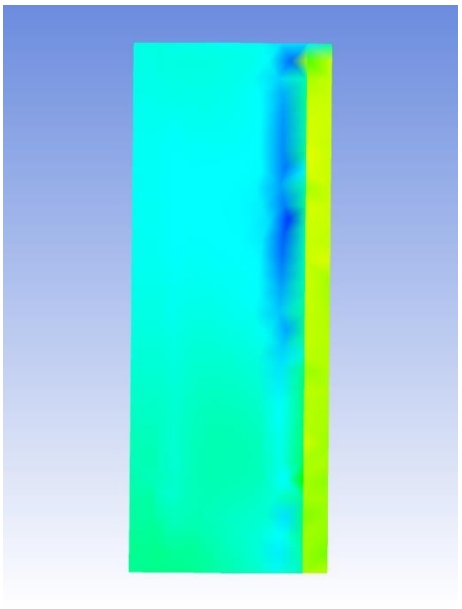

Figure 4.31 Side face 37.5 mm corner cut

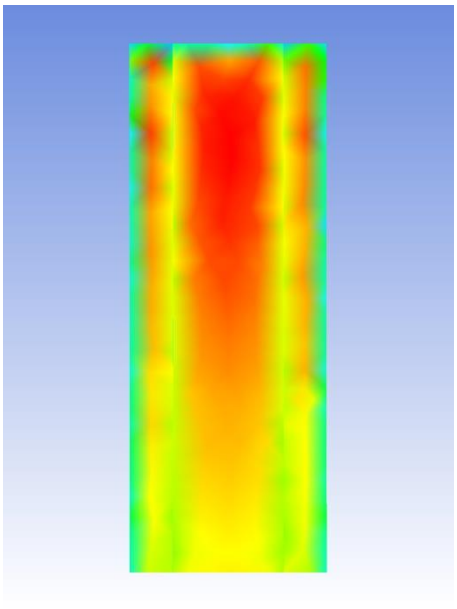

Figure 4.32 Front face 43.75 mm corner cut

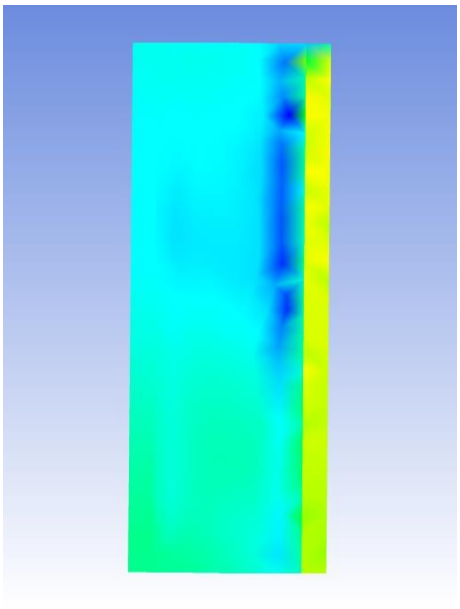

Figure 4.33 Side face 43.75 mm corner cut

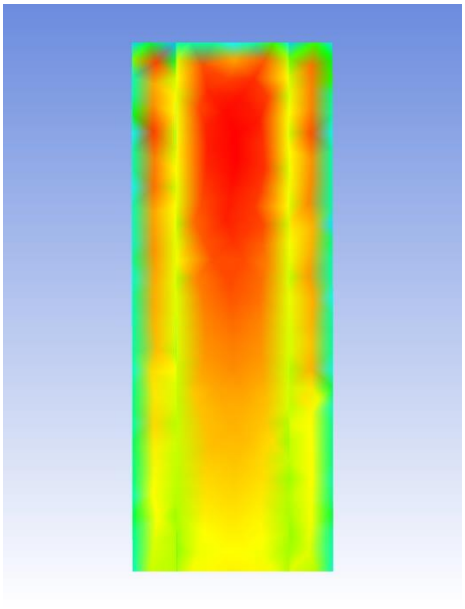

Figure 4.34 Front face 50 mm corner

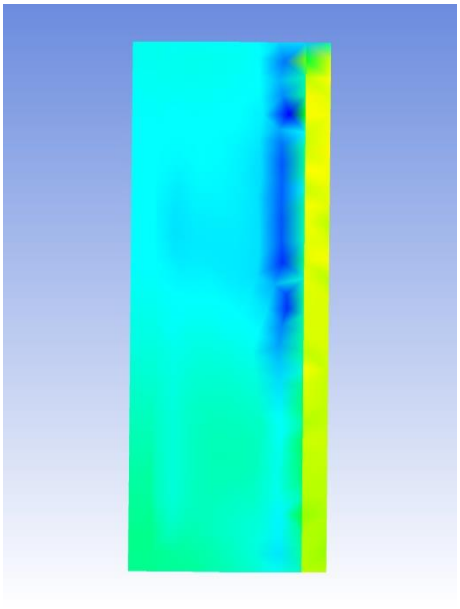

Figure 4.35 Side face 50 mm corner cut

4.3 Interference Study

4.3.1 Interference effect on along win response

The interference factor (IF) is the ratio of wind load on PM under influence of interference to the wind response of an isolated PM (Eq. 4.1). To assess wind interference effects along wind direction the force along the normal x-direction has been computed for all principal models with different configurations of IM locations and orientations.

$$IF = \frac{Force/Pressure\ on\ PM\ in\ presence\ of\ IM}{Force/Pressure\ on\ isolated\ PM} \tag{4.1}$$

The interference effect on PM is assessed by plotting IF values against different height ratios and different orientations of IM. The IF values less than unity suggest a shielding effect on PM. The values of IF more than unity suggest enhanced wind loading. In our study, no case of enhanced loading is observed. When the IM is placed at HB blockage condition it is observed that the IF values are very low due to shielding effect. Optimum shielding of 90% is observed for the IM model of 600 mm at 60-degree orientation (Fig. 4.36). No shielding was observed in the case of 100 mm high IM. In the case of NB and HB blockage conditions the shielding increased with a decrease in height ratio too, thus reducing the value of the IF factor (Figs. 4.37 and 4.38). The HB and NB blockage configuration showed optimum reduction at 45-degree and 60-degree orientations respectively. The maximum interference effect was observed for no blockage condition at 0-degree orientation. The maximum variation was observed for H_r ratio 5 and 6 within the range of 16-39% increment for blockage ratio in ascending order except for the exceptional case of H_r 6 in full blockage configuration.

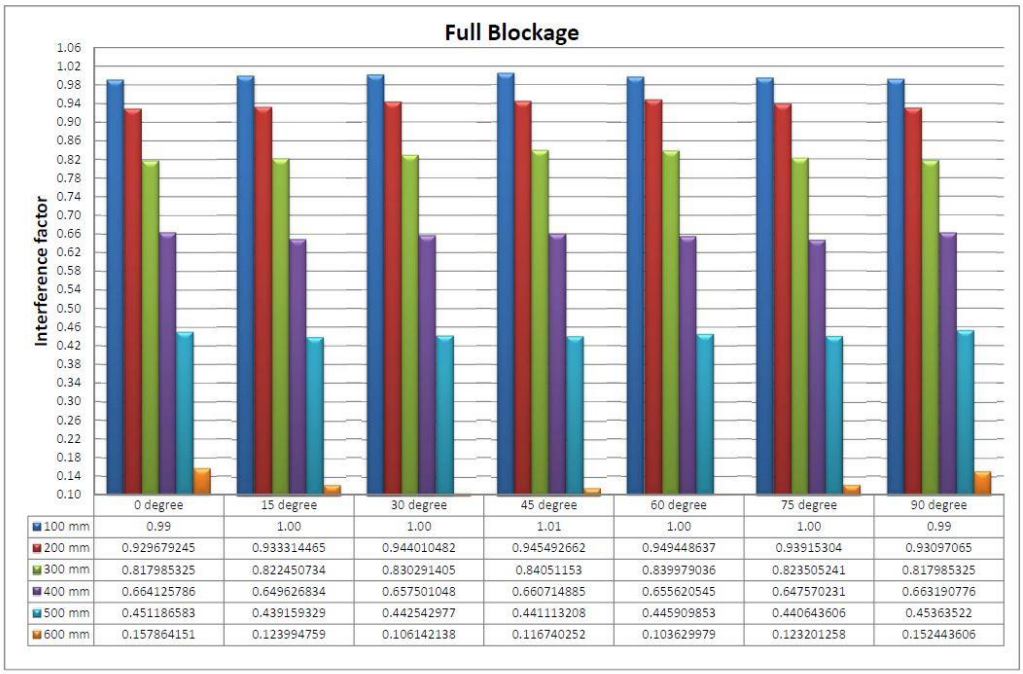

	0 degree	15 degree	30 degree	45 degree	60 degree	75 degree	90 degree
100 mm	0.99	1.00	1.00	1.01	1.00	1.00	0.99
200 mm	0.929679245	0.933314465	0.944010482	0.945492662	0.949448637	0.93915304	0.93097065
300 mm	0.817985325	0.822450734	0.830291405	0.84051153	0.839979036	0.823505241	0.817985325
400 mm	0.664125786	0.649626834	0.657501048	0.660714885	0.655620545	0.647570231	0.663190776
500 mm	0.451186583	0.439159329	0.442542977	0.441113208	0.445909853	0.440643606	0.45363522
600 mm	0.157864151	0.123994759	0.106142138	0.116740252	0.103629979	0.123201258	0.152443606

Figure 4.36 Interference factor for FB configuration

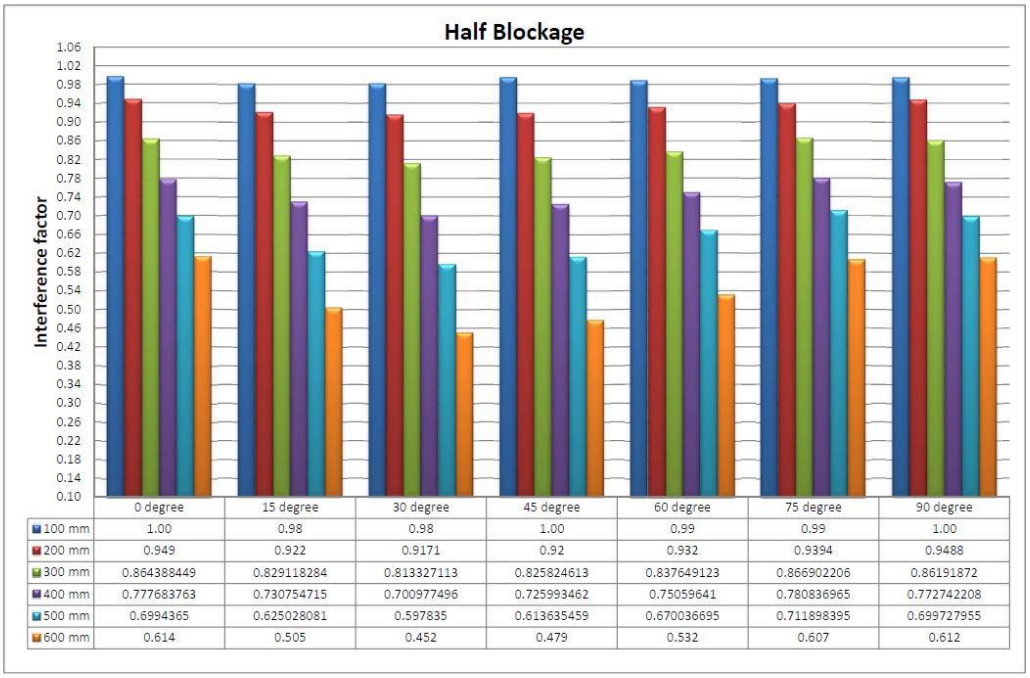

	0 degree	15 degree	30 degree	45 degree	60 degree	75 degree	90 degree
100 mm	1.00	0.98	0.98	1.00	0.99	0.99	1.00
200 mm	0.949	0.922	0.9171	0.92	0.932	0.9394	0.9488
300 mm	0.864388449	0.829118284	0.813327113	0.825824613	0.837649123	0.866902206	0.86191872
400 mm	0.777683763	0.730754715	0.700977496	0.725993462	0.75059641	0.780836965	0.772742208
500 mm	0.6994365	0.625028081	0.597835	0.613635459	0.670036695	0.711898395	0.699727955
600 mm	0.614	0.505	0.452	0.479	0.532	0.607	0.612

Figure 4.37 Interference factor for HB configuration

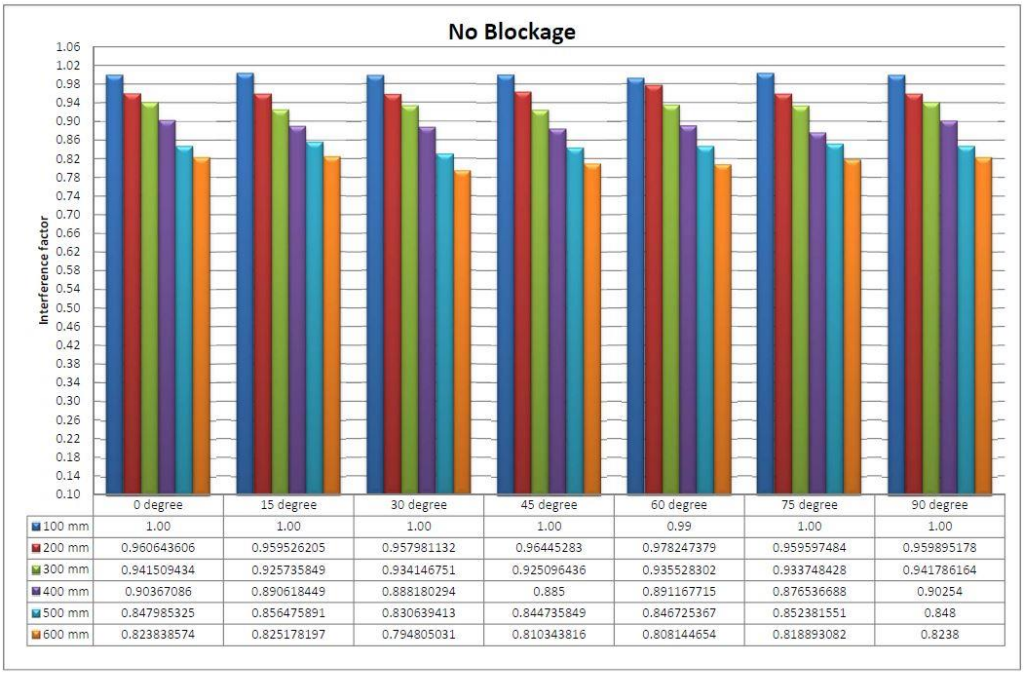

	0 degree	15 degree	30 degree	45 degree	60 degree	75 degree	90 degree
100 mm	1.00	1.00	1.00	1.00	0.99	1.00	1.00
200 mm	0.960643606	0.959526205	0.957981132	0.96445283	0.978247379	0.959597484	0.959895178
300 mm	0.941509434	0.925735849	0.934146751	0.925096436	0.935528302	0.933748428	0.941786164
400 mm	0.90367086	0.890618449	0.888180294	0.885	0.891167715	0.876536688	0.90254
500 mm	0.847985325	0.856475891	0.830639413	0.844735849	0.846725367	0.852381551	0.848
600 mm	0.823838574	0.825178197	0.794805031	0.810343816	0.808144654	0.818893082	0.8238

Figure 4.38 Interference factor for NB configuration

4.3.2 Interference effect on across wind response

The across wind response of interference effects through interference factor of the normal force in the y-direction on PM showed great variations and anomalies. In some cases, the across wind response suggested 4 to 5 folds magnitudes that of isolated structure. This section explores the power spectral density function and pressure coefficients for a better understanding of the interference effect on across wind response. This section discusses IM heights of 300 mm and 400 mm in different configurations as their responses were exceptional in the normal y-direction in comparison to other model heights.

The power spectral density of lift coefficient ($nS(n)/\sigma_{Cfy}$) versus strouhal number (nD/H) has been plotted using hannings FFT model. Power spectral densities of force coefficient in y-direction were plotted against strouhal number for

different orientations of IM. It is evident from the PSD plots that the spectra of both the model heights flow over the isolated structures spectra, thus producing large magnitudes of force coefficients across wind direction than an isolated structure. The gap between PSD response is least for FB blockage condition thus magnitudes of the force coefficients were in closer proximities to that of an isolated structure (Fig. 4.39 and 4.40). Fig. 4.43 and 4.44 suggest that for NB condition for IM models of height 300 and 400-mm power spectra of orientations 0-degree and 15-degree only provide a stable response for across wind forces. Power spectra of half blockage conditions also give acceptable responses only at 0-degree and 30-degree for 300 mm (Fig. 4.41), and 0-degree for 400 mm models (Fig. 4.42). Thus, the along wind interference parameter IF alone can't justify the interference effects. It was observed as the H_r of building decreases the pressure spectra extends to high-frequency scales, on contrary for lower heights of IM the pressure spectra was observed the same as an isolated building. The unstable orientation angles of the 300 mm and 400 mm IM were further explored by evaluating transient pressure coefficient analysis on a polyline.

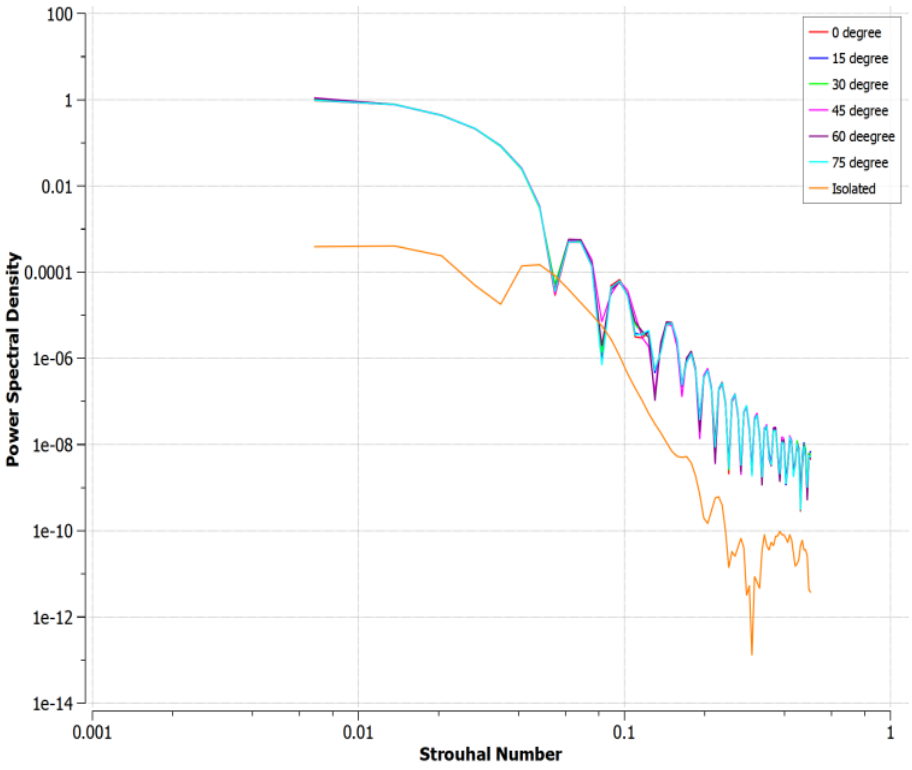

Figure 4.39 PSD for 300 mm IM at FB configuration

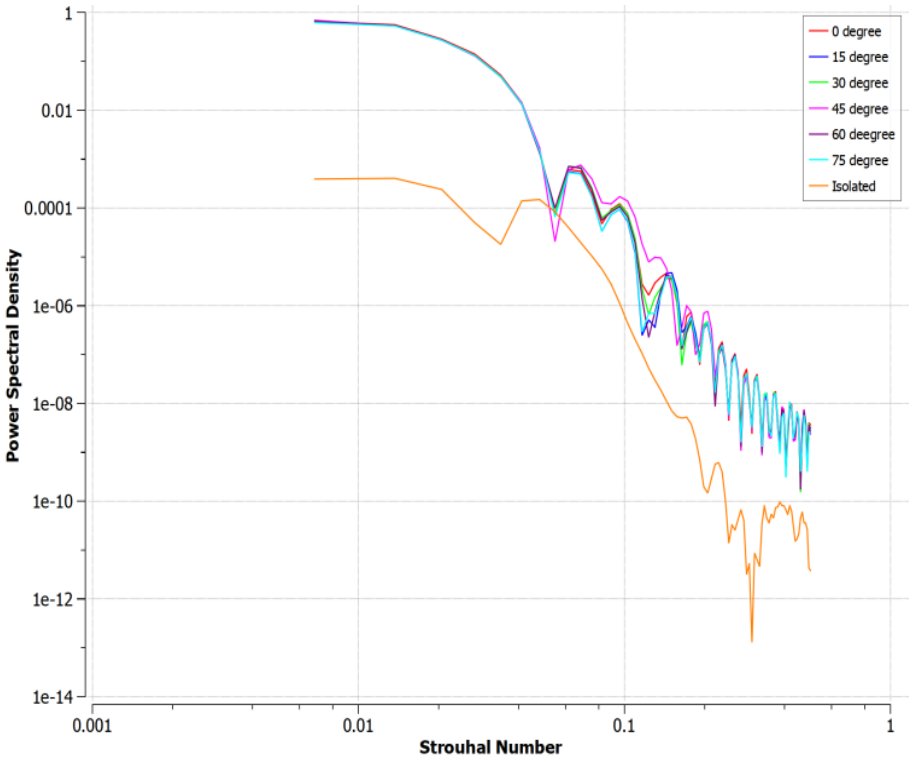

Figure 4.40 PSD for 400 mm IM at FB configuration

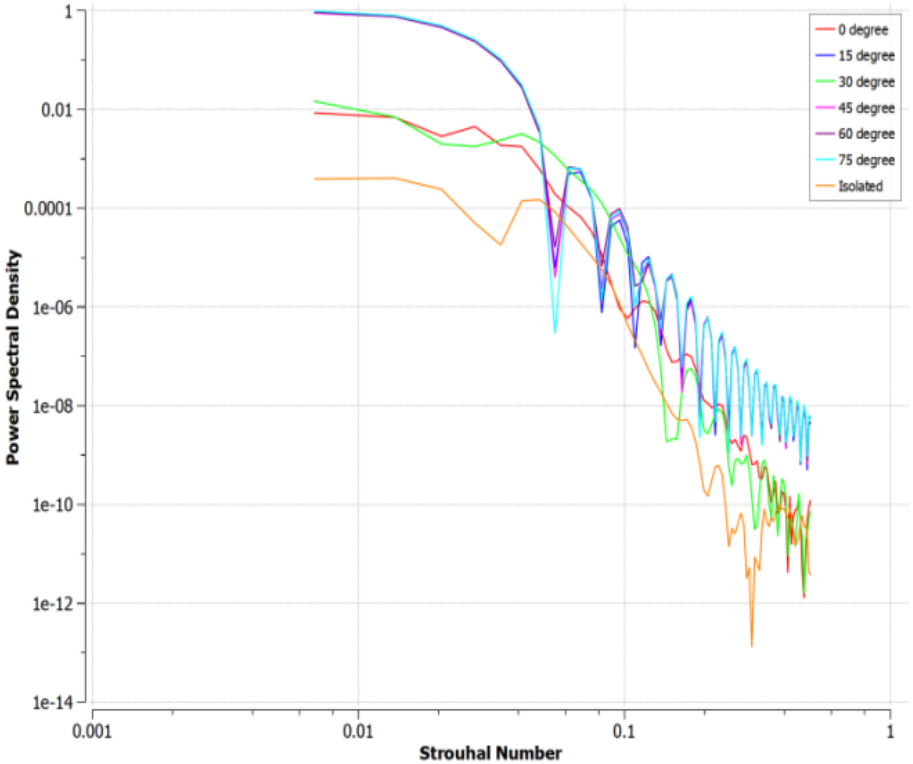

Figure 4.41 PSD for 300 mm IM at HB configuration

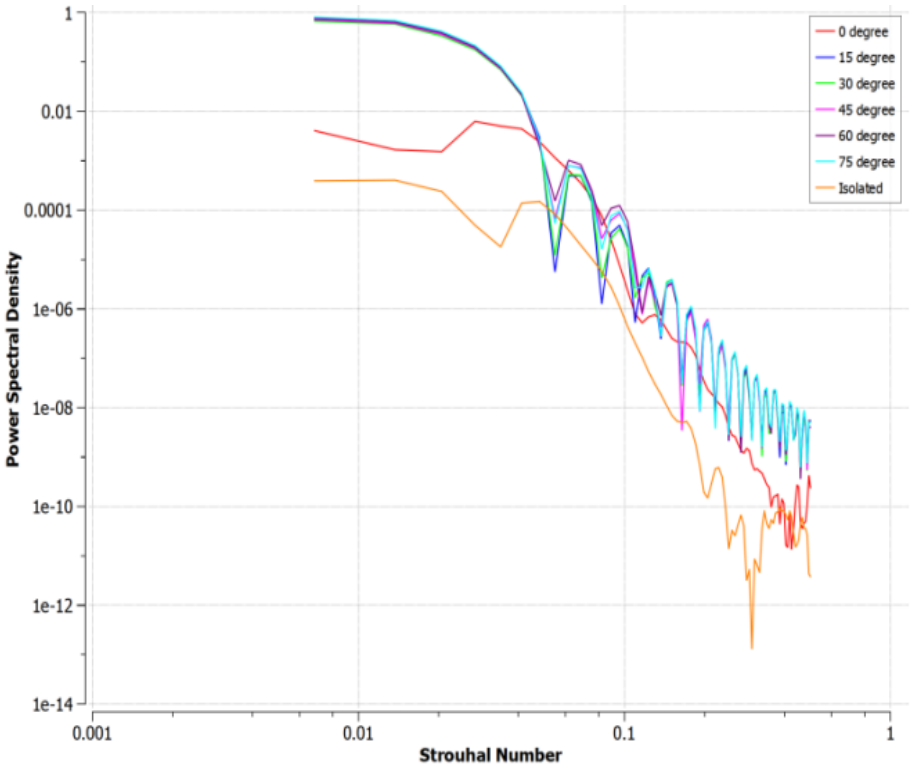

Figure 4.42 PSD for 400 mm IM at HB configuration

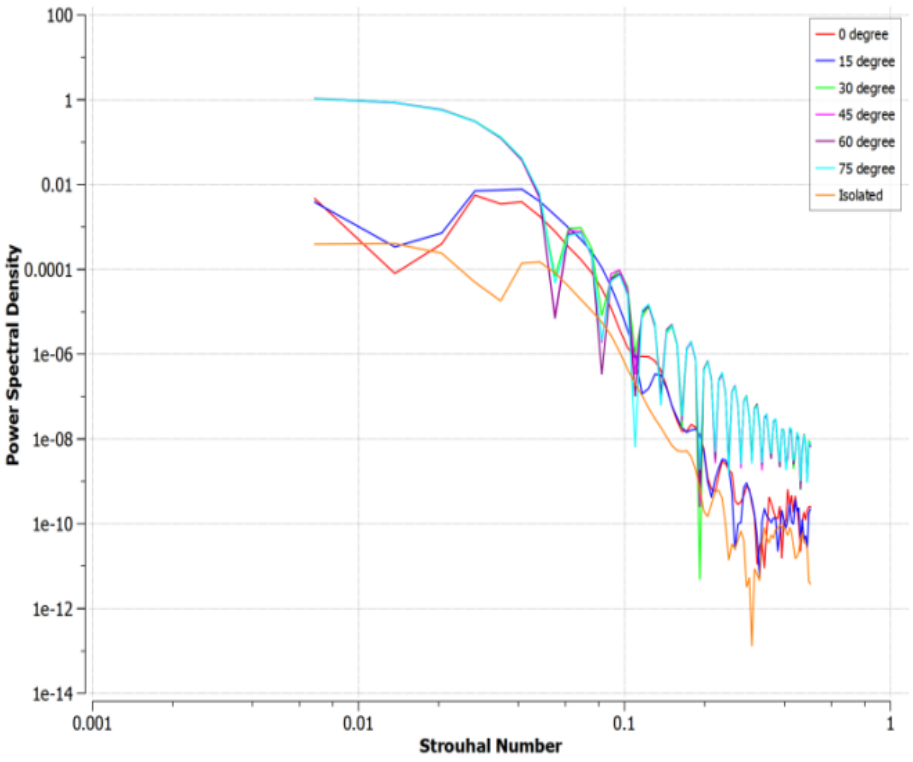

Figure 4.43 PSD for 300 mm IM at NB configuration

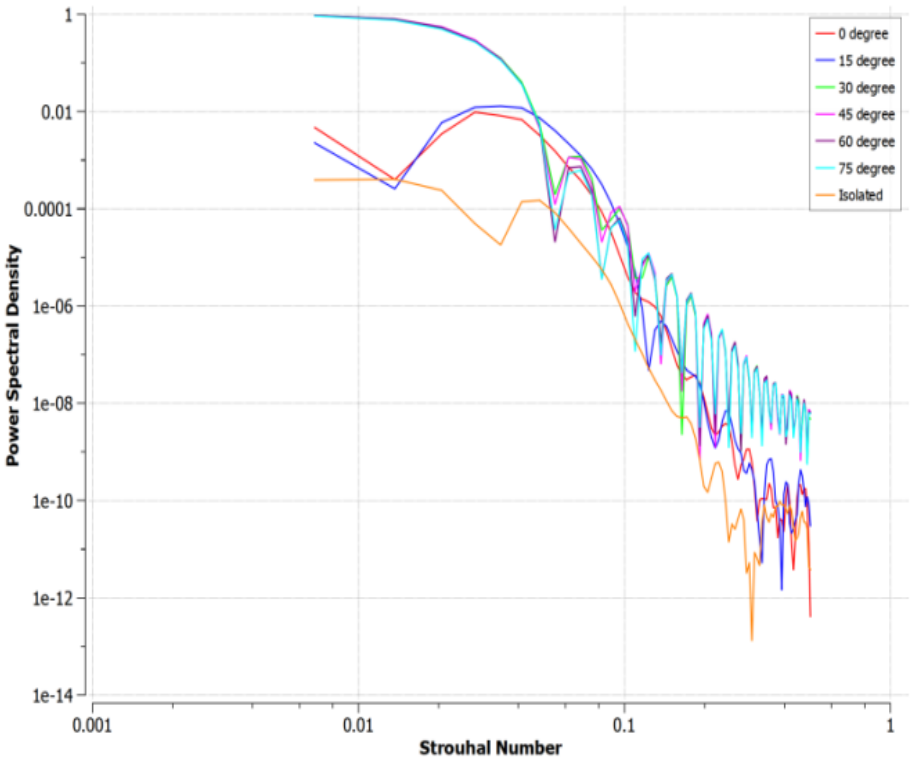

Figure 4.44 PSD for 400 mm IM at HB configuration

4.3.3 Horizontal pressure coefficient

The pressure variation due to different orientation of IM of height 300 mm and 400 mm in all blockage conditions has been discussed in this section. A perimeter is placed at 0.9H height i.e. 540 mm from the base on the PM in the form of a polyline to measure the external pressure coefficient.

A series of six probe points are also placed on this pressure belt to monitor the transient pressure variations as shown in Fig. 3.7. The coefficient of pressure variations for H_r 3 and 4 are highlighted in this section as these cased showed most variation in across wind responses of PM. It is evident from the C_p plot (Fig. 4.45 and 4.46) that for orientation of 30, 45, 60, and 75-degree for no blockage condition in case of 300 mm and 400 mm IM the negative C_p on the side faces increases up to maximum 24%. This increment is responsible for more turbulence in

the wake regions of the PM. For the same height ratios in full blockage condition, the C_p values (Figs. 4.49 and 4.50) are increased up to 27 % with respect to an isolated model. Although, the full blockage C_p variation doesn't contribute much to across wind response as the opposite side face pressure coefficients diminish the response.

In the case of the half blockage condition, windward projections for side faces reverse in magnitudes as streamlines projected from IM disturb the flow profile around PM as shown in Fig. 4.47 and 4.48. Half shielding of the PM creates a wake region between two models, thus creating negative pressure points on the front face.

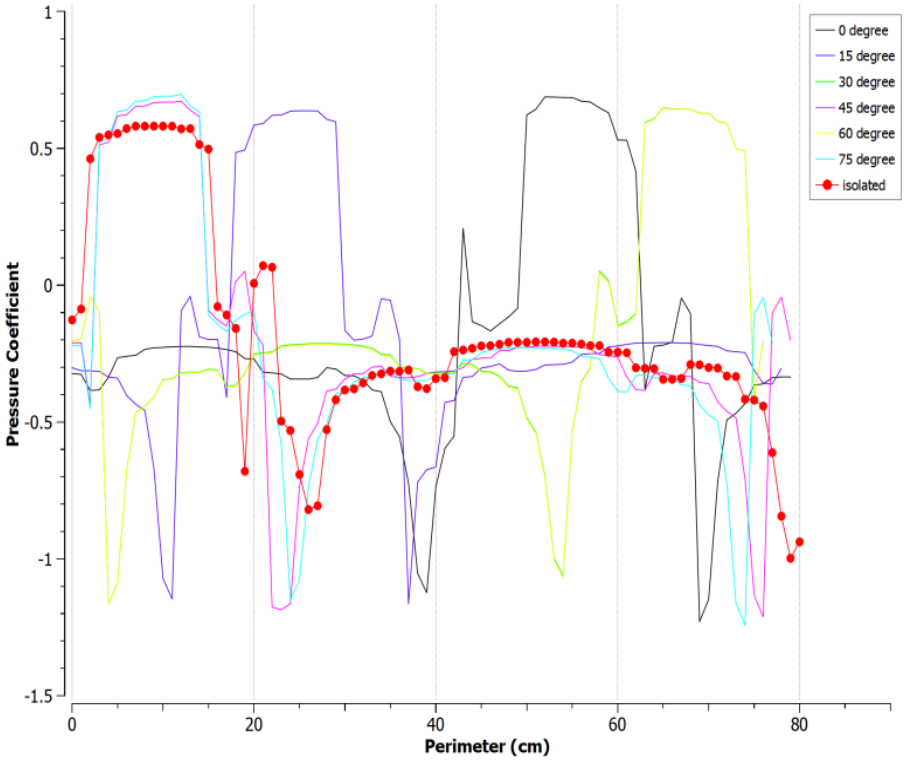

Figure 4.45 C_p curve for 300 mm IM at NB configuration

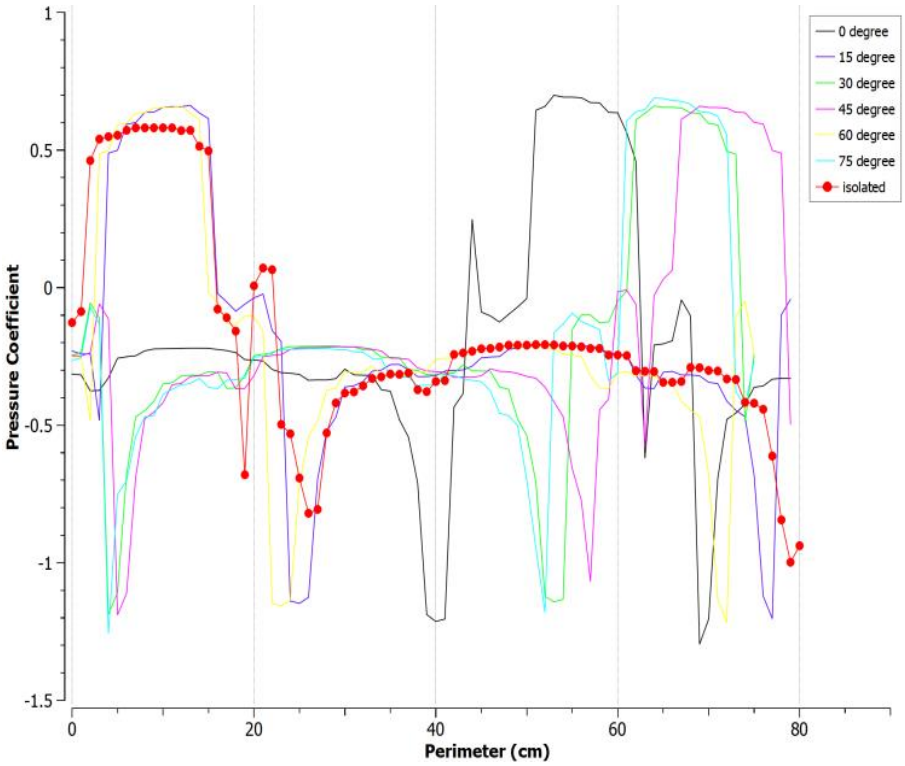

Figure 4.46 C_p curve for 400 mm IM at NB configuration

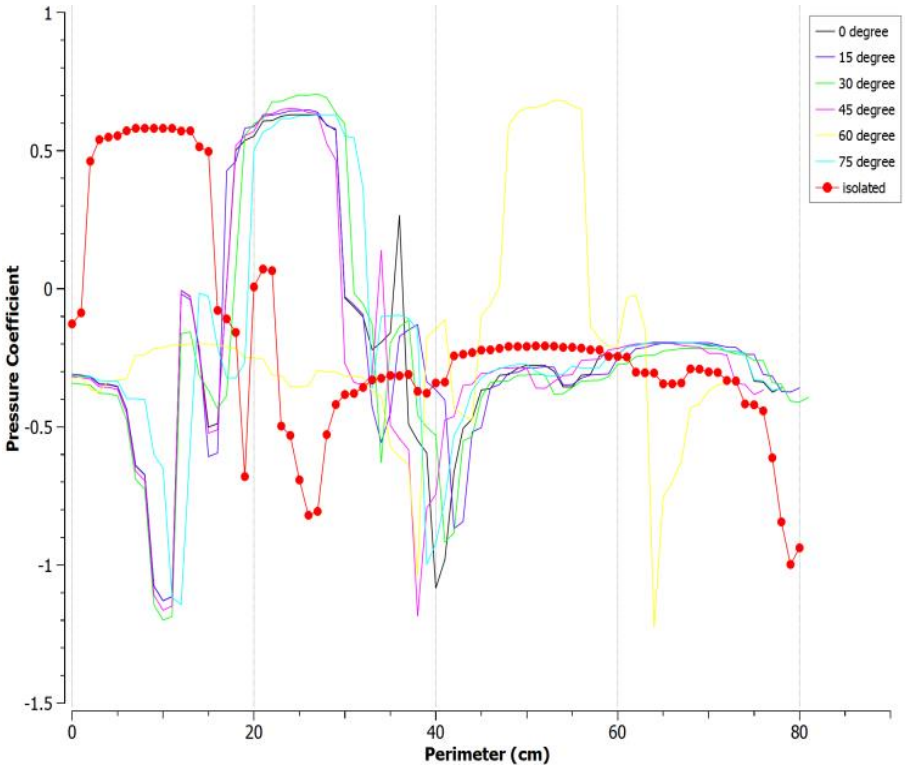

Figure 4.47 C_p curve for 300 mm IM at HB configuration

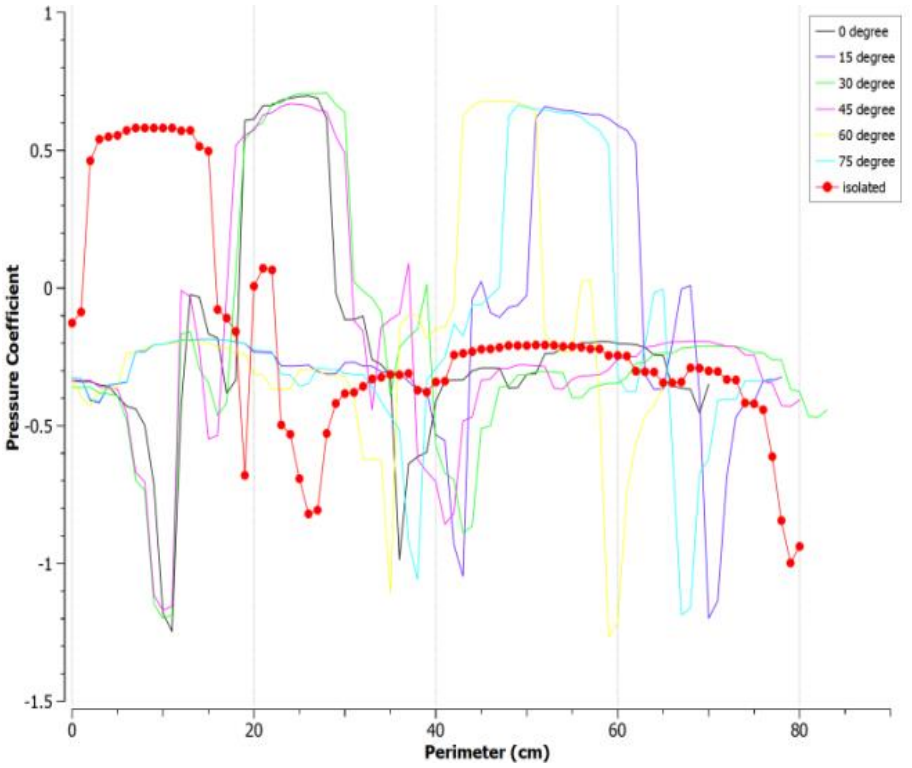

Figure 4.48 C_p curve for 400 mm IM at HB configuration

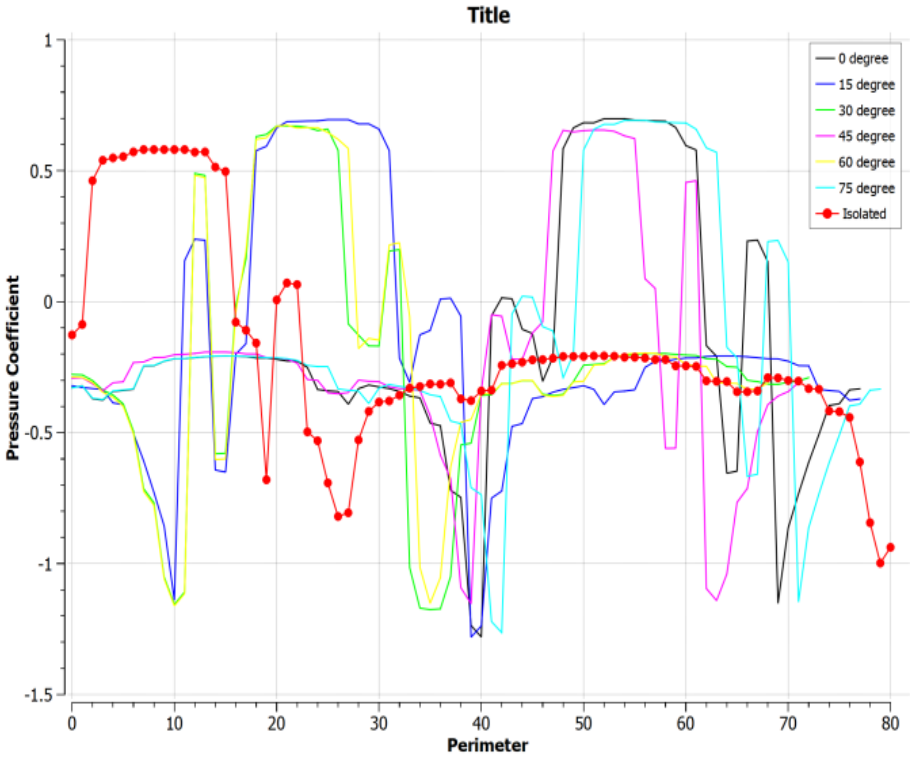

Figure 4.49 C_p curve for 300 mm IM at FB configuration

The transient pressure study on the front face later suggested suction points on the front faces of the PM. The common projection in all the blockage conditions is that the most unstable nature of across wind response was generated for a 60-degree orientation of IM.

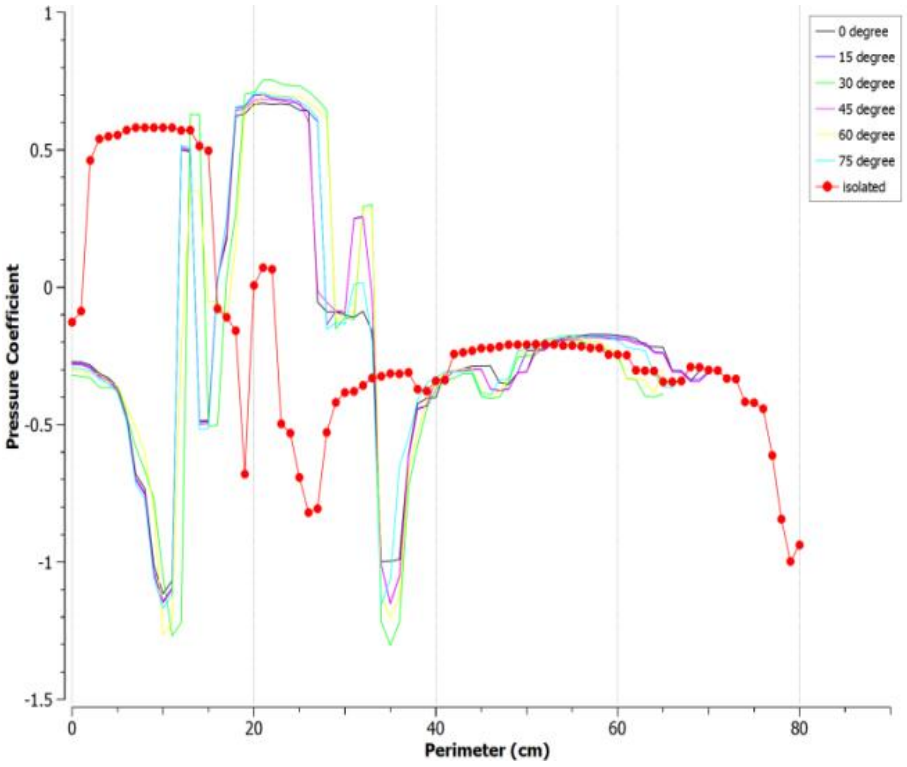

Figure 4.50 C_p curve for 400 mm IM at FB configuration

4.3.4 Kinetic energy fluctuations and Turbulence

On monitoring probability density function many subsequent peaks were observed. These subsequent peaks may suggest vortex shedding and reattachment of the separated turbulent flow. These flow conditions produce turbulence in the wake regions of the principal modal. The vortex shedding and turbulence both contribute to the kinetic energy (KE) in the wake region. A section plane was created at the top of PM to analyze the pattern of these turbulences employing kinetic energy fluctuations and compared them with the isolated model.

The vortex shedding and turbulence both contribute to the kinetic energy in the wake region. The most unstable wind response cases have been compared here. It is observed in most of these cases suction is developed on both roof and the front face of the PM which was evident from the C_p plots on the polyline Furthermore, these cases had wake regions developed on the right side of PM. These responses also showed prolonged wake religions and a higher magnitude of turbulence as compared to the isolated principal model kinetic energy plot. The corner cuts of the principal model may be responsible for this across wind wake regions. This can be justified by an interference study on square sectional models of the same cross-sections as corner cut models.

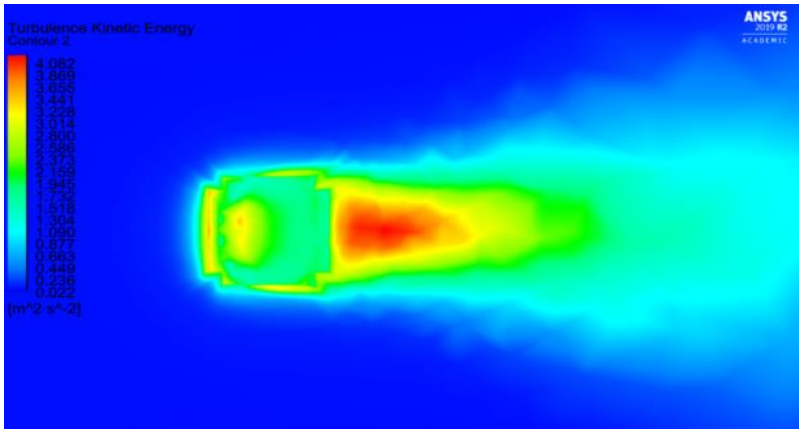

Figure 4.51 KE spectrum for isolated PM

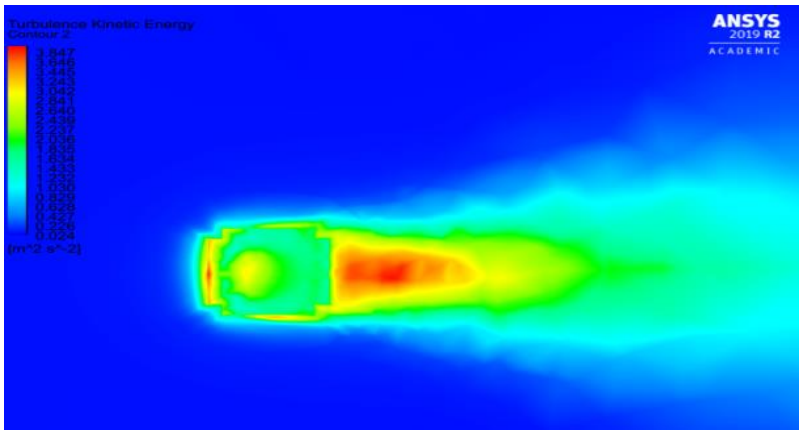

Figure 4.52 KE spectrum for PM for 15-degree IM 300 at NB

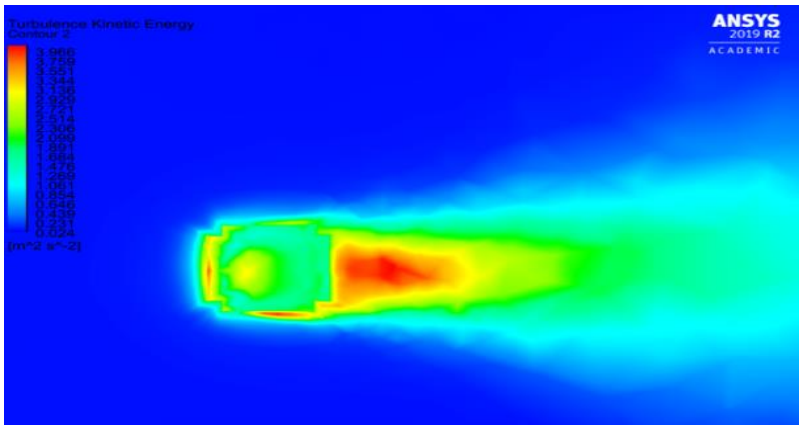

Figure 4.53 KE spectrum for PM for 60-degree IM 300 at NB

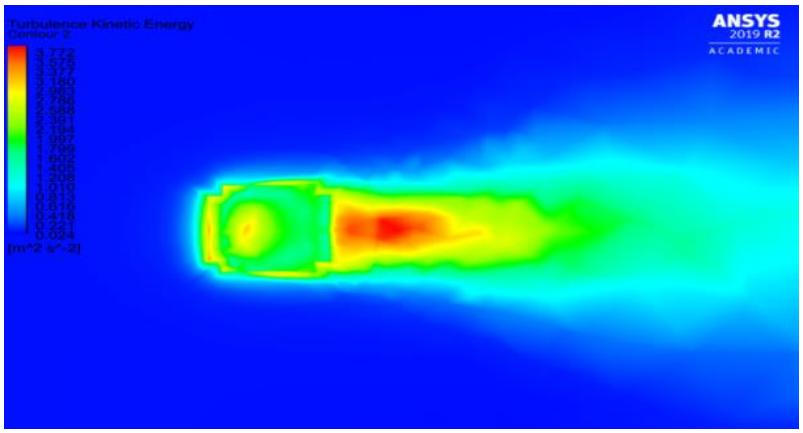

Figure 4.54 KE spectrum for PM for 60-degree IM 300 at HB

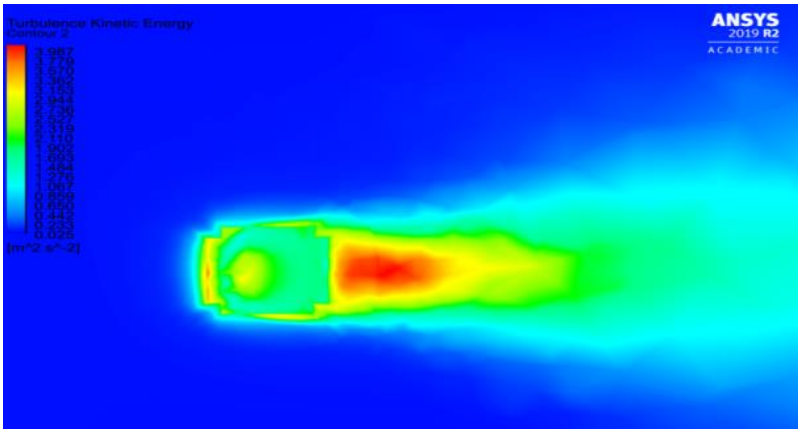

Figure 4.55 KE spectrum for PM for 45-degree IM 400 at NB

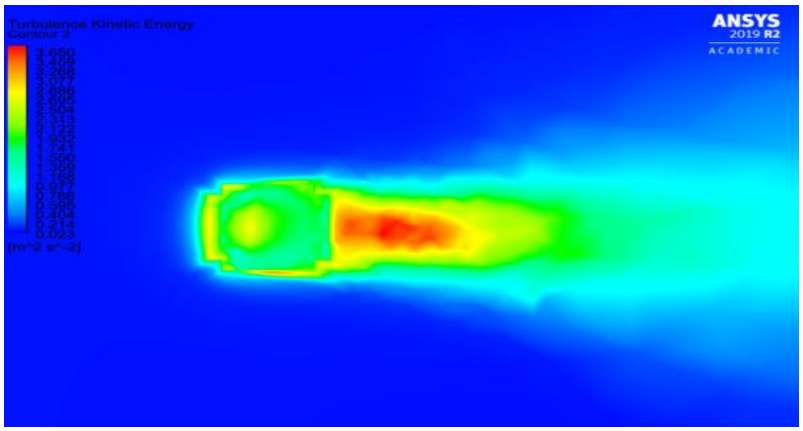

Figure 4.56 KE spectrum for PM for 15-degree IM 400 at HB

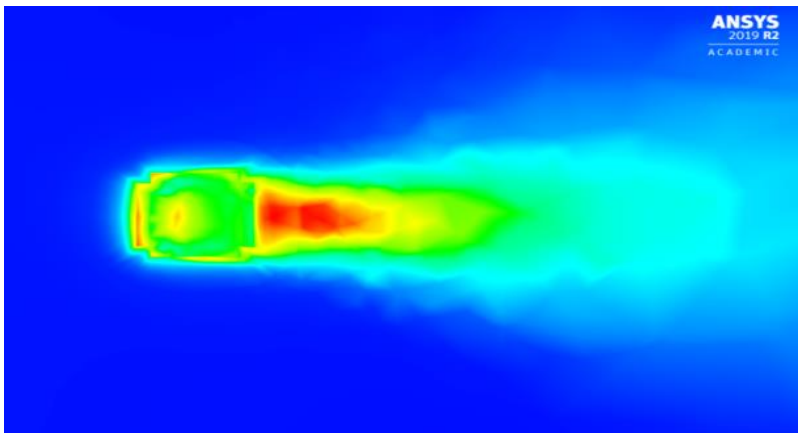

Figure 4.57 KE spectrum for PM for 60-degree IM 400 at HB

4.3.5 Velocity Streamlines

The velocity streamlines for corner cut sections are compared with an isolated square model in this section. Fig. 4.59 and 4.60 suggest that IM does mot disturb the flow lines from the PM, but the wake region flow profiles are different in these cases than an isolated square model. A wider wake is observed in these cases. In most of the NB configuration the streamlines from IM don't interfere with the PM. In case of HB configuration (Fig. 4.61, 4.63 and 4.64) the interference effects were more prominent than the NB case.

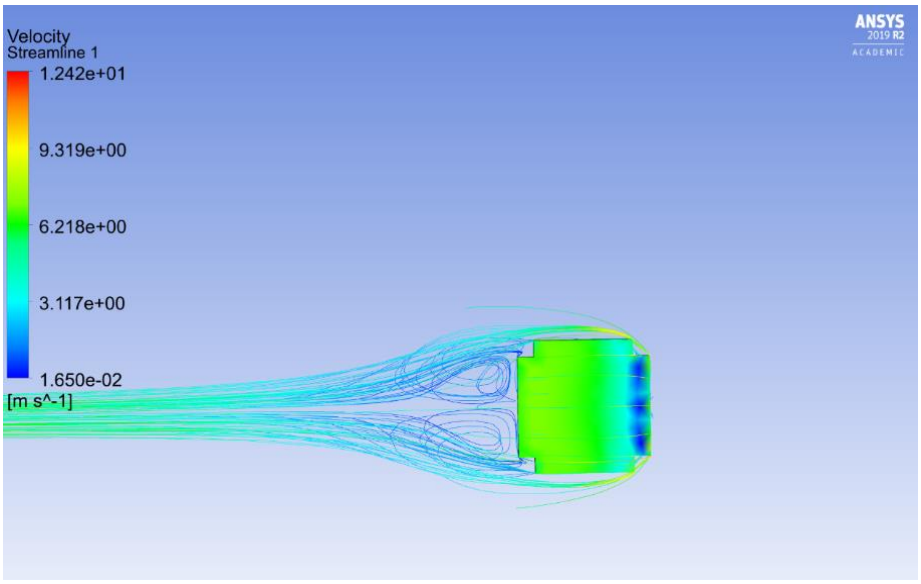

Figure 4.58 Velocity streamlines for isolated PM

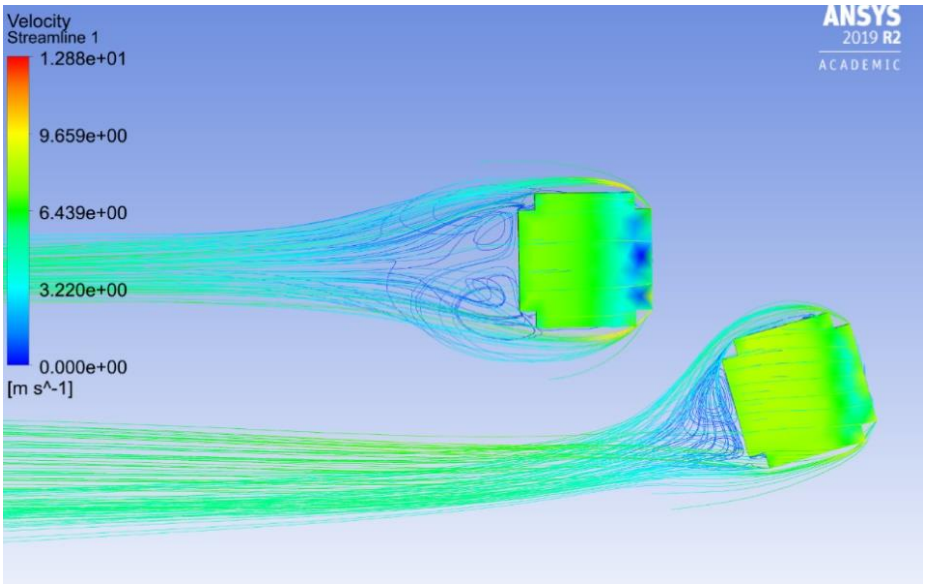

Figure 4.59 Velocity streamlines for PM for 15-degree IM 300 at NB

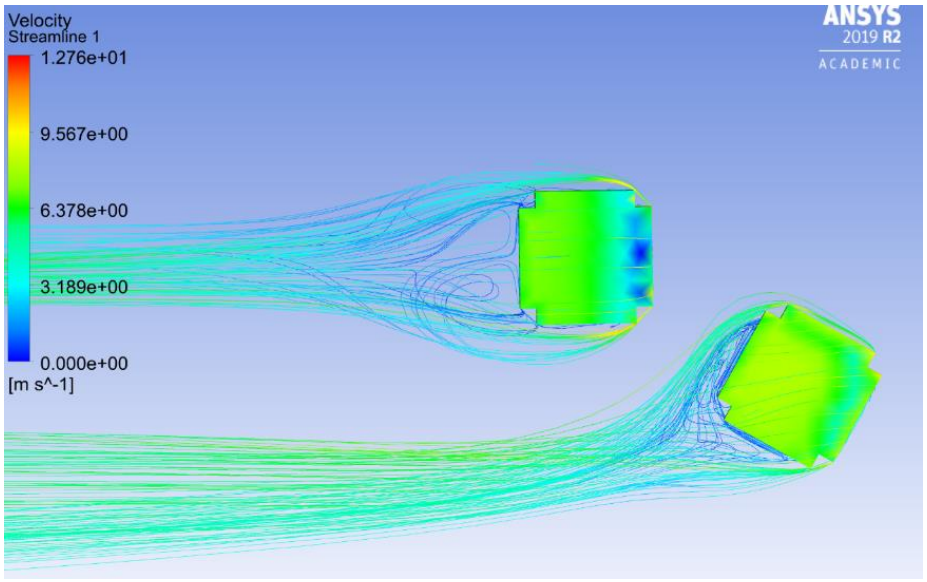

Figure 4.60 Velocity streamlines for PM for 60-degree IM 300 at NB

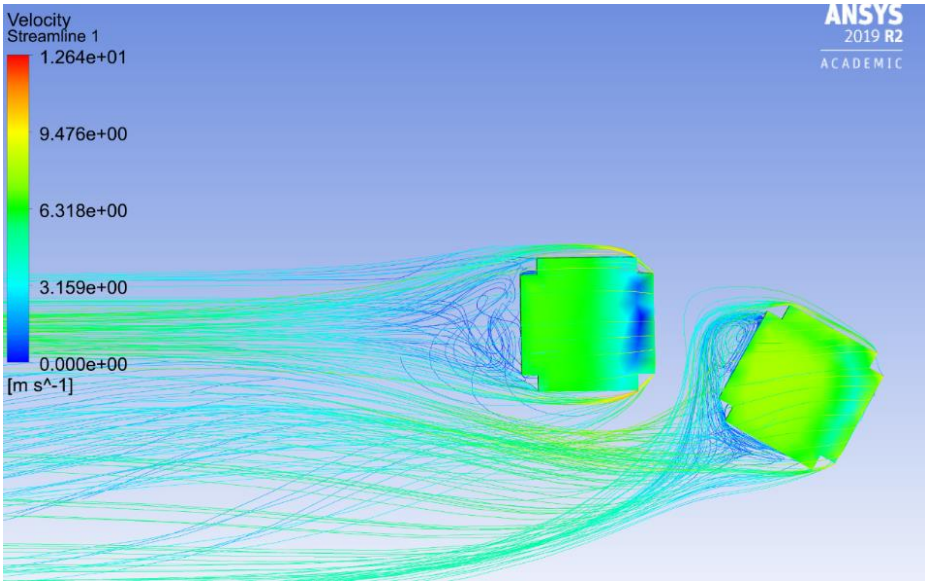

Figure 4.61 Velocity streamlines for PM for 60-degree IM 300 at HB

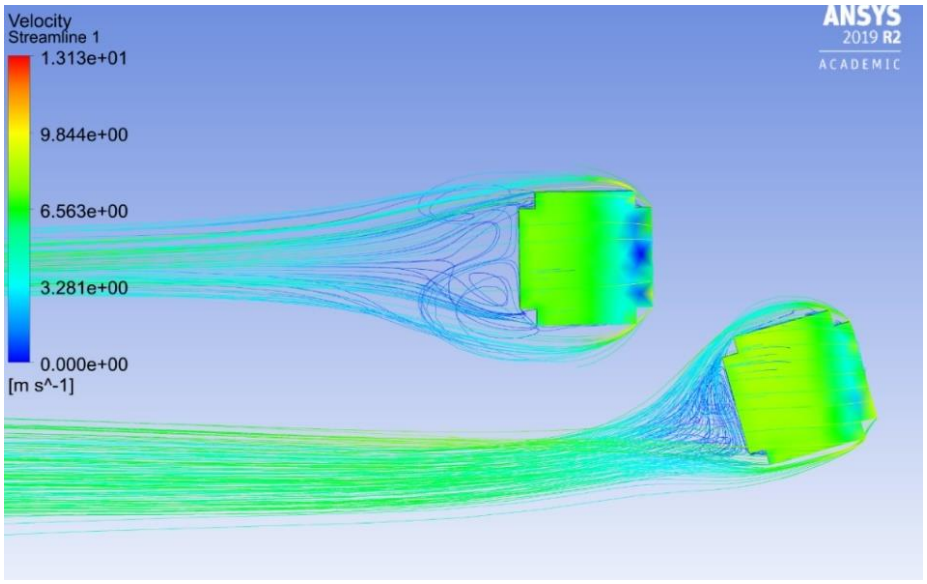

Figure 4.62 Velocity streamlines for PM for 45-degree IM 400 at NB

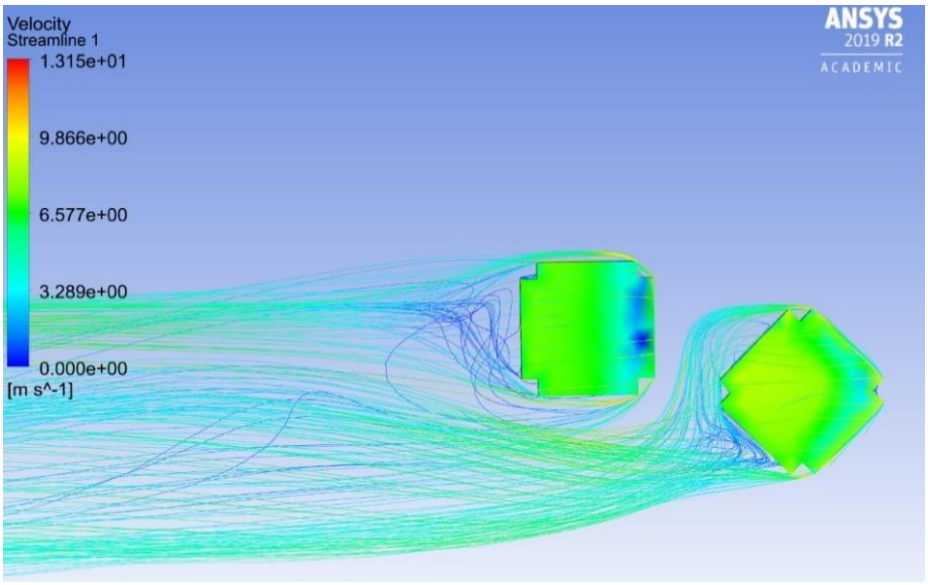

Figure 4.63 Velocity streamlines for PM for 15-degree IM 400 at HB

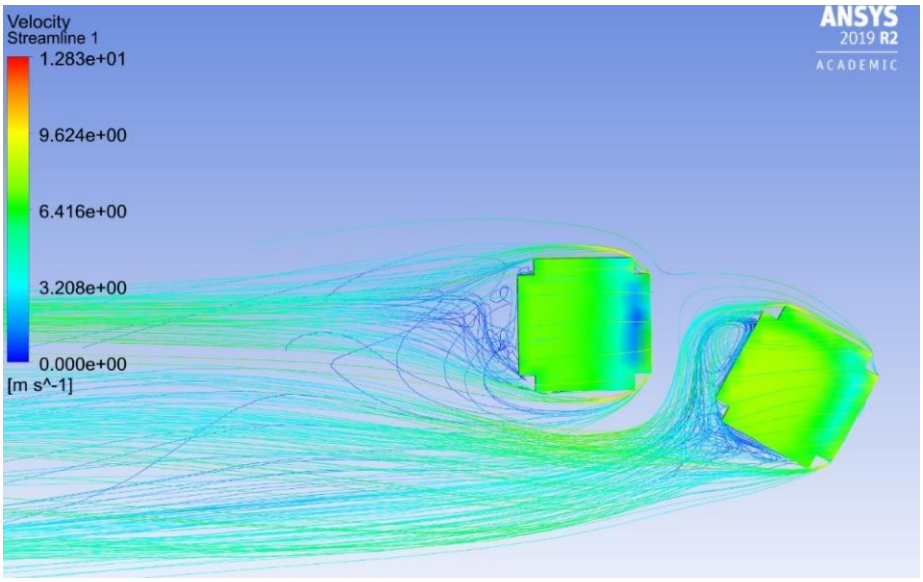

Figure 4.64 Velocity streamlines for PM for 60-degree IM 400 at HB

Chapter 5 CONCLUSION

5.1 Corner Study

In this study, the prediction of along wind components with numerical simulations has shown great accuracy. The findings of this study have led to comprehensive understanding of the aerodynamic and response characteristics of super-tall buildings with various cross-sections. It has been observed that the computational fluid dynamics simulations in the numerical model agree with the experimental results. The results are in better agreement on the front face and across wind responses but show a slight discrepancy in lift forces. Some modifications in the fluid domain and meshing have to be performed in more complex models to generate more convergent results. The k-ε turbulence model has shown great performance in numerical simulations. This study suggests that numerical simulations can be reliable for more complex wind simulations. This evaluation suggests the suitability of low-dimensional steady computational fluid dynamics modeling for performance assessment. The case study for corner modifications suggests the following

- Minor modifications like corner cutting may lead to reductions in drag force and moment by 25% and 20% respectively.

- Corner modification showed better performance upto 12-15% modifications in section. More than 22% reduction leads to aerodynamic instability of the structure.

- Streamline study and pressure field of the models show suction near the corner cut the walls which may be responsible for drag force reductions.

- The introduction of corner cutting (chamfer and fillet) in building plans can be effective in aerodynamic mitigation but requires a complete understanding of the building aerodynamics and wind responses.

5.2 Interference Study

Interference effects on corner configured high rise building models have been investigated for three blockage conditions in this study. The efficacy of interference model orientations and height ratio has been examined in detail. Several findings have been enlisted as follows.

- The maximum value of the interference factor was achieved equal to unity. The shielding effects were prominent for all three cases as the spacing between the models was kept as low as 0.2H.

- The interference factor showed good results in along wind response study but for across wind response, other parameters have to be trusted. The shielding effect was prominent throughout all the cases but 24-27% increment in negative C_p on some faces inclined to this conclusion. This suggests corner cut models may be responsible for such across wind response.

- In all three blockage configurations, the 60-degree orientation of IM interfered the most with PM, thus producing the strongest wind responses.

- For interfering model heights less than H/3 interference effect was negligible which justifies the codal provisions.

- Kinetic energy fluctuations and force spectra suggested that some orientations of IM which produced the least stable wind response can be used for future parametric studies.

- Corner cut configured building models provide a good option to curb interference effect as suction developed at corner cuts may have reduced drag forces and flow separation.

APPENDICES

Appendix 1

```
! $List = getValue("DATA READER","Timestep List"); #this looks for all trn.files

! print "$List \n"; #shows the result of the search

! @Wert = split(/,/,$List); #makes it accessible for further tasks

! $lastFrame=$List[$#timestepList]; # very nice, this gives you the number of the last frame, nice for animations

! foreach $List(@Wert){ #the MAINTASK, do the line and graph and export for every trn.file, see below

> load timestep = $List #load the timestep

! print "calculating for TIMESTEP $List \n";

! ($time, $timeunits) = evaluate("Time");

! }
```

Appendix 2

Table A 2.1 Pressure coefficient on polyline for 100 mm IM in NB configuration

Perimeter	0°	15°	30°	45°	60°	75°
0.00	-0.32	-0.32	-0.17	-0.16	-0.18	-0.32
1.00	-0.33	-0.32	-0.18	-0.17	-0.17	-0.31
2.00	-0.39	-0.33	-0.18	-0.17	-0.03	-0.32
3.00	-0.39	-0.33	-0.40	-0.38	-0.08	-0.32
4.00	-0.34	-0.33	0.52	0.51	-1.18	-0.32
5.00	-0.27	-0.35	0.53	0.52	-1.11	-0.34
6.00	-0.26	-0.35	0.62	0.60	-0.69	-0.34
7.00	-0.26	-0.41	0.63	0.61	-0.47	-0.40
8.00	-0.24	-0.44	0.66	0.63	-0.45	-0.43
9.00	-0.23	-0.47	0.66	0.64	-0.41	-0.46
10.00	-0.23	-0.69	0.67	0.65	-0.35	-0.67
11.00	-0.23	-1.10	0.67	0.65	-0.35	-1.07
12.00	-0.23	-1.17	0.67	0.65	-0.33	-1.15
13.00	-0.22	-0.09	0.67	0.65	-0.33	-0.08
14.00	-0.22	-0.04	0.64	0.62	-0.33	-0.03
15.00	-0.22	-0.14	0.61	0.60	-0.32	-0.15
16.00	-0.23	-0.15	-0.11	0.06	-0.33	-0.16
17.00	-0.23	-0.16	-0.15	0.03	-0.40	-0.17
18.00	-0.24	-0.48	-0.17	-0.01	-0.39	-0.38
19.00	-0.27	0.45	0.00	-0.55	-0.34	0.51
20.00	-0.27	0.54	0.04	-0.11	-0.27	0.52
21.00	-0.32	0.63	-0.32	-0.08	-0.26	0.61
22.00	-0.32	0.63	-0.38	-0.07	-0.26	0.62
23.00	-0.33	0.66	-0.57	-0.37	-0.24	0.64
24.00	-0.35	0.66	-1.12	-0.41	-0.23	0.64
25.00	-0.34	0.67	-1.06	-0.43	-0.23	0.65
26.00	-0.34	0.67	-0.74	-1.06	-0.23	0.65
27.00	-0.34	0.67	-0.57	-0.94	-0.22	0.65
28.00	-0.30	0.67	-0.51	-0.66	-0.22	0.65
29.00	-0.31	0.64	-0.40	-0.49	-0.22	0.61
30.00	-0.33	0.62	-0.39	-0.47	-0.23	0.59
31.00	-0.33	-0.06	-0.35	-0.37	-0.23	0.02
32.00	-0.35	-0.10	-0.33	-0.37	-0.24	-0.01
33.00	-0.39	-0.12	-0.33	-0.32	-0.25	-0.06
34.00	-0.40	-0.16	-0.31	-0.32	-0.27	-0.51
35.00	-0.51	-0.14	-0.30	-0.32	-0.28	-0.26
36.00	-0.57	-0.11	-0.34	-0.30	-0.33	-0.24

Table A 2.1 (continued)

37.00	-0.74	0.21	-0.35	-0.34	-0.33	-0.22
38.00	-1.05	-0.38	-0.35	-0.34	-0.34	-0.04
39.00	-1.12	-0.45	-0.35	-0.34	-0.36	-0.39
40.00	-0.57	-1.21	-0.33	-0.34	-0.36	-0.44
41.00	-0.38	-1.22	-0.32	-0.32	-0.36	-1.14
42.00	-0.32	-1.20	-0.32	-0.32	-0.36	-1.15
43.00	0.03	-0.72	-0.27	-0.27	-0.31	-1.13
44.00	-0.01	-0.54	-0.27	-0.27	-0.31	-0.65
45.00	-0.17	-0.49	-0.24	-0.27	-0.32	-0.48
46.00	-0.15	-0.38	-0.24	-0.24	-0.32	-0.43
47.00	-0.11	-0.38	-0.23	-0.24	-0.33	-0.35
48.00	0.61	-0.34	-0.23	-0.22	-0.35	-0.35
49.00	0.64	-0.33	-0.22	-0.22	-0.36	-0.33
50.00	0.67	-0.33	-0.22	-0.22	-0.44	-0.32
51.00	0.67	-0.31	-0.22	-0.22	-0.49	-0.32
52.00	0.67	-0.30	-0.23	-0.22	-0.67	-0.30
53.00	0.67	-0.34	-0.23	-0.22	-1.18	-0.30
54.00	0.66	-0.35	-0.23	-0.22	-1.20	-0.34
55.00	0.66	-0.35	-0.24	-0.22	-1.19	-0.35
56.00	0.63	-0.35	-0.26	-0.23	-0.46	-0.35
57.00	0.62	-0.33	-0.26	-0.25	-0.40	-0.34
58.00	0.53	-0.32	-0.27	-0.25	-0.02	-0.32
59.00	0.52	-0.32	-0.34	-0.26	-0.22	-0.32
60.00	-0.39	-0.27	-0.39	-0.33	-0.25	-0.32
61.00	-0.18	-0.27	-0.40	-0.38	-0.30	-0.27
62.00	-0.18	-0.24	-0.33	-0.38	-0.56	-0.26
63.00	-0.17	-0.23	-0.32	-0.32	-0.08	-0.24
64.00	-0.03	-0.23	-0.33	-0.31	0.01	-0.23
65.00	-0.08	-0.23	-0.33	-0.32	0.05	-0.22
66.00	-1.19	-0.22	-0.33	-0.32	0.62	-0.22
67.00	-1.11	-0.22	-0.35	-0.32	0.63	-0.22
68.00	-0.69	-0.22	-0.35	-0.34	0.67	-0.22
69.00	-0.47	-0.22	-0.41	-0.34	0.67	-0.22
70.00	-0.45	-0.23	-0.45	-0.40	0.67	-0.22
71.00	-0.41	-0.23	-0.47	-0.44	0.67	-0.22
72.00	-0.35	-0.24	-0.69	-0.46	0.66	-0.23
73.00	-0.35	-0.26	-1.11	-0.67	0.65	-0.23
74.00	-0.33	-0.26	-1.19	-1.08	0.63	-0.25
75.00	-0.33	-0.27	-0.08	-1.16	0.54	-0.25
76.00	-0.33	-0.34	-0.03	-0.08	0.54	-0.26

Table A 2.2 Pressure coefficient on polyline for 200 mm IM in NB configuration

Perimeter	0°	15°	30°	45°	60°	75°
0	-0.33	-0.35	-0.2	-0.16	-0.19	-0.19
1	-0.33	-0.34	-0.2	-0.56	-0.18	-0.2
2	-0.34	-0.34	-0.19	0.44	-0.03	-0.2
3	-0.34	-0.41	-0.04	0.51	-0.09	-0.35
4	-0.34	-0.41	-0.09	0.62	-1.16	0.43
5	-0.36	-0.36	-1.22	0.63	-1.08	0.54
6	-0.36	-0.28	-1.14	0.66	-0.67	0.54
7	-0.43	-0.27	-0.71	0.66	-0.46	0.63
8	-0.46	-0.27	-0.49	0.68	-0.44	0.65
9	-0.49	-0.25	-0.46	0.68	-0.41	0.67
10	-0.72	-0.24	-0.43	0.68	-0.34	0.67
11	-1.14	-0.24	-0.36	0.68	-0.34	0.68
12	-1.22	-0.24	-0.36	0.61	-0.32	0.68
13	-0.09	-0.24	-0.34	0.61	-0.32	0.69
14	-0.04	-0.23	-0.34	0.61	-0.32	0.68
15	-0.19	-0.23	-0.34	-0.08	-0.31	0.64
16	-0.2	-0.23	-0.33	-0.31	-0.31	0.61
17	-0.2	-0.24	-0.33	-0.31	-0.38	-0.14
18	-0.35	-0.25	-0.4	-0.29	-0.38	-0.17
19	0.43	-0.26	-0.4	-0.21	-0.33	-0.19
20	0.54	-0.28	-0.35	-0.26	-0.26	-0.15
21	0.54	-0.29	-0.27	-0.47	-0.25	-0.13
22	0.64	-0.34	-0.27	-1.12	-0.25	-0.12
23	0.65	-0.34	-0.26	-1.05	-0.23	-0.19
24	0.67	-0.35	-0.24	-0.74	-0.22	-0.23
25	0.68	-0.37	-0.23	-0.56	-0.22	-1.24
26	0.69	-0.37	-0.23	-0.51	-0.22	-1.25
27	0.69	-0.37	-0.23	-0.39	-0.22	-1.23
28	0.69	-0.37	-0.23	-0.39	-0.22	-0.74
29	0.69	-0.32	-0.23	-0.35	-0.22	-0.55
30	0.64	-0.32	-0.23	-0.34	-0.22	-0.5
31	0.62	-0.34	-0.23	-0.33	-0.22	-0.39
32	-0.14	-0.34	-0.23	-0.31	-0.23	-0.38
33	-0.17	-0.36	-0.24	-0.31	-0.24	-0.35
34	-0.19	-0.39	-0.25	-0.35	-0.26	-0.33
35	-0.15	-0.39	-0.28	-0.35	-0.26	-0.33
36	-0.13	-0.5	-0.28	-0.35	-0.31	-0.31
37	-0.11	-0.56	-0.33	-0.35	-0.31	-0.31

Table A 2.2 (continued)

38	-0.19	-0.75	-0.33	-0.33	-0.31	-0.36
39	-0.23	-1.22	-0.34	-0.33	-0.33	-0.36
40	-1.24	-1.24	-0.36	-0.33	-0.33	-0.36
41	-1.25	-1.23	-0.36	-0.28	-0.33	-0.36
42	-1.23	-0.25	-0.36	-0.27	-0.32	-0.34
43	-0.74	-0.21	-0.35	-0.25	-0.29	-0.33
44	-0.55	-0.07	-0.31	-0.24	-0.3	-0.33
45	-0.5	-0.08	-0.31	-0.23	-0.32	-0.28
46	-0.38	-0.1	-0.33	-0.23	-0.32	-0.28
47	-0.38	-0.63	-0.33	-0.23	-0.34	-0.25
48	-0.35	-0.23	-0.35	-0.23	-0.37	-0.25
49	-0.33	-0.2	-0.38	-0.23	-0.38	-0.24
50	-0.33	0.56	-0.39	-0.23	-0.48	-0.23
51	-0.31	0.59	-0.5	-0.23	-0.54	-0.23
52	-0.31	0.62	-0.55	-0.24	-0.7	-0.23
53	-0.35	0.7	-0.74	-0.24	-0.99	-0.23
54	-0.36	0.71	-1.22	-0.26	-1.06	-0.23
55	-0.36	0.7	-1.25	-0.27	-0.53	-0.23
56	-0.36	0.69	-1.24	-0.27	-0.34	-0.23
57	-0.34	0.69	-0.23	-0.35	-0.29	-0.24
58	-0.33	0.68	-0.19	-0.4	0.01	-0.26
59	-0.33	0.68	-0.1	-0.4	-0.02	-0.27
60	-0.28	0.66	-0.12	-0.33	-0.12	-0.27
61	-0.28	0.66	-0.14	-0.33	-0.1	-0.35
62	-0.25	0.55	-0.19	-0.34	-0.07	-0.4
63	-0.24	0.55	-0.17	-0.34	0.59	-0.4
64	-0.23	-0.43	-0.13	-0.34	0.6	-0.33
65	-0.23	-0.2	0.61	-0.36	0.65	-0.33
66	-0.23	-0.2	0.64	-0.36	0.64	-0.34
67	-0.23	-0.19	0.69	-0.43	0.64	-0.34
68	-0.23	-0.04	0.69	-0.46	0.64	-0.34
69	-0.23	-0.09	0.69	-0.48	0.63	-0.36
70	-0.23	-1.26	0.69	-0.71	0.63	-0.36
71	-0.23	-1.18	0.67	-1.13	0.6	-0.43
72	-0.24	-0.74	0.67	-1.21	0.6	-0.46
73	-0.26	-0.5	0.65	-0.11	0.51	-0.49
74	-0.27	-0.48	0.63	-0.05	0.5	-0.72
75	-0.27	-0.44	0.54	-0.15	-0.4	-1.14
76	-0.35	-0.37	0.54	-0.16	-0.19	-1.22

Table A 2.3 Pressure coefficient on polyline for 300 mm IM in NB configuration

Perimeter	0°	15°	30°	45°	60°	75°
0	-0.32	-0.3	-0.2	-0.21	-0.2	-0.22
1	-0.33	-0.31	-0.2	-0.21	-0.19	-0.22
2	-0.38	-0.31	-0.04	-0.44	-0.04	-0.45
3	-0.38	-0.32	-0.1	0.51	-0.1	0.52
4	-0.34	-0.34	-1.16	0.52	-1.17	0.54
5	-0.26	-0.34	-1.09	0.62	-1.09	0.63
6	-0.26	-0.4	-0.68	0.62	-0.68	0.64
7	-0.26	-0.44	-0.47	0.65	-0.47	0.67
8	-0.23	-0.46	-0.44	0.66	-0.44	0.67
9	-0.23	-0.67	-0.41	0.67	-0.41	0.69
10	-0.23	-1.07	-0.35	0.67	-0.35	0.69
11	-0.22	-1.15	-0.34	0.67	-0.34	0.69
12	-0.22	-0.09	-0.32	0.67	-0.32	0.7
13	-0.22	-0.04	-0.32	0.64	-0.32	0.66
14	-0.23	-0.19	-0.32	0.62	-0.32	0.63
15	-0.23	-0.2	-0.31	-0.09	-0.31	-0.11
16	-0.23	-0.2	-0.31	-0.13	-0.31	-0.14
17	-0.24	-0.41	-0.37	-0.15	-0.37	-0.17
18	-0.24	0.48	-0.37	0.01	-0.37	-0.13
19	-0.27	0.49	-0.32	0.05	-0.32	-0.11
20	-0.27	0.59	-0.25	-0.17	-0.25	-0.09
21	-0.32	0.59	-0.25	-0.22	-0.25	-0.34
22	-0.32	0.62	-0.24	-1.18	-0.25	-0.38
23	-0.32	0.62	-0.22	-1.19	-0.23	-0.58
24	-0.34	0.64	-0.22	-1.16	-0.22	-1.15
25	-0.34	0.64	-0.22	-0.74	-0.22	-1.08
26	-0.34	0.64	-0.21	-0.56	-0.22	-0.74
27	-0.34	0.64	-0.21	-0.51	-0.22	-0.56
28	-0.3	0.61	-0.21	-0.39	-0.22	-0.51
29	-0.31	0.6	-0.21	-0.38	-0.22	-0.4
30	-0.33	-0.17	-0.22	-0.34	-0.22	-0.39
31	-0.33	-0.2	-0.22	-0.32	-0.22	-0.35
32	-0.35	-0.2	-0.22	-0.32	-0.23	-0.34
33	-0.38	-0.19	-0.23	-0.3	-0.23	-0.34
34	-0.39	-0.05	-0.25	-0.3	-0.26	-0.31
35	-0.5	-0.05	-0.25	-0.33	-0.26	-0.31
36	-0.55	-0.2	-0.3	-0.34	-0.3	-0.34
37	-0.72	-1.17	-0.3	-0.34	-0.3	-0.35

Table A 2.3 (continued)

38	-1.05	-0.72	-0.31	-0.33	-0.31	-0.35
39	-1.12	-0.67	-0.32	-0.32	-0.32	-0.35
40	-0.74	-0.66	-0.32	-0.32	-0.32	-0.33
41	-0.6	-0.43	-0.32	-0.32	-0.32	-0.33
42	-0.55	-0.42	-0.32	-0.31	-0.32	-0.32
43	0.21	-0.34	-0.29	-0.3	-0.29	-0.27
44	-0.13	-0.33	-0.29	-0.27	-0.29	-0.27
45	-0.15	-0.3	-0.32	-0.27	-0.32	-0.25
46	-0.17	-0.3	-0.32	-0.27	-0.32	-0.24
47	-0.14	-0.29	-0.33	-0.24	-0.34	-0.23
48	-0.12	-0.31	-0.37	-0.24	-0.37	-0.23
49	-0.08	-0.31	-0.38	-0.23	-0.38	-0.23
50	0.62	-0.31	-0.48	-0.23	-0.49	-0.23
51	0.64	-0.31	-0.54	-0.22	-0.54	-0.23
52	0.69	-0.29	-0.7	-0.22	-0.7	-0.23
53	0.69	-0.29	-1	-0.22	-1	-0.23
54	0.69	-0.29	-1.06	-0.22	-1.07	-0.23
55	0.69	-0.28	-0.54	-0.23	-0.54	-0.24
56	0.67	-0.25	-0.35	-0.23	-0.36	-0.26
57	0.67	-0.25	-0.3	-0.23	-0.3	-0.26
58	0.65	-0.25	0.05	-0.25	0.05	-0.27
59	0.63	-0.23	0.02	-0.26	0.01	-0.34
60	0.53	-0.22	-0.15	-0.26	-0.15	-0.39
61	0.53	-0.22	-0.13	-0.34	-0.14	-0.39
62	0.42	-0.21	-0.1	-0.38	-0.11	-0.33
63	-0.38	-0.21	0.6	-0.38	0.59	-0.33
64	-0.22	-0.21	0.61	-0.32	0.61	-0.34
65	-0.22	-0.21	0.65	-0.32	0.65	-0.34
66	-0.21	-0.21	0.64	-0.33	0.64	-0.34
67	-0.05	-0.21	0.64	-0.33	0.64	-0.36
68	-0.1	-0.21	0.64	-0.33	0.64	-0.37
69	-1.23	-0.22	0.63	-0.36	0.63	-0.44
70	-1.15	-0.22	0.63	-0.36	0.63	-0.47
71	-0.72	-0.22	0.6	-0.43	0.6	-0.5
72	-0.49	-0.24	0.59	-0.46	0.59	-0.73
73	-0.47	-0.24	0.5	-0.49	0.5	-1.16
74	-0.43	-0.25	0.49	-0.71	0.49	-1.24
75	-0.37	-0.31	-0.42	-1.13	-0.42	-0.1
76	-0.36	-0.36	-0.2	-1.21	-0.2	-0.05

Table A 2.4 Pressure coefficient on polyline for 400 mm IM in NB configuration

Perimeter	0°	15°	30°	45°	60°	75°
0	-0.31	-0.23	-0.25	-0.25	-0.25	-0.26
1	-0.32	-0.24	-0.24	-0.25	-0.25	-0.26
2	-0.38	-0.24	-0.06	-0.24	-0.49	-0.07
3	-0.37	-0.48	-0.11	-0.06	0.49	-0.13
4	-0.33	0.49	-1.19	-0.11	0.5	-1.26
5	-0.26	0.5	-1.11	-1.19	0.59	-0.75
6	-0.25	0.59	-0.68	-1.11	0.6	-0.7
7	-0.25	0.6	-0.47	-0.69	0.63	-0.54
8	-0.23	0.64	-0.45	-0.48	0.64	-0.47
9	-0.22	0.64	-0.41	-0.45	0.65	-0.47
10	-0.22	0.66	-0.35	-0.42	0.66	-0.39
11	-0.22	0.66	-0.35	-0.35	0.66	-0.37
12	-0.22	0.66	-0.32	-0.35	0.66	-0.35
13	-0.22	0.66	-0.32	-0.32	0.63	-0.35
14	-0.22	0.63	-0.32	-0.32	0.61	-0.33
15	-0.22	0.61	-0.31	-0.32	-0.02	-0.36
16	-0.23	-0.02	-0.31	-0.31	-0.05	-0.37
17	-0.23	-0.05	-0.37	-0.31	-0.13	-0.34
18	-0.24	-0.09	-0.36	-0.37	-0.13	-0.33
19	-0.26	-0.06	-0.32	-0.37	-0.1	-0.33
20	-0.26	-0.04	-0.25	-0.32	-0.1	-0.25
21	-0.27	-0.02	-0.24	-0.25	-0.16	-0.25
22	-0.3	-0.16	-0.24	-0.25	-1.15	-0.23
23	-0.31	-0.2	-0.22	-0.24	-1.16	-0.23
24	-0.31	-1.14	-0.22	-0.22	-1.13	-0.23
25	-0.32	-1.15	-0.21	-0.22	-0.71	-0.22
26	-0.34	-1.13	-0.21	-0.22	-0.54	-0.22
27	-0.34	-0.7	-0.21	-0.22	-0.48	-0.22
28	-0.34	-0.52	-0.21	-0.22	-0.37	-0.22
29	-0.33	-0.47	-0.21	-0.22	-0.37	-0.23
30	-0.3	-0.36	-0.22	-0.22	-0.31	-0.23
31	-0.32	-0.36	-0.22	-0.22	-0.31	-0.23
32	-0.32	-0.34	-0.23	-0.22	-0.31	-0.23
33	-0.32	-0.3	-0.23	-0.22	-0.29	-0.26
34	-0.37	-0.3	-0.25	-0.23	-0.32	-0.26
35	-0.38	-0.28	-0.25	-0.26	-0.32	-0.32
36	-0.48	-0.28	-0.26	-0.26	-0.32	-0.32
37	-0.54	-0.3	-0.3	-0.26	-0.32	-0.33

Table A 2.4 (continued)

38	-0.71	-0.32	-0.3	-0.29	-0.31	-0.36
39	-1.19	-0.32	-0.32	-0.3	-0.3	-0.35
40	-1.21	-0.32	-0.31	-0.31	-0.26	-0.35
41	-1.2	-0.3	-0.31	-0.31	-0.26	-0.32
42	-0.43	-0.3	-0.31	-0.33	-0.26	-0.32
43	-0.39	-0.3	-0.28	-0.33	-0.23	-0.33
44	0.25	-0.29	-0.3	-0.33	-0.23	-0.34
45	-0.09	-0.26	-0.3	-0.32	-0.22	-0.34
46	-0.1	-0.25	-0.3	-0.3	-0.22	-0.38
47	-0.13	-0.25	-0.36	-0.3	-0.22	-0.46
48	-0.1	-0.22	-0.37	-0.31	-0.22	-0.47
49	-0.07	-0.22	-0.48	-0.31	-0.22	-0.5
50	-0.04	-0.21	-0.54	-0.32	-0.22	-0.7
51	0.65	-0.21	-0.71	-0.33	-0.22	-0.95
52	0.66	-0.21	-1.12	-0.36	-0.22	-1.18
53	0.7	-0.21	-1.14	-0.42	-0.23	-0.16
54	0.69	-0.21	-1.13	-0.47	-0.24	-0.13
55	0.69	-0.21	-0.15	-0.66	-0.25	-0.09
56	0.69	-0.21	-0.1	-0.77	-0.25	-0.12
57	0.67	-0.21	-0.1	-1.07	-0.32	-0.14
58	0.67	-0.22	-0.13	-0.44	-0.37	-0.15
59	0.64	-0.24	-0.12	-0.41	-0.37	-0.34
60	0.64	-0.24	-0.05	-0.01	-0.31	-0.31
61	0.56	-0.25	-0.01	-0.01	-0.31	0.61
62	0.46	-0.32	0.61	-0.06	-0.32	0.64
63	-0.62	-0.36	0.63	-0.58	-0.32	0.65
64	-0.21	-0.37	0.66	-0.03	-0.32	0.69
65	-0.2	-0.31	0.66	0.03	-0.35	0.69
66	-0.19	-0.3	0.66	0.06	-0.35	0.68
67	-0.04	-0.32	0.65	0.61	-0.41	0.68
68	-0.1	-0.32	0.64	0.63	-0.45	0.67
69	-1.3	-0.32	0.63	0.66	-0.47	0.64
70	-1.21	-0.34	0.6	0.66	-0.68	0.64
71	-0.69	-0.35	0.59	0.66	-1.13	0.62
72	-0.48	-0.41	0.5	0.65	-1.22	0.56
73	-0.46	-0.45	0.49	0.64	-0.1	-0.38
74	-0.42	-0.47	-0.49	0.64	-0.05	-0.43
75	-0.36	-0.68	-0.25	0.6	-0.24	-0.27
76	-0.36	-1.12	-0.2	0.6	-0.2	-0.05

Table A 2.5 Pressure coefficient on polyline for 500 mm IM in NB configuration

Perimeter	0°	15°	30°	45°	60°	75°
0	-0.3	-0.23	-0.33	-0.23	-0.29	-0.66
1	-0.34	-0.25	-0.32	-0.24	-0.29	-0.65
2	-0.34	-0.25	-0.08	-0.82	-0.12	-0.64
3	-0.31	-0.72	-0.06	0.37	-0.1	-0.13
4	-0.31	-0.55	-0.12	0.49	-0.16	-0.19
5	-0.3	0.49	-1.1	0.57	-1.08	-1.09
6	-0.23	0.52	-0.68	0.57	-0.67	-0.66
7	-0.23	0.59	-0.63	0.62	-0.63	-0.64
8	-0.22	0.62	-0.55	0.62	-0.55	-0.61
9	-0.21	0.63	-0.42	0.65	-0.43	-0.46
10	-0.21	0.65	-0.41	0.66	-0.42	-0.37
11	-0.21	0.66	-0.34	0.66	-0.35	-0.37
12	-0.2	0.67	-0.31	0.67	-0.32	-0.37
13	-0.2	0.67	-0.3	0.65	-0.31	-0.32
14	-0.2	0.67	-0.32	0.64	-0.32	-0.32
15	-0.21	0.66	-0.33	-0.13	-0.32	-0.3
16	-0.21	0.6	-0.34	-0.17	-0.33	-0.33
17	-0.21	-0.13	-0.33	-0.09	-0.33	-0.33
18	-0.21	-0.17	-0.3	-0.07	-0.3	-0.33
19	-0.23	-0.29	-0.3	-0.05	-0.29	-0.3
20	-0.23	-0.28	-0.24	-0.07	-0.24	-0.29
21	-0.31	0.22	-0.24	-0.19	-0.24	-0.24
22	-0.31	0.2	-0.23	-1.18	-0.23	-0.24
23	-0.31	-1.07	-0.22	-0.67	-0.23	-0.23
24	-0.35	-1.09	-0.22	-0.66	-0.22	-0.22
25	-0.34	-0.95	-0.21	-0.66	-0.22	-0.22
26	-0.29	-0.7	-0.21	-0.42	-0.22	-0.22
27	-0.3	-0.61	-0.21	-0.4	-0.22	-0.22
28	-0.3	-0.47	-0.21	-0.33	-0.22	-0.22
29	-0.32	-0.46	-0.21	-0.31	-0.22	-0.22
30	-0.32	-0.35	-0.21	-0.3	-0.22	-0.22
31	-0.35	-0.34	-0.22	-0.3	-0.23	-0.22
32	-0.36	-0.3	-0.22	-0.29	-0.23	-0.22
33	-0.37	-0.29	-0.22	-0.32	-0.25	-0.23
34	-0.43	-0.28	-0.25	-0.32	-0.26	-0.23
35	-0.56	-0.32	-0.25	-0.32	-0.26	-0.25
36	-0.65	-0.32	-0.32	-0.3	-0.31	-0.25
37	-1.08	-0.32	-0.32	-0.29	-0.31	-0.26

Table A 2.5 (continued)

38	-1.18	-0.3	-0.37	-0.25	-0.31	-0.32
39	-1.16	-0.29	-0.37	-0.25	-0.32	-0.32
40	0.11	-0.29	-0.3	-0.22	-0.33	-0.32
41	0.15	-0.24	-0.3	-0.22	-0.33	-0.35
42	-0.06	-0.24	-0.3	-0.21	-0.32	-0.35
43	-0.08	-0.22	-0.3	-0.21	-0.29	-0.34
44	-0.1	-0.21	-0.3	-0.21	-0.3	-0.3
45	-0.16	-0.21	-0.32	-0.21	-0.31	-0.31
46	-0.14	-0.21	-0.33	-0.21	-0.31	-0.32
47	-0.1	-0.21	-0.4	-0.21	-0.33	-0.32
48	0.63	-0.21	-0.47	-0.22	-0.43	-0.33
49	0.65	-0.21	-0.65	-0.22	-0.43	-0.35
50	0.68	-0.21	-0.84	-0.22	-0.44	-0.42
51	0.68	-0.21	-1.15	-0.23	-0.69	-0.43
52	0.67	-0.22	-0.61	-0.23	-0.78	-0.48
53	0.67	-0.22	-0.55	-0.24	-1.25	-0.63
54	0.64	-0.23	-0.51	-0.3	-1.22	-0.94
55	0.62	-0.23	0.06	-0.36	-0.51	-1.06
56	0.61	-0.28	-0.11	-0.36	0.22	-1.11
57	0.57	-0.29	-0.13	-0.29	0.26	-0.63
58	0.57	-0.33	-0.45	-0.29	-0.06	-0.59
59	0.52	-0.33	-0.4	-0.3	-0.09	-0.52
60	-0.81	-0.3	0.02	-0.3	-0.11	0.12
61	-0.23	-0.29	0.59	-0.3	-0.15	-0.13
62	-0.22	-0.3	0.63	-0.33	-0.12	-0.15
63	-0.21	-0.33	0.7	-0.33	-0.1	-0.16
64	-0.09	-0.39	0.7	-0.39	0.66	-0.19
65	-0.15	-0.4	0.67	-0.42	0.66	-0.5
66	-1.08	-0.5	0.67	-0.44	0.67	0.1
67	-0.68	-0.55	0.67	-0.62	0.68	0.18
68	-0.63	-0.56	0.63	-1.01	0.68	0.21
69	-0.5	-0.89	0.6	-1.08	0.66	0.65
70	-0.44	-0.93	0.58	-0.09	0.66	0.65
71	-0.43	-0.3	0.56	-0.04	0.65	0.69
72	-0.36	-0.25	0.5	-0.22	0.63	0.68
73	-0.34	-0.45	-0.57	0.64	0.61	0.68
74	-0.32	-0.47	-0.65	0.64	0.55	0.68
75	-0.31	-0.68	-0.25	0.6	0.55	0.66
76	-0.36	-1.12	-0.2	0.6	0.5	0.62

Table A 2.6 Pressure coefficient on polyline for 600 mm IM in NB configuration

Perimeter	0°	15°	30°	45°	60°	75°
0	-0.34	-0.46	-0.41	-0.4	-0.4	-0.41
1	-0.27	-0.47	-0.43	-0.42	-0.42	-0.43
2	-0.29	-0.75	-0.44	-0.43	-0.43	-0.43
3	-0.29	-0.62	-0.82	-1.06	-1.13	-0.88
4	-0.31	0.46	-0.75	0.28	0.34	0.36
5	-0.34	0.52	0.42	0.3	0.41	0.45
6	-0.41	0.57	0.49	0.45	0.41	0.55
7	-0.42	0.63	0.52	0.46	0.53	0.57
8	-0.47	0.64	0.55	0.56	0.58	0.6
9	-0.59	0.64	0.61	0.56	0.61	0.63
10	-0.62	0.66	0.64	0.62	0.63	0.64
11	-0.93	0.66	0.68	0.63	0.65	0.66
12	-0.19	0.63	0.67	0.63	0.67	0.66
13	-0.14	-0.04	0.66	0.66	0.67	0.63
14	-0.43	-0.1	0.16	0.64	0.67	0.58
15	-0.45	-0.04	0.14	0.64	0.67	0.54
16	-0.46	-0.04	0.09	0.04	0.67	-0.21
17	-0.94	-0.03	-0.39	0.01	0.01	-0.23
18	-0.7	0.05	-0.15	-0.02	-0.03	-0.13
19	0.49	-0.03	-0.12	0	-0.34	-0.11
20	0.52	-1.11	-0.1	0.02	-0.33	0.07
21	0.64	-0.98	0.06	0.03	0.09	0.29
22	0.67	-0.58	-0.41	-0.13	0.07	0.3
23	0.69	-0.52	-0.47	-0.17	-0.08	-0.23
24	0.7	-0.38	-0.53	-1.12	-1.23	-0.63
25	0.72	-0.34	-1.15	-1.13	-0.91	-0.68
26	0.72	-0.3	-1.06	-1.11	-0.73	-1.05
27	0.7	-0.3	-0.69	-0.68	-0.53	-0.75
28	0.68	-0.29	-0.57	-0.51	-0.44	-0.61
29	0.16	-0.28	-0.44	-0.45	-0.35	-0.38
30	0.13	-0.27	-0.38	-0.35	-0.33	-0.37
31	0.09	-0.3	-0.35	-0.34	-0.3	-0.35
32	-0.35	-0.3	-0.33	-0.29	-0.3	-0.29
33	-0.32	-0.3	-0.32	-0.29	-0.3	-0.28
34	0.25	-0.28	-0.31	-0.29	-0.28	-0.28
35	0.32	-0.28	-0.3	-0.26	-0.28	-0.27
36	-0.56	-0.28	-0.29	-0.29	-0.31	-0.27
37	-0.6	-0.23	-0.28	-0.29	-0.31	-0.3

Table A 2.6 (continued)

38	-0.63	-0.22	-0.33	-0.29	-0.3	-0.3
39	-1.19	-0.2	-0.34	-0.3	-0.29	-0.3
40	-0.92	-0.2	-0.34	-0.28	-0.29	-0.28
41	-0.7	-0.2	-0.3	-0.28	-0.29	-0.28
42	-0.5	-0.2	-0.3	-0.28	-0.25	-0.28
43	-0.46	-0.2	-0.29	-0.23	-0.25	-0.24
44	-0.45	-0.2	-0.23	-0.23	-0.25	-0.23
45	-0.37	-0.2	-0.23	-0.21	-0.22	-0.23
46	-0.34	-0.2	-0.21	-0.21	-0.22	-0.21
47	-0.34	-0.2	-0.21	-0.2	-0.21	-0.21
48	-0.33	-0.21	-0.2	-0.2	-0.21	-0.2
49	-0.32	-0.21	-0.2	-0.2	-0.21	-0.2
50	-0.32	-0.22	-0.2	-0.2	-0.21	-0.2
51	-0.35	-0.21	-0.2	-0.2	-0.21	-0.2
52	-0.36	-0.21	-0.2	-0.21	-0.21	-0.2
53	-0.36	-0.26	-0.2	-0.21	-0.22	-0.2
54	-0.32	-0.27	-0.2	-0.21	-0.22	-0.2
55	-0.32	-0.27	-0.21	-0.21	-0.22	-0.21
56	-0.25	-0.32	-0.21	-0.21	-0.23	-0.21
57	-0.25	-0.31	-0.22	-0.21	-0.22	-0.22
58	-0.23	-0.23	-0.21	-0.21	-0.22	-0.21
59	-0.22	-0.24	-0.21	-0.26	-0.27	-0.21
60	-0.22	-0.24	-0.27	-0.32	-0.27	-0.25
61	-0.22	-0.25	-0.27	-0.32	-0.29	-0.26
62	-0.22	-0.28	-0.29	-0.24	-0.29	-0.26
63	-0.22	-0.33	-0.3	-0.24	-0.29	-0.29
64	-0.22	-0.33	-0.29	-0.24	-0.28	-0.28
65	-0.23	-0.45	-0.28	-0.24	-0.26	-0.24
66	-0.23	-0.46	-0.24	-0.24	-0.27	-0.26
67	-0.23	-0.7	-0.24	-0.27	-0.3	-0.28
68	-0.24	-0.73	-0.26	-0.27	-0.36	-0.34
69	-0.23	-0.28	-0.32	-0.32	-0.37	-0.35
70	-0.22	-0.22	-0.33	-0.35	-0.46	-0.47
71	-0.3	-0.43	-0.42	-0.36	-0.52	-0.47
72	-0.3	-0.25	-0.48	-0.49	-0.55	-0.51
73	-0.31	-0.45	-0.5	-0.73	-0.82	-0.71
74	-0.35	-0.47	-0.79	-0.78	-0.2	-0.74
75	-0.31	-0.68	-0.11	-0.11	-0.17	-0.27
76	-0.36	-1.12	-0.07	-0.07	0.5	-0.22

Table A 2.7 Pressure coefficient on polyline for 100 mm IM in HB configuration

Perimeter	0°	15°	30°	45°	60°	75°
0	-0.31	-0.31	-0.33	-0.31	-0.31	-0.32
1	-0.31	-0.31	-0.33	-0.31	-0.31	-0.32
2	-0.31	-0.31	-0.33	-0.35	-0.31	-0.32
3	-0.34	-0.34	-0.36	-0.37	-0.34	-0.35
4	-0.34	-0.34	-0.36	-0.33	-0.34	-0.35
5	-0.35	-0.35	-0.37	-0.33	-0.35	-0.36
6	-0.42	-0.43	-0.46	-0.24	-0.43	-0.44
7	-0.62	-0.63	-0.67	-0.24	-0.62	-0.65
8	-0.65	-0.66	-0.7	-0.23	-0.65	-0.68
9	-1.05	-1.07	-1.12	-0.22	-1.05	-1.1
10	-1.1	-1.12	-1.18	-0.21	-1.1	-1.16
11	-1.09	-1.11	-1.16	-0.21	-1.09	-1.14
12	0	0.03	0	-0.21	0	0.03
13	-0.02	0.01	-0.02	-0.21	-0.03	0.01
14	-0.21	-0.23	-0.23	-0.2	-0.21	-0.24
15	-0.53	-0.34	-0.51	-0.2	-0.53	-0.35
16	-0.51	-0.32	-0.5	-0.2	-0.52	-0.33
17	0.47	-0.23	-0.02	-0.21	0.47	-0.23
18	0.5	0.53	0.53	-0.22	0.5	0.54
19	0.61	0.59	0.57	-0.22	0.61	0.61
20	0.61	0.61	0.59	-0.25	0.61	0.63
21	0.61	0.62	0.65	-0.25	0.61	0.63
22	0.62	0.63	0.66	-0.26	0.62	0.65
23	0.62	0.64	0.67	-0.29	0.62	0.66
24	0.63	0.63	0.68	-0.3	0.63	0.65
25	0.63	0.63	0.68	-0.31	0.63	0.65
26	0.64	0.63	0.68	-0.31	0.64	0.65
27	0.62	0.58	0.66	-0.32	0.62	0.6
28	0.07	0.56	0.66	-0.34	0.07	0.58
29	0.02	-0.03	-0.04	-0.34	0.02	-0.03
30	-0.01	-0.06	-0.09	-0.29	0	-0.06
31	-0.04	-0.1	-0.33	-0.28	-0.04	-0.1
32	-0.25	-0.55	-0.33	-0.28	-0.25	-0.57
33	-0.22	-0.3	-0.28	-0.29	-0.23	-0.3
34	-0.21	-0.28	0.35	-0.29	-0.21	-0.28
35	0.18	-0.26	-0.68	-0.29	0.18	-0.26
36	-0.67	-0.07	-0.74	-0.32	-0.67	-0.06
37	-0.71	-0.63	-0.78	-0.33	-0.71	-0.65

Table A 2.7 (continued)

38	-0.74	-0.69	-0.97	-0.37	-0.74	-0.7
39	-0.9	-0.71	-0.92	-0.46	-0.9	-0.74
40	-0.86	-0.84	-0.59	-0.51	-0.86	-0.88
41	-0.54	-0.81	-0.58	-0.79	-0.54	-0.85
42	-0.52	-0.5	-0.41	-0.8	-0.53	-0.52
43	-0.37	-0.49	-0.4	-0.77	-0.38	-0.5
44	-0.37	-0.36	-0.34	-0.68	-0.37	-0.37
45	-0.31	-0.36	-0.34	-0.66	-0.31	-0.36
46	-0.31	-0.31	-0.31	-0.61	-0.31	-0.32
47	-0.29	-0.31	-0.31	0.1	-0.29	-0.32
48	-0.29	-0.29	-0.31	-0.24	-0.29	-0.3
49	-0.29	-0.29	-0.31	-0.26	-0.29	-0.3
50	-0.29	-0.29	-0.38	-0.28	-0.29	-0.3
51	-0.36	-0.29	-0.37	-0.1	-0.36	-0.31
52	-0.36	-0.36	-0.35	-0.06	-0.35	-0.38
53	-0.34	-0.36	-0.33	-0.01	-0.33	-0.38
54	-0.32	-0.33	-0.33	0.55	-0.32	-0.35
55	-0.32	-0.32	-0.33	0.6	-0.32	-0.33
56	-0.31	-0.32	-0.32	0.62	-0.32	-0.33
57	-0.26	-0.32	-0.28	0.62	-0.26	-0.27
58	-0.25	-0.26	-0.28	0.63	-0.26	-0.27
59	-0.22	-0.26	-0.27	0.63	-0.22	-0.27
60	-0.22	-0.26	-0.24	0.62	-0.22	-0.23
61	-0.21	-0.22	-0.23	0.61	-0.2	-0.23
62	-0.2	-0.22	-0.23	0.61	-0.2	-0.22
63	-0.2	-0.21	-0.22	0.55	-0.2	-0.21
64	-0.2	-0.2	-0.22	0.54	-0.2	-0.21
65	-0.2	-0.2	-0.22	0.5	-0.21	-0.21
66	-0.21	-0.2	-0.22	0.02	-0.21	-0.21
67	-0.21	-0.2	-0.22	-0.47	-0.22	-0.21
68	-0.22	-0.2	-0.22	-0.48	-0.22	-0.21
69	-0.22	-0.21	-0.23	-0.22	-0.24	-0.22
70	-0.23	-0.22	-0.23	-0.02	-0.24	-0.23
71	-0.24	-0.22	-0.23	0	-0.24	-0.23
72	-0.24	-0.23	-0.25	-1.08	-0.33	-0.25
73	-0.32	-0.23	-0.25	-1.1	-0.34	-0.25
74	-0.32	-0.23	-0.26	-1.05	-0.37	-0.33
75	-0.33	-0.24	-0.35	-0.65	-0.35	-0.33
76	-0.36	-0.33	-0.35	-0.62	0.5	-0.34

Table A 2.8 Pressure coefficient on polyline for 200 mm IM in HB configuration

Perimeter	0°	15°	30°	45°	60°	75°
0	-0.31	-0.31	-0.34	-0.34	-0.31	-0.29
1	-0.31	-0.31	-0.34	-0.34	-0.31	-0.3
2	-0.32	-0.34	-0.38	-0.34	-0.32	-0.3
3	-0.34	-0.35	-0.4	-0.37	-0.34	-0.33
4	-0.34	-0.35	-0.39	-0.37	-0.35	-0.33
5	-0.35	-0.31	-0.34	-0.38	-0.35	-0.41
6	-0.43	-0.3	-0.33	-0.47	-0.44	-0.42
7	-0.63	-0.24	-0.26	-0.68	-0.64	-0.47
8	-0.66	-0.24	-0.26	-0.71	-0.67	-0.67
9	-1.06	-0.22	-0.24	-1.13	-1.08	-1.09
10	-1.11	-0.22	-0.24	-1.18	-1.13	-1.14
11	-1.1	-0.21	-0.23	-1.17	-1.12	-0.38
12	0	-0.2	-0.23	-0.16	0.02	-0.01
13	-0.03	-0.2	-0.22	-0.15	0	-0.02
14	-0.23	-0.2	-0.22	-0.31	-0.24	-0.22
15	-0.5	-0.2	-0.22	-0.36	-0.35	-0.32
16	-0.48	-0.2	-0.22	-0.42	-0.34	-0.32
17	0	-0.21	-0.23	-0.38	-0.24	-0.27
18	0.5	-0.22	-0.23	0.08	0.53	0.52
19	0.54	-0.22	-0.25	0.55	0.59	0.58
20	0.56	-0.26	-0.25	0.6	0.61	0.6
21	0.61	-0.26	-0.25	0.61	0.61	0.62
22	0.61	-0.26	-0.28	0.67	0.63	0.64
23	0.63	-0.31	-0.28	0.67	0.64	0.63
24	0.63	-0.32	-0.33	0.69	0.63	0.64
25	0.63	-0.32	-0.34	0.69	0.63	0.64
26	0.63	-0.35	-0.34	0.69	0.63	0.64
27	0.63	-0.35	-0.35	0.69	0.58	0.64
28	0.6	-0.29	-0.37	0.69	0.57	0.65
29	0.58	-0.29	-0.39	0.64	-0.01	0.61
30	0.04	-0.29	-0.39	0.6	-0.04	0.59
31	0	-0.29	-0.32	-0.03	-0.07	-0.19
32	-0.03	-0.31	-0.32	-0.07	-0.53	-0.23
33	-0.26	-0.31	-0.32	-0.11	-0.28	-0.26
34	-0.45	-0.35	-0.32	-0.57	-0.26	0.05
35	-0.34	-0.36	-0.35	-0.33	-0.24	0.09
36	-0.21	-0.49	-0.35	-0.3	-0.05	0.11
37	-0.19	-0.51	-0.35	-0.07	-0.62	-0.34

Table A 2.8 (continued)

38	-0.16	-0.83	-0.41	-0.06	-0.68	-0.4
39	0.08	-0.86	-0.55	-0.09	-0.7	-0.43
40	-0.5	-0.7	-0.57	-0.9	-0.83	-1.04
41	-0.54	-0.67	-0.91	-0.93	-0.8	-0.98
42	-0.59	-0.61	-0.95	-0.89	-0.5	-0.84
43	-1	0.03	-0.52	-0.87	-0.49	-0.56
44	-0.91	-0.27	-0.49	-0.53	-0.36	-0.49
45	-0.52	-0.3	-0.44	-0.52	-0.35	-0.38
46	-0.51	-0.32	-0.35	-0.39	-0.31	-0.34
47	-0.36	-0.14	-0.39	-0.38	-0.31	-0.31
48	-0.36	-0.11	-0.38	-0.34	-0.29	-0.3
49	-0.31	-0.08	-0.17	-0.33	-0.29	-0.29
50	-0.31	0.56	-0.13	-0.32	-0.29	-0.29
51	-0.29	0.58	0.58	-0.32	-0.29	-0.31
52	-0.29	0.63	0.62	-0.31	-0.36	-0.36
53	-0.29	0.63	0.69	-0.37	-0.35	-0.36
54	-0.29	0.63	0.7	-0.38	-0.33	-0.32
55	-0.33	0.64	0.7	-0.38	-0.33	-0.31
56	-0.34	0.63	0.7	-0.38	-0.32	-0.31
57	-0.34	0.62	0.69	-0.35	-0.32	-0.25
58	-0.33	0.61	0.68	-0.35	-0.32	-0.25
59	-0.31	0.59	0.68	-0.35	-0.3	-0.22
60	-0.31	0.53	0.62	-0.28	-0.26	-0.22
61	-0.31	-0.23	0.6	-0.28	-0.25	-0.21
62	-0.25	-0.33	0.56	-0.24	-0.25	-0.21
63	-0.25	-0.34	0.08	-0.24	-0.22	-0.21
64	-0.25	-0.24	-0.38	-0.23	-0.22	-0.21
65	-0.22	0	-0.43	-0.22	-0.21	-0.21
66	-0.22	0.02	-0.36	-0.22	-0.2	-0.21
67	-0.21	-1.12	-0.31	-0.22	-0.2	-0.21
68	-0.2	-1.13	-0.15	-0.22	-0.2	-0.22
69	-0.2	-1.08	-0.16	-0.22	-0.2	-0.23
70	-0.2	-0.67	-1.17	-0.22	-0.2	-0.25
71	-0.2	-0.64	-1.18	-0.23	-0.21	-0.25
72	-0.2	-0.43	-1.13	-0.23	-0.22	-0.26
73	-0.21	-0.35	-0.71	-0.23	-0.22	-0.31
74	-0.21	-0.34	-0.68	-0.25	-0.24	-0.31
75	-0.21	-0.34	-0.47	-0.25	-0.24	-0.31
76	-0.22	-0.31	-0.38	-0.26	-0.32	-0.31

Table A 2.9 Pressure coefficient on polyline for 300 mm IM in HB configuration

Perimeter	0°	15°	30°	45°	60°	75°
0	-0.31	-0.31	-0.34	-0.32	-0.33	-0.31
1	-0.31	-0.32	-0.35	-0.32	-0.32	-0.32
2	-0.32	-0.32	-0.35	-0.33	-0.37	-0.32
3	-0.35	-0.35	-0.38	-0.36	-0.37	-0.33
4	-0.35	-0.35	-0.38	-0.36	-0.33	-0.33
5	-0.35	-0.36	-0.39	-0.36	-0.33	-0.33
6	-0.44	-0.44	-0.48	-0.45	-0.33	-0.4
7	-0.64	-0.64	-0.69	-0.66	-0.24	-0.4
8	-0.67	-0.68	-0.73	-0.7	-0.24	-0.4
9	-1.08	-1.08	-1.14	-1.11	-0.22	-0.6
10	-1.13	-1.13	-1.2	-1.16	-0.21	-0.65
11	-1.11	-1.11	-1.19	-1.15	-0.2	-1.12
12	-0.01	-0.02	-0.16	-0.01	-0.2	-1.14
13	-0.03	-0.04	-0.16	-0.03	-0.2	-0.56
14	-0.23	-0.22	-0.32	-0.24	-0.2	-0.02
15	-0.5	-0.61	-0.37	-0.52	-0.2	-0.03
16	-0.49	-0.59	-0.43	-0.51	-0.2	-0.21
17	0.01	0.43	-0.39	0.02	-0.21	-0.32
18	0.5	0.46	0.07	0.52	-0.22	-0.32
19	0.54	0.58	0.56	0.55	-0.25	-0.27
20	0.55	0.59	0.6	0.57	-0.25	0.5
21	0.61	0.63	0.62	0.63	-0.25	0.57
22	0.61	0.63	0.68	0.63	-0.31	0.58
23	0.62	0.64	0.68	0.65	-0.31	0.62
24	0.63	0.64	0.69	0.65	-0.35	0.62
25	0.63	0.65	0.7	0.65	-0.36	0.63
26	0.63	0.65	0.7	0.64	-0.35	0.63
27	0.63	0.64	0.71	0.63	-0.3	0.63
28	0.59	0.59	0.69	0.53	-0.3	0.63
29	0.57	0.58	0.64	0.47	-0.3	0.63
30	-0.03	-0.03	0.6	-0.27	-0.32	0.55
31	-0.07	-0.06	-0.02	-0.34	-0.32	0.55
32	-0.1	-0.09	-0.06	-0.35	-0.32	0.37
33	-0.22	-0.43	-0.13	-0.31	-0.37	-0.36
34	-0.19	-0.56	-0.63	0.14	-0.39	-0.1
35	-0.16	-0.45	-0.2	-0.49	-0.57	-0.1
36	0.26	-0.17	-0.14	-0.54	-0.61	-0.1
37	-0.49	-0.15	-0.11	-0.58	-0.64	-0.11

Table A 2.9 (continued)

38	-0.55	-0.13	-0.46	-1.18	-1.04	-0.15
39	-0.59	-0.34	-0.5	-0.79	-0.17	-1
40	-1.08	-0.37	-0.53	-0.74	-0.15	-0.92
41	-0.98	-0.4	-0.92	-0.48	-0.11	-0.77
42	-0.66	-0.87	-0.88	-0.46	-0.43	-0.53
43	-0.51	-0.84	-0.55	-0.35	-0.46	-0.47
44	-0.47	-0.52	-0.53	-0.35	-0.48	-0.37
45	-0.37	-0.5	-0.39	-0.31	-0.1	-0.32
46	-0.36	-0.36	-0.34	-0.3	-0.06	-0.3
47	-0.31	-0.35	-0.34	-0.29	0.01	-0.29
48	-0.31	-0.31	-0.33	-0.29	0.59	-0.28
49	-0.29	-0.3	-0.31	-0.29	0.64	-0.27
50	-0.28	-0.29	-0.31	-0.29	0.66	-0.27
51	-0.28	-0.29	-0.31	-0.36	0.66	-0.3
52	-0.28	-0.28	-0.31	-0.36	0.67	-0.32
53	-0.3	-0.28	-0.38	-0.34	0.68	-0.31
54	-0.36	-0.35	-0.38	-0.31	0.68	-0.31
55	-0.36	-0.35	-0.36	-0.31	0.66	-0.28
56	-0.31	-0.32	-0.34	-0.26	0.65	-0.29
57	-0.31	-0.31	-0.33	-0.26	-0.14	-0.29
58	-0.24	-0.31	-0.33	-0.26	-0.18	-0.29
59	-0.24	-0.31	-0.32	-0.22	-0.21	-0.24
60	-0.24	-0.25	-0.27	-0.22	-0.21	-0.24
61	-0.21	-0.25	-0.27	-0.21	-0.03	-0.21
62	-0.21	-0.22	-0.25	-0.2	-0.02	-0.21
63	-0.2	-0.21	-0.24	-0.2	-0.14	-0.2
64	-0.19	-0.2	-0.24	-0.2	-1.23	-0.2
65	-0.19	-0.2	-0.23	-0.2	-0.75	-0.19
66	-0.19	-0.2	-0.22	-0.2	-0.7	-0.19
67	-0.2	-0.2	-0.22	-0.21	-0.62	-0.19
68	-0.2	-0.2	-0.22	-0.21	-0.43	-0.19
69	-0.2	-0.2	-0.22	-0.21	-0.42	-0.2
70	-0.21	-0.2	-0.22	-0.23	-0.37	-0.2
71	-0.21	-0.2	-0.22	-0.23	-0.35	-0.21
72	-0.23	-0.21	-0.23	-0.24	-0.34	-0.23
73	-0.23	-0.21	-0.24	-0.34	-0.33	-0.23
74	-0.23	-0.24	-0.24	-0.35	-0.24	-0.23
75	-0.33	-0.24	-0.26	-0.38	-0.24	-0.33
76	-0.34	-0.31	-0.26	-0.37	-0.32	-0.33

Table A 2.10 Pressure coefficient on polyline for 400 mm IM in HB configuration

Perimeter	0°	15°	30°	45°	60°	75°
0	-0.34	-0.33	-0.36	-0.33	-0.33	-0.33
1	-0.34	-0.33	-0.36	-0.34	-0.4	-0.33
2	-0.35	-0.41	-0.36	-0.34	-0.43	-0.4
3	-0.46	-0.42	-0.38	-0.36	-0.37	-0.41
4	-0.37	-0.35	-0.38	-0.36	-0.37	-0.35
5	-0.37	-0.35	-0.39	-0.37	-0.36	-0.35
6	-0.36	-0.34	-0.48	-0.45	-0.24	-0.34
7	-0.25	-0.23	-0.7	-0.67	-0.24	-0.23
8	-0.24	-0.23	-0.73	-0.7	-0.22	-0.23
9	-0.22	-0.21	-1.15	-1.12	-0.21	-0.21
10	-0.21	-0.2	-1.2	-1.17	-0.2	-0.2
11	-0.2	-0.2	-1.19	-1.15	-0.2	-0.2
12	-0.2	-0.19	-0.17	-0.01	-0.19	-0.19
13	-0.2	-0.19	-0.16	-0.03	-0.19	-0.19
14	-0.2	-0.19	-0.29	-0.22	-0.2	-0.19
15	-0.2	-0.19	-0.34	-0.55	-0.2	-0.19
16	-0.2	-0.19	-0.46	-0.54	-0.22	-0.19
17	-0.22	-0.19	-0.42	-0.01	-0.22	-0.19
18	-0.22	-0.2	0.05	0.52	-0.24	-0.2
19	-0.24	-0.2	0.54	0.56	-0.24	-0.2
20	-0.24	-0.23	0.58	0.57	-0.31	-0.23
21	-0.31	-0.23	0.6	0.63	-0.32	-0.23
22	-0.32	-0.24	0.67	0.64	-0.37	-0.23
23	-0.37	-0.28	0.67	0.66	-0.37	-0.31
24	-0.37	-0.28	0.7	0.67	-0.37	-0.32
25	-0.29	-0.28	0.71	0.67	-0.3	-0.36
26	-0.29	-0.28	0.71	0.66	-0.3	-0.35
27	-0.29	-0.3	0.71	0.65	-0.3	-0.29
28	-0.3	-0.31	0.71	0.64	-0.32	-0.3
29	-0.33	-0.31	0.67	0.55	-0.32	-0.3
30	-0.33	-0.27	0.64	0.49	-0.32	-0.31
31	-0.33	-0.27	0.02	-0.12	-0.39	-0.31
32	-0.41	-0.28	-0.01	-0.16	-0.62	-0.32
33	-0.63	-0.28	-0.04	-0.44	-0.62	-0.36
34	-0.63	-0.3	-0.09	-0.14	-0.62	-0.41
35	-0.63	-0.31	-0.39	-0.11	-1.11	-0.46
36	-1.06	-0.31	-0.22	-0.09	-0.14	-0.52
37	-0.21	-0.34	-0.18	0.09	-0.1	-0.92

Table A 2.10 (continued)

38	-0.16	-0.37	-0.15	-0.62	-0.1	-1.06
39	-0.16	-0.37	0.01	-0.67	-0.18	-0.33
40	0.13	-0.53	-0.57	-0.7	-0.15	-0.29
41	-0.43	-0.55	-0.67	-0.86	-0.14	-0.25
42	-0.43	-0.93	-0.7	-0.82	-0.06	-0.13
43	-0.02	-1.05	-0.89	-0.48	0.63	-0.18
44	0.56	-0.04	-0.86	-0.47	0.66	-0.06
45	0.59	0.02	-0.51	-0.33	0.68	-0.06
46	0.69	-0.09	-0.5	-0.33	0.68	-0.03
47	0.7	-0.11	-0.36	-0.29	0.68	0
48	0.69	-0.07	-0.36	-0.29	0.68	0.62
49	0.69	-0.06	-0.32	-0.28	0.67	0.67
50	0.68	-0.03	-0.32	-0.28	0.66	0.66
51	0.67	0.62	-0.3	-0.28	0.64	0.65
52	0.67	0.66	-0.3	-0.28	-0.17	0.65
53	0.62	0.65	-0.3	-0.36	-0.22	0.64
54	0.61	0.65	-0.31	-0.37	-0.23	0.64
55	-0.33	0.64	-0.4	-0.33	-0.23	0.64
56	-0.38	0.63	-0.4	-0.32	0.02	0.62
57	-0.18	0.63	-0.36	-0.32	0.03	0.59
58	-0.16	0.63	-0.35	-0.31	-0.41	0.57
59	-0.03	0.62	-0.35	-0.3	-1.27	0.52
60	-0.02	0.59	-0.35	-0.26	-1.22	-0.32
61	-0.43	0.57	-0.32	-0.25	-0.74	-0.38
62	-1.25	0.52	-0.27	-0.25	-0.57	-0.38
63	-1.18	-0.31	-0.27	-0.22	-0.46	-0.21
64	-0.72	-0.37	-0.24	-0.21	-0.43	-0.02
65	-0.5	-0.37	-0.24	-0.2	-0.36	0
66	-0.44	-0.2	-0.24	-0.2	-0.33	-0.58
67	-0.43	0	-0.22	-0.19	-0.62	-1.19
68	-0.39	0.01	-0.22	-0.19	-0.43	-1.16
69	-0.36	-0.39	-0.21	-0.19	-0.42	-0.67
70	-0.35	-1.2	-0.21	-0.19	-0.37	-0.62
71	-0.34	-1.13	-0.21	-0.2	-0.35	-0.41
72	-0.23	-0.68	-0.21	-0.21	-0.34	-0.4
73	-0.23	-0.47	-0.21	-0.21	-0.33	-0.4
74	-0.23	-0.42	-0.22	-0.24	-0.24	-0.34
75	-0.33	-0.41	-0.23	-0.24	-0.24	-0.34
76	-0.34	-0.34	-0.24	-0.34	-0.32	-0.34

Table A 2.11 Pressure coefficient on polyline for 500 mm IM in HB configuration

Perimeter	0°	15°	30°	45°	60°	75°
0	-0.35	-0.39	-0.37	-0.45	-0.34	-0.3
1	-0.4	-0.33	-0.36	-0.44	-0.39	-0.34
2	-0.43	-0.32	-0.32	-0.39	-0.41	-0.36
3	-0.81	-0.3	-0.3	-0.37	-0.75	-0.67
4	-0.53	-0.29	-0.3	-0.37	-0.5	-0.47
5	-0.52	-0.32	-0.31	-0.38	-0.49	-0.46
6	-0.5	-0.36	-0.38	-0.45	-0.48	-0.45
7	-0.25	-0.6	-0.61	-0.72	-0.27	-0.25
8	-0.25	-0.65	-0.64	-0.76	-0.26	-0.25
9	-0.25	-0.69	-1.1	-1.34	-0.24	-0.23
10	-0.25	-1.18	-1.16	-1.41	-0.22	-0.23
11	-0.24	-0.02	-1.15	-1.39	-0.22	-0.22
12	-0.22	0.12	0.11	0.06	-0.22	-0.21
13	-0.22	0.11	0.09	0.05	-0.21	-0.21
14	-0.22	-0.1	0	-0.01	-0.21	-0.2
15	-0.21	-0.46	-0.62	-0.81	-0.2	-0.2
16	-0.21	-0.47	-0.61	-0.81	-0.2	-0.2
17	-0.21	-0.41	0.01	-0.09	-0.21	-0.2
18	-0.21	0.5	0.56	0.68	-0.21	-0.2
19	-0.22	0.54	0.59	0.73	-0.24	-0.21
20	-0.26	0.54	0.59	0.73	-0.31	-0.23
21	-0.26	0.58	0.57	0.72	-0.31	-0.24
22	-0.26	0.61	0.58	0.72	-0.31	-0.24
23	-0.34	0.61	0.6	0.75	-0.36	-0.31
24	-0.34	0.66	0.62	0.78	-0.36	-0.31
25	-0.35	0.67	0.63	0.78	-0.35	-0.32
26	-0.36	0.69	0.66	0.78	-0.29	-0.36
27	-0.36	0.73	0.69	0.8	-0.29	-0.36
28	-0.35	0.75	0.68	0.79	-0.29	-0.35
29	-0.34	0.75	0.3	0.76	-0.3	-0.29
30	-0.34	0.44	0.28	0.13	-0.36	-0.29
31	-0.3	0.08	0.27	0.09	-0.37	-0.28
32	-0.3	0.07	0.05	0.07	-0.59	-0.29
33	-0.31	0.08	0.14	0.1	-0.66	-0.31
34	-0.34	0.04	0.51	0.17	-1.11	-0.33
35	-0.38	0.03	-0.28	0.44	-0.08	-0.44
36	-0.56	-0.02	-0.45	-0.38	-0.03	-0.48
37	-0.57	-1.11	-0.49	-0.53	-0.01	-0.75

Table A 2.11 (continued)

38	-0.65	-1.03	-0.98	-0.59	0.07	-0.87
39	-1.07	-0.86	-0.74	-1.22	0.05	-0.92
40	-1.21	-0.52	-0.55	-0.82	0.06	-0.25
41	-0.01	-0.45	-0.44	-0.8	0.36	-0.21
42	0.05	-0.34	-0.34	-0.56	0.72	-0.19
43	-0.04	-0.3	-0.33	-0.49	0.72	0.06
44	-0.04	-0.3	-0.29	-0.49	0.71	0.05
45	-0.08	-0.29	-0.28	-0.49	0.7	-0.2
46	-0.03	-0.29	-0.28	-0.37	0.67	0.68
47	0.01	-0.3	-0.28	-0.33	0.66	0.69
48	0.32	-0.3	-0.28	-0.33	0.63	0.7
49	0.76	-0.31	-0.28	-0.33	0.63	0.7
50	0.8	-0.41	-0.37	-0.32	0.62	0.67
51	0.79	-0.4	-0.38	-0.32	0.61	0.65
52	0.78	-0.33	-0.38	-0.33	0.4	0.64
53	0.78	-0.33	-0.33	-0.34	-0.48	0.62
54	0.73	-0.26	-0.33	-0.45	-0.54	0.6
55	0.73	-0.25	-0.33	-0.44	-0.51	0.61
56	0.69	-0.25	-0.25	-0.41	-0.13	0.57
57	0.68	-0.21	-0.25	-0.38	0.09	-0.39
58	0.63	-0.21	-0.25	-0.38	0.1	-0.46
59	0.61	-0.2	-0.22	-0.38	-0.5	-0.44
60	-0.48	-0.2	-0.21	-0.36	-1.23	-0.12
61	-0.58	-0.2	-0.21	-0.31	-1.19	0.11
62	-0.56	-0.2	-0.21	-0.3	-0.65	0.13
63	-0.13	-0.21	-0.21	-0.3	-0.39	-0.02
64	0.1	-0.21	-0.21	-0.26	-0.39	-1.2
65	0.12	-0.22	-0.21	-0.25	-0.39	-0.68
66	-0.04	-0.23	-0.23	-0.24	-0.31	-0.63
67	-1.27	-0.24	-0.23	-0.24	-0.31	-0.59
68	-0.73	-0.24	-0.24	-0.24	-0.33	-0.35
69	-0.68	-0.24	-0.24	-0.25	-0.42	-0.31
70	-0.64	-0.48	-0.23	-0.25	-0.37	-0.28
71	-0.38	-0.49	-0.23	-0.25	-0.35	-0.28
72	-0.33	-0.5	-0.24	-0.25	-0.34	-0.29
73	-0.3	-0.77	-0.49	-0.27	-0.33	-0.4
74	-0.32	-0.42	-0.5	-0.28	-0.24	-0.34
75	-0.33	-0.41	-0.66	-0.28	-0.24	-0.34
76	-0.34	-0.34	-0.6	-0.29	-0.32	-0.34

Table A 2.12 Pressure coefficient on polyline for 600 mm IM in HB configuration

Perimeter	0°	15°	30°	45°	60°	75°
0	-0.22	-0.26	-0.3	-0.34	-0.25	-0.21
1	-0.21	-0.22	-0.28	-0.32	-0.23	-0.2
2	-0.2	-0.22	-0.25	-0.28	-0.22	-0.19
3	-0.2	-0.21	-0.24	-0.25	-0.2	-0.19
4	-0.2	-0.21	-0.23	-0.25	-0.2	-0.19
5	-0.21	-0.23	-0.25	-0.25	-0.2	-0.21
6	-0.23	-0.24	-0.25	-0.27	-0.21	-0.21
7	-0.29	-0.3	-0.27	-0.4	-0.21	-0.21
8	-0.3	-0.32	-0.35	-0.42	-0.27	-0.3
9	-0.32	-0.33	-0.38	-0.65	-0.3	-0.4
10	-0.46	-0.49	-0.6	-0.68	-0.33	-0.51
11	-0.25	-0.24	-0.24	-0.67	-0.59	-0.15
12	-0.23	-0.2	-0.19	-0.33	-0.18	-0.1
13	-0.23	-0.21	-0.19	-0.33	-0.13	-0.11
14	-0.38	-0.29	-0.27	-0.28	-0.14	-0.32
15	-0.41	-0.64	-0.28	-0.46	-0.28	-0.34
16	-0.72	-0.66	-0.53	-0.67	-0.29	-0.74
17	-0.71	-0.63	-0.5	-0.69	-0.64	-0.7
18	-0.64	-0.11	-0.02	-0.6	-0.6	0.05
19	-0.01	-0.03	0.02	-0.53	0.02	0.1
20	0.06	-0.03	0.04	-0.3	0.06	0.17
21	0.11	0.04	0.1	-0.08	0.11	0.3
22	0.15	0.05	0.18	-0.06	0.18	0.35
23	0.3	0.17	0.34	-0.04	0.27	0.38
24	0.37	0.17	0.38	0.02	0.45	0.54
25	0.53	0.19	0.42	0.04	0.49	0.67
26	0.58	0.38	0.62	0.11	0.51	0.7
27	0.73	0.49	0.68	0.25	0.69	0.44
28	0.76	0.65	0.5	0.28	0.5	0.37
29	0.31	0.54	0.47	0.31	0.46	0.34
30	0.29	0.53	0.45	0.54	0.43	0
31	0.28	0.52	0.45	0.67	0.07	0.04
32	0.39	0.5	0.48	0.74	0.32	0.15
33	0.4	0.39	0.21	0.46	0.34	0.14
34	0	0.41	0.18	0.45	0.35	0.1
35	-0.06	0.42	0.04	0.44	0.51	0.05
36	-1.07	-0.09	-1.32	0.45	-0.25	-1
37	-0.92	-0.14	-1.1	0.48	-0.32	-0.66

Table A 2.12 (continued)

38	-0.54	-0.19	-0.64	0.69	-0.4	-0.56
39	-0.49	-1.11	-0.6	-0.49	-1.07	-0.48
40	-0.33	-0.6	-0.39	-0.62	-0.98	-0.36
41	-0.32	-0.6	-0.39	-0.66	-0.72	-0.3
42	-0.29	-0.59	-0.37	-1.05	-0.52	-0.29
43	-0.29	-0.35	-0.35	-1.02	-0.44	-0.27
44	-0.3	-0.3	-0.35	-0.57	-0.32	-0.27
45	-0.3	-0.3	-0.35	-0.56	-0.28	-0.27
46	-0.31	-0.3	-0.35	-0.39	-0.27	-0.27
47	-0.41	-0.3	-0.37	-0.38	-0.28	-0.36
48	-0.41	-0.33	-0.38	-0.35	-0.28	-0.37
49	-0.41	-0.33	-0.53	-0.35	-0.29	-0.32
50	-0.34	-0.33	-0.53	-0.36	-0.29	-0.31
51	-0.33	-0.41	-0.42	-0.36	-0.41	-0.22
52	-0.33	-0.5	-0.41	-0.37	-0.41	-0.21
53	-0.24	-0.49	-0.41	-0.38	-0.33	-0.19
54	-0.24	-0.39	-0.3	-0.51	-0.33	-0.19
55	-0.24	-0.39	-0.3	-0.51	-0.25	-0.18
56	-0.21	-0.39	-0.3	-0.45	-0.25	-0.18
57	-0.2	-0.27	-0.26	-0.43	-0.24	-0.19
58	-0.2	-0.23	-0.25	-0.41	-0.2	-0.19
59	-0.2	-0.23	-0.25	-0.4	-0.2	-0.2
60	-0.2	-0.22	-0.25	-0.39	-0.2	-0.21
61	-0.2	-0.22	-0.25	-0.33	-0.2	-0.22
62	-0.21	-0.22	-0.26	-0.33	-0.2	-0.24
63	-0.21	-0.23	-0.28	-0.28	-0.21	-0.18
64	-0.22	-0.23	-0.29	-0.28	-0.23	-0.17
65	-0.24	-0.25	-0.32	-0.27	-0.23	-0.3
66	-0.24	-0.25	-0.34	-0.28	-0.26	-0.31
67	-0.18	-0.28	-0.27	-0.28	-0.28	-0.32
68	-0.18	-0.29	-0.26	-0.29	-0.2	-0.41
69	-0.3	-0.21	-0.46	-0.29	-0.19	-0.39
70	-0.31	-0.2	-0.48	-0.3	-0.39	-0.28
71	-0.31	-0.38	-0.7	-0.34	-0.4	-0.28
72	-0.44	-0.39	-0.71	-0.39	-0.41	-0.29
73	-0.25	-0.4	-0.67	-0.4	-0.57	-0.4
74		-0.6	-0.5	-0.26	-0.54	-0.34
75	-0.33	-0.27	-0.66	-0.25	-0.24	-0.34
76	-0.34	-0.34	-0.6	-0.52	-0.32	-0.34

Table A 2.13 Pressure coefficient on polyline for 100 mm IM in FB configuration

Perimeter	0°	15°	30°	45°	60°	75°
0	-0.34	-0.29	-0.33	-0.29	-0.34	-0.33
1	-0.33	-0.29	-0.34	-0.29	-0.33	-0.34
2	-0.38	-0.31	-0.34	-0.31	-0.38	-0.34
3	-0.38	-0.35	-0.35	-0.35	-0.38	-0.34
4	-0.35	-0.37	-0.4	-0.37	-0.35	-0.4
5	-0.35	-0.4	-0.4	-0.4	-0.35	-0.4
6	-0.34	-0.5	-0.51	-0.5	-0.34	-0.51
7	-0.26	-0.72	-0.62	-0.72	-0.26	-0.62
8	-0.26	-0.77	-0.74	-0.77	-0.26	-0.74
9	-0.24	-1.05	-0.87	-1.05	-0.24	-0.86
10	-0.23	-1.16	-1.15	-1.15	-0.23	-1.15
11	-0.23	-1.11	0.14	-1.11	-0.23	0.14
12	-0.23	0.48	0.22	0.48	-0.23	0.22
13	-0.23	0.47	0.22	0.47	-0.22	0.22
14	-0.22	-0.61	-0.67	-0.61	-0.22	-0.68
15	-0.22	-0.61	-0.68	-0.61	-0.22	-0.69
16	-0.22	-0.05	-0.23	-0.04	-0.22	-0.23
17	-0.22	0.18	-0.19	0.14	-0.22	-0.19
18	-0.23	0.61	0.56	0.61	-0.23	0.56
19	-0.23	0.62	0.58	0.62	-0.23	0.58
20	-0.23	0.66	0.65	0.66	-0.23	0.65
21	-0.23	0.67	0.67	0.66	-0.24	0.67
22	-0.24	0.66	0.68	0.66	-0.24	0.68
23	-0.26	0.66	0.68	0.65	-0.26	0.68
24	-0.26	0.66	0.68	0.64	-0.34	0.68
25	-0.26	0.64	0.68	0.65	-0.35	0.68
26	-0.34	0.61	0.68	0.56	-0.35	0.68
27	-0.35	0.57	0.68	-0.09	-0.39	0.68
28	-0.35	-0.21	0.67	-0.14	-0.34	0.67
29	-0.39	-0.16	0.67	-0.17	-0.33	0.67
30	-0.34	-0.17	0.65	-0.17	-0.33	0.65
31	-0.33	0.21	0.57	0.21	-0.34	0.57
32	-0.33	0.22	-0.23	0.21	-0.35	-0.23
33	-0.34	-0.07	-0.32	-0.07	-0.37	-0.32
34	-0.35	-1.02	-0.14	-1.02	-0.38	-0.14
35	-0.37	-1.15	-0.12	-1.16	-0.47	-0.12
36	-0.38	-1.06	0	-1.06	-0.48	0
37	-0.47	-0.64	0	-0.64	-0.72	0.01

Table A 2.13 (continued)

38	-0.48	-0.47	-0.06	-0.47	-0.75	-0.06
39	-0.73	-0.46	-1.28	-0.46	-1.23	-1.27
40	-0.75	-0.36	-1.24	-0.36	-1.28	-1.23
41	-1.24	-0.36	-0.75	-0.36	-0.06	-0.75
42	-1.28	-0.32	-0.72	-0.32	0	-0.72
43	-0.06	-0.32	-0.48	-0.32	0	-0.48
44	0	-0.3	-0.47	-0.3	-0.12	-0.47
45	0	-0.3	-0.38	-0.3	-0.14	-0.37
46	-0.12	-0.35	-0.37	-0.35	-0.33	-0.37
47	-0.14	-0.36	-0.35	-0.36	-0.23	-0.35
48	-0.33	-0.36	-0.34	-0.35	0.57	-0.34
49	-0.23	-0.31	-0.33	-0.31	0.65	-0.33
50	0.57	-0.25	-0.33	-0.25	0.67	-0.33
51	0.65	-0.25	-0.34	-0.25	0.67	-0.34
52	0.67	-0.25	-0.39	-0.25	0.68	-0.39
53	0.67	-0.22	-0.35	-0.22	0.68	-0.35
54	0.69	-0.21	-0.35	-0.21	0.68	-0.35
55	0.69	-0.21	-0.34	-0.21	0.68	-0.34
56	0.69	-0.21	-0.26	-0.21	0.68	-0.26
57	0.68	-0.21	-0.26	-0.21	0.68	-0.24
58	0.68	-0.22	-0.26	-0.22	0.67	-0.24
59	0.68	-0.22	-0.24	-0.22	0.65	-0.23
60	0.68	-0.24	-0.23	-0.24	0.58	-0.23
61	0.65	-0.25	-0.23	-0.25	0.56	-0.23
62	0.58	-0.31	-0.23	-0.31	-0.19	-0.22
63	0.57	-0.31	-0.23	-0.31	-0.23	-0.22
64	-0.19	-0.32	-0.22	-0.31	-0.68	-0.22
65	-0.23	-0.34	-0.22	-0.34	-0.67	-0.22
66	-0.68	-0.34	-0.22	-0.34	0.22	-0.22
67	-0.67	-0.32	-0.22	-0.32	0.22	-0.23
68	0.22	-0.29	-0.23	-0.29	0.14	-0.23
69	0.22	-0.21	-0.23	-0.29	-1.15	-0.23
70	0.14	-0.2	-0.23	-0.3	-0.86	-0.24
71	-1.16	-0.38	-0.23	-0.34	-0.73	-0.26
72	-0.87	-0.39	-0.24	-0.39	-0.62	-0.26
73	-0.74	-0.4	-0.26	-0.4	-0.51	-0.34
74	-0.62	-0.6	-0.26	-0.26	-0.4	-0.34
75	-0.51	-0.27	-0.34	-0.25	-0.4	-0.35
76	-0.41	-0.34	-0.35	-0.52	-0.34	-0.38

Table A 2.14 Pressure coefficient on polyline for 200 mm IM in FB configuration

Perimeter	0°	15°	30°	45°	60°	75°
0	-0.33	-0.33	-0.33	-0.33	-0.29	-0.29
1	-0.32	-0.32	-0.33	-0.33	-0.29	-0.29
2	-0.37	-0.37	-0.34	-0.34	-0.31	-0.31
3	-0.37	-0.38	-0.34	-0.34	-0.35	-0.35
4	-0.34	-0.34	-0.4	-0.4	-0.37	-0.37
5	-0.34	-0.34	-0.4	-0.4	-0.4	-0.4
6	-0.33	-0.34	-0.51	-0.51	-0.51	-0.51
7	-0.25	-0.25	-0.62	-0.62	-0.73	-0.73
8	-0.25	-0.25	-0.74	-0.74	-0.78	-0.78
9	-0.23	-0.24	-0.87	-0.87	-1.06	-1.06
10	-0.23	-0.23	-1.16	-1.15	-1.16	-1.16
11	-0.23	-0.23	0.14	0.14	-1.11	-1.11
12	-0.22	-0.22	0.22	0.22	0.47	0.48
13	-0.22	-0.22	0.22	0.22	0.47	0.47
14	-0.22	-0.22	-0.66	-0.67	-0.62	-0.62
15	-0.22	-0.22	-0.67	-0.68	-0.62	-0.62
16	-0.22	-0.22	-0.22	-0.23	-0.05	-0.05
17	-0.22	-0.22	-0.18	-0.19	0.13	0.18
18	-0.22	-0.22	0.57	0.56	0.61	0.62
19	-0.22	-0.22	0.59	0.58	0.62	0.62
20	-0.22	-0.22	0.66	0.65	0.66	0.67
21	-0.23	-0.23	0.68	0.68	0.66	0.67
22	-0.23	-0.23	0.68	0.68	0.66	0.66
23	-0.25	-0.25	0.68	0.68	0.65	0.66
24	-0.25	-0.25	0.68	0.68	0.64	0.66
25	-0.25	-0.26	0.69	0.69	0.65	0.64
26	-0.33	-0.33	0.69	0.69	0.57	0.61
27	-0.34	-0.34	0.69	0.69	-0.08	0.58
28	-0.34	-0.34	0.67	0.67	-0.13	-0.2
29	-0.38	-0.38	0.67	0.67	-0.16	-0.16
30	-0.33	-0.33	0.65	0.65	-0.16	-0.16
31	-0.32	-0.32	0.57	0.57	0.21	0.21
32	-0.33	-0.33	-0.24	-0.23	0.22	0.22
33	-0.33	-0.34	-0.33	-0.32	-0.07	-0.06
34	-0.35	-0.35	-0.14	-0.14	-1.02	-1.02
35	-0.36	-0.37	-0.13	-0.12	-1.16	-1.15
36	-0.37	-0.37	0	0	-1.06	-1.06
37	-0.47	-0.47	0	0	-0.64	-0.64

Table A 2.14 (continued)

38	-0.48	-0.48	-0.07	-0.06	-0.47	-0.47
39	-0.72	-0.72	-1.29	-1.28	-0.46	-0.46
40	-0.75	-0.75	-1.24	-1.24	-0.36	-0.36
41	-1.23	-1.23	-0.76	-0.75	-0.36	-0.36
42	-1.27	-1.28	-0.73	-0.73	-0.32	-0.32
43	-0.06	-0.06	-0.48	-0.48	-0.32	-0.32
44	0.01	0	-0.47	-0.47	-0.3	-0.3
45	0	0	-0.38	-0.38	-0.3	-0.3
46	-0.12	-0.12	-0.37	-0.37	-0.35	-0.35
47	-0.14	-0.14	-0.35	-0.35	-0.36	-0.36
48	-0.32	-0.33	-0.34	-0.34	-0.35	-0.35
49	-0.23	-0.24	-0.33	-0.33	-0.31	-0.31
50	0.57	0.57	-0.32	-0.32	-0.25	-0.25
51	0.65	0.65	-0.34	-0.34	-0.25	-0.24
52	0.67	0.67	-0.39	-0.39	-0.24	-0.24
53	0.67	0.67	-0.35	-0.35	-0.22	-0.21
54	0.69	0.68	-0.34	-0.34	-0.21	-0.21
55	0.69	0.69	-0.34	-0.34	-0.2	-0.2
56	0.69	0.69	-0.26	-0.26	-0.2	-0.2
57	0.68	0.68	-0.24	-0.24	-0.2	-0.2
58	0.68	0.68	-0.24	-0.24	-0.22	-0.22
59	0.68	0.68	-0.23	-0.23	-0.22	-0.22
60	0.68	0.68	-0.23	-0.23	-0.24	-0.24
61	0.65	0.65	-0.23	-0.23	-0.25	-0.25
62	0.58	0.58	-0.22	-0.22	-0.3	-0.3
63	0.57	0.57	-0.22	-0.22	-0.3	-0.3
64	-0.19	-0.18	-0.22	-0.22	-0.31	-0.31
65	-0.23	-0.22	-0.22	-0.22	-0.32	-0.33
66	-0.68	-0.67	-0.22	-0.22	-0.33	-0.33
67	-0.67	-0.66	-0.22	-0.22	-0.32	-0.32
68	0.22	0.22	-0.23	-0.23	-0.31	-0.31
69	0.23	0.23	-0.23	-0.23	-0.3	-0.3
70	0.14	0.15	-0.24	-0.24	-0.86	-0.24
71	-1.15	-1.14	-0.25	-0.25	-0.73	-0.26
72	-0.86	-0.86	-0.25	-0.25	-0.62	-0.26
73	-0.74	-0.73	-0.34	-0.34	-0.51	-0.34
74	-0.62	-0.61	-0.34	-0.34	-0.4	-0.34
75	-0.51	-0.51	-0.35	-0.35	-0.4	-0.35
76	-0.4	-0.4	-0.38	-0.38	-0.34	-0.38

Table A 2.15 Pressure coefficient on polyline for 300 mm IM in FB configuration

Perimeter	0°	15°	30°	45°	60°	75°
0	-0.33	-0.32	-0.28	-0.29	-0.29	-0.33
1	-0.32	-0.33	-0.28	-0.29	-0.29	-0.32
2	-0.37	-0.33	-0.3	-0.31	-0.31	-0.37
3	-0.38	-0.34	-0.34	-0.34	-0.35	-0.37
4	-0.34	-0.39	-0.36	-0.31	-0.37	-0.34
5	-0.34	-0.39	-0.39	-0.31	-0.4	-0.34
6	-0.33	-0.5	-0.49	-0.23	-0.5	-0.33
7	-0.25	-0.61	-0.71	-0.23	-0.73	-0.24
8	-0.25	-0.73	-0.77	-0.21	-0.78	-0.24
9	-0.23	-0.86	-1.05	-0.21	-1.06	-0.23
10	-0.22	-1.14	-1.16	-0.2	-1.16	-0.22
11	-0.22	0.16	-1.11	-0.2	-1.11	-0.22
12	-0.21	0.24	0.49	-0.2	0.48	-0.21
13	-0.21	0.23	0.48	-0.19	0.47	-0.21
14	-0.21	-0.64	-0.58	-0.19	-0.6	-0.21
15	-0.21	-0.65	-0.58	-0.19	-0.6	-0.21
16	-0.21	-0.2	-0.02	-0.19	-0.04	-0.21
17	-0.21	-0.16	0.16	-0.2	0.19	-0.21
18	-0.22	0.58	0.63	-0.2	0.62	-0.21
19	-0.22	0.59	0.64	-0.21	0.63	-0.21
20	-0.22	0.66	0.67	-0.21	0.67	-0.21
21	-0.23	0.69	0.67	-0.22	0.68	-0.22
22	-0.23	0.69	0.67	-0.24	0.66	-0.22
23	-0.25	0.69	0.67	-0.3	0.67	-0.24
24	-0.34	0.69	0.65	-0.3	0.66	-0.25
25	-0.34	0.7	0.66	-0.35	0.65	-0.25
26	-0.34	0.7	0.58	-0.35	0.62	-0.33
27	-0.39	0.7	-0.09	-0.35	0.59	-0.34
28	-0.33	0.68	-0.13	-0.3	-0.18	-0.34
29	-0.32	0.68	-0.17	-0.3	-0.14	-0.39
30	-0.33	0.66	-0.17	-0.31	-0.15	-0.33
31	-0.33	0.58	0.19	-0.33	0.22	-0.32
32	-0.34	-0.22	0.2	-0.33	0.23	-0.32
33	-0.36	-0.31	-1.02	-0.33	-0.06	-0.33
34	-0.37	-0.13	-1.17	-0.34	-1.01	-0.34
35	-0.46	-0.11	-1.18	-0.44	-1.15	-0.36
36	-0.47	0.01	-1.17	-0.59	-1.05	-0.36
37	-0.72	0.01	-1.05	-0.68	-0.63	-0.46

Table A 2.15 (continued)

38	-0.75	-0.06	-0.55	-1.09	-0.46	-0.47
39	-1.24	-1.28	-0.54	-1.15	-0.45	-0.71
40	-1.28	-1.24	-0.36	-0.34	-0.35	-0.74
41	-0.05	-0.75	-0.36	-0.05	-0.35	-1.22
42	0.01	-0.72	-0.31	-0.06	-0.31	-1.26
43	0.01	-0.48	-0.31	-0.22	-0.31	-0.05
44	-0.11	-0.47	-0.3	-0.22	-0.3	0.02
45	-0.12	-0.37	-0.3	-0.12	-0.3	0.02
46	-0.3	-0.36	-0.35	-0.08	-0.36	-0.1
47	-0.21	-0.35	-0.36	0.58	-0.36	-0.11
48	0.59	-0.33	-0.35	0.65	-0.36	-0.29
49	0.66	-0.33	-0.31	0.65	-0.31	-0.2
50	0.68	-0.32	-0.24	0.65	-0.3	0.58
51	0.68	-0.33	-0.24	0.66	-0.24	0.66
52	0.7	-0.39	-0.24	0.66	-0.24	0.68
53	0.7	-0.34	-0.21	0.65	-0.21	0.68
54	0.7	-0.34	-0.21	0.63	-0.2	0.69
55	0.69	-0.34	-0.2	0.62	-0.2	0.69
56	0.69	-0.25	-0.2	0.09	-0.2	0.69
57	0.69	-0.23	-0.2	0.05	-0.2	0.69
58	0.69	-0.23	-0.2	-0.56	-0.21	0.69
59	0.67	-0.22	-0.2	-0.56	-0.21	0.68
60	0.6	-0.22	-0.2	0.46	-0.24	0.68
61	0.58	-0.21	-0.21	0.46	-0.25	0.66
62	-0.17	-0.21	-0.22	-1.1	-0.25	0.59
63	-0.21	-0.21	-0.22	-1.14	-0.31	0.57
64	-0.66	-0.21	-0.25	-1.04	-0.31	-0.17
65	-0.65	-0.21	-0.25	-0.77	-0.31	-0.22
66	0.23	-0.21	-0.3	-0.71	-0.33	-0.67
67	0.24	-0.21	-0.31	-0.5	-0.33	-0.66
68	0.15	-0.22	-0.31	-0.39	-0.31	0.23
69	-1.15	-0.22	-0.32	-0.36	-0.3	0.23
70	-0.86	-0.23	-0.31	-0.34	-0.86	0.15
71	-0.73	-0.24	-0.3	-0.31	-0.73	-1.15
72	-0.61	-0.24	-0.29	-0.25	-0.62	-0.86
73	-0.51	-0.33	-0.34	-0.34	-0.51	-0.73
74	-0.4	-0.34	-0.34	-0.34	-0.4	-0.61
75	-0.39	-0.34	-0.35	-0.35	-0.4	-0.51
76	-0.34	-0.38	-0.38	-0.38	-0.34	-0.4

Table A 2.16 Pressure coefficient on polyline for 400 mm IM in FB configuration

Perimeter	0°	15°	30°	45°	60°	75°
0	-0.27	-0.28	-0.32	-0.28	-0.3	-0.29
1	-0.27	-0.28	-0.32	-0.28	-0.31	-0.3
2	-0.28	-0.29	-0.33	-0.3	-0.31	-0.31
3	-0.31	-0.32	-0.37	-0.33	-0.32	-0.34
4	-0.33	-0.34	-0.37	-0.34	-0.34	-0.35
5	-0.36	-0.37	-0.37	-0.38	-0.36	-0.39
6	-0.46	-0.47	-0.47	-0.48	-0.43	-0.49
7	-0.68	-0.7	-0.58	-0.7	-0.51	-0.72
8	-0.73	-0.75	-0.67	-0.76	-0.6	-0.77
9	-1.01	-1.04	-0.77	-1.04	-0.81	-1.06
10	-1.12	-1.14	-1.05	-1.15	-1.27	-1.17
11	-1.07	-1.09	-1.27	-1.1	-1.22	-1.12
12	0.5	0.51	-1.22	0.5	-0.23	0.52
13	0.49	0.5	0.63	0.5	0.35	0.51
14	-0.49	-0.49	0.63	-0.5	0.35	-0.52
15	-0.48	-0.49	-0.51	-0.5	-0.05	-0.51
16	0.03	0.03	-0.5	0.02	-0.05	0.02
17	0.17	0.25	0.04	0.19	-0.12	0.25
18	0.62	0.65	0.27	0.64	0.16	0.66
19	0.63	0.66	0.7	0.65	0.65	0.66
20	0.67	0.7	0.71	0.68	0.66	0.71
21	0.67	0.7	0.75	0.68	0.7	0.71
22	0.67	0.69	0.76	0.68	0.71	0.7
23	0.67	0.68	0.74	0.68	0.7	0.69
24	0.66	0.68	0.73	0.67	0.69	0.69
25	0.65	0.66	0.73	0.68	0.69	0.68
26	0.64	0.64	0.71	0.6	0.67	0.65
27	-0.05	0.6	0.68	-0.01	0.65	0.62
28	-0.09	-0.14	0.65	-0.05	0.61	-0.15
29	-0.09	-0.09	-0.15	-0.09	-0.12	-0.13
30	-0.1	-0.09	-0.11	-0.09	-0.08	-0.13
31	-0.11	0.25	-0.12	0.25	-0.09	0.01
32	-0.09	0.26	0.29	0.26	0.28	0.02
33	-0.16	-0.03	0.3	-0.03	0.29	-0.2
34	-1	-1.01	-1.22	-1.01	-1.12	-1.16
35	-1	-1.15	-1.3	-1.15	-1.2	-1.06
36	-0.99	-1.05	-1.22	-1.05	-1.13	-0.65
37	-0.61	-0.62	-0.72	-0.62	-0.67	-0.55

Table A 2.16 (continued)

38	-0.42	-0.44	-0.58	-0.44	-0.53	-0.41
39	-0.4	-0.43	-0.44	-0.43	-0.41	-0.35
40	-0.4	-0.34	-0.37	-0.34	-0.34	-0.33
41	-0.31	-0.34	-0.34	-0.33	-0.31	-0.31
42	-0.31	-0.3	-0.33	-0.3	-0.31	-0.31
43	-0.29	-0.3	-0.32	-0.3	-0.29	-0.31
44	-0.29	-0.3	-0.32	-0.3	-0.3	-0.31
45	-0.29	-0.3	-0.4	-0.3	-0.38	-0.39
46	-0.29	-0.37	-0.41	-0.37	-0.39	-0.39
47	-0.35	-0.38	-0.4	-0.38	-0.38	-0.34
48	-0.35	-0.37	-0.35	-0.37	-0.33	-0.33
49	-0.31	-0.31	-0.26	-0.31	-0.24	-0.23
50	-0.31	-0.23	-0.25	-0.31	-0.24	-0.23
51	-0.22	-0.23	-0.25	-0.23	-0.23	-0.22
52	-0.21	-0.22	-0.21	-0.23	-0.2	-0.19
53	-0.21	-0.19	-0.2	-0.2	-0.19	-0.19
54	-0.19	-0.19	-0.19	-0.19	-0.18	-0.18
55	-0.18	-0.18	-0.19	-0.19	-0.18	-0.18
56	-0.18	-0.18	-0.2	-0.18	-0.18	-0.18
57	-0.17	-0.18	-0.21	-0.18	-0.2	-0.18
58	-0.17	-0.18	-0.21	-0.18	-0.2	-0.18
59	-0.17	-0.18	-0.23	-0.19	-0.22	-0.19
60	-0.18	-0.18	-0.25	-0.19	-0.24	-0.19
61	-0.18	-0.19	-0.33	-0.19	-0.33	-0.22
62	-0.19	-0.2	-0.34	-0.21	-0.33	-0.23
63	-0.21	-0.2	-0.4	-0.21	-0.34	-0.23
64	-0.22	-0.23	-0.4	-0.24	-0.38	-0.32
65	-0.22	-0.24	-0.39	-0.24	-0.3	-0.36
66	-0.3	-0.3	-0.3	-0.31	-0.33	-0.37
67	-0.31	-0.3	-0.31	-0.31	-0.33	-0.33
68	-0.34	-0.34	-0.31	-0.34	-0.31	0.23
69	-0.31	-0.34	-0.32	-0.34	-0.3	0.23
70	-0.86	-0.31	-0.31	-0.31	-0.86	0.15
71	-0.73	-0.24	-0.3	-0.31	-0.73	-1.15
72	-0.61	-0.24	-0.29	-0.25	-0.62	-0.86
73	-0.51	-0.33	-0.34	-0.34	-0.51	-0.73
74	-0.4	-0.34	-0.34	-0.34	-0.4	-0.61
75	-0.39	-0.34	-0.35	-0.35	-0.4	-0.51
76	-0.34	-0.38	-0.38	-0.38	-0.34	-0.4

Table A 2.17 Pressure coefficient on polyline for 500 mm IM in FB configuration

Perimeter	0°	15°	30°	45°	60°	75°
0	-0.27	-0.29	-0.3	-0.33	-0.3	-0.29
1	-0.27	-0.3	-0.3	-0.31	-0.31	-0.28
2	-0.35	-0.41	-0.27	-0.29	-0.46	-0.25
3	-0.43	-0.53	-0.26	-0.29	-0.49	-0.25
4	-0.43	-0.39	-0.25	-0.29	-0.38	-0.25
5	-0.35	-0.39	-0.25	-0.29	-0.37	-0.28
6	-0.35	-0.38	-0.27	-0.37	-0.37	-0.37
7	-0.23	-0.19	-0.36	-0.49	-0.22	-0.62
8	-0.23	-0.19	-0.4	-0.58	-0.19	-0.67
9	-0.22	-0.18	-0.49	-0.69	-0.19	-0.92
10	-0.18	-0.18	-0.71	-0.98	-0.18	-1.02
11	-0.16	-0.16	-1.13	-1.2	-0.17	-0.96
12	-0.16	-0.16	-1.09	-1.15	-0.17	0.61
13	-0.16	-0.15	-0.12	0.72	-0.16	0.6
14	-0.16	-0.16	0.45	0.73	-0.16	-0.16
15	-0.16	-0.17	0.45	0.04	-0.16	-0.16
16	-0.18	-0.18	0.23	0.04	-0.17	0.2
17	-0.18	-0.2	0.23	0.1	-0.18	0.31
18	-0.21	-0.2	0.11	0.35	-0.19	0.72
19	-0.21	-0.21	0.29	0.8	-0.21	0.72
20	-0.37	-0.38	0.76	0.8	-0.22	0.71
21	-0.38	-0.39	0.76	0.79	-0.22	0.7
22	-0.38	-0.54	0.72	0.79	-0.41	0.7
23	-0.53	-0.52	0.73	0.78	-0.42	0.73
24	-0.51	-0.31	0.72	0.78	-0.54	0.73
25	-0.32	-0.28	0.72	0.77	-0.49	0.73
26	-0.28	-0.27	0.69	0.8	-0.32	0.79
27	-0.27	-0.26	0.71	0.82	-0.31	0.8
28	-0.26	-0.24	0.69	0.79	-0.28	0.29
29	-0.24	-0.24	0.13	0.03	-0.26	0.12
30	-0.24	-0.3	0.09	0.14	-0.26	0.12
31	-0.3	-0.31	0.14	0.14	-0.29	0.23
32	-0.31	-0.33	0.15	0.14	-0.36	0.16
33	-0.32	-0.56	0.36	0.14	-0.5	0.16
34	-0.57	-0.89	0.34	-0.1	-0.73	-0.11
35	-0.99	-0.92	-0.88	-1.15	-1.08	-1.14
36	-1.03	-0.31	-1	-1.05	-0.94	-1.02
37	-0.34	0.14	-0.68	-0.62	0.47	-0.63

Table A 2.17 (continued)

38	0.17	0.24	-0.5	-0.5	0.47	-0.39
39	0.17	0.21	-0.33	-0.34	0.18	-0.34
40	0.18	-0.14	-0.29	-0.3	0.18	-0.31
41	0.19	-0.11	-0.26	-0.28	0.17	-0.26
42	0.09	0.65	-0.26	-0.3	0.21	-0.29
43	0.64	0.66	-0.27	-0.3	0.74	-0.3
44	0.66	0.67	-0.31	-0.35	0.75	-0.31
45	0.61	0.64	-0.31	-0.36	0.74	-0.35
46	0.61	0.66	-0.51	-0.61	0.74	-0.56
47	0.61	0.66	-0.57	-0.62	0.74	-0.58
48	0.6	0.7	-0.42	-0.45	0.73	-0.43
49	0.6	0.69	-0.41	-0.44	0.72	-0.42
50	0.61	0.7	-0.4	-0.43	0.75	-0.41
51	0.66	0.72	-0.2	-0.23	0.75	-0.22
52	0.67	0.28	-0.2	-0.21	0.24	-0.2
53	0.4	0.22	-0.19	-0.19	0.05	-0.2
54	0.28	-0.09	-0.18	-0.19	0.2	-0.2
55	-0.09	-0.09	-0.17	-0.18	0.2	-0.2
56	-0.09	0.61	-0.16	-0.17	0.41	-0.18
57	0.6	0.61	-0.16	-0.17	0.42	-0.18
58	0.6	-1	-0.16	-0.17	-0.14	-0.17
59	-0.96	-1.05	-0.16	-0.18	-1.08	-0.17
60	-1.01	-0.94	-0.17	-0.18	-1.12	-0.17
61	-0.91	-0.67	-0.17	-0.19	-0.71	-0.18
62	-0.66	-0.61	-0.18	-0.22	-0.5	-0.2
63	-0.6	-0.38	-0.19	-0.22	-0.4	-0.2
64	-0.36	-0.29	-0.22	-0.23	-0.36	-0.23
65	-0.27	-0.26	-0.36	-0.4	-0.27	-0.26
66	-0.25	-0.26	-0.36	-0.54	-0.25	-0.26
67	-0.24	-0.25	-0.37	-0.54	-0.25	-0.39
68	-0.24	-0.34	-0.47	-0.51	-0.26	-0.4
69	-0.31	-0.34	-0.44	-0.34	-0.28	-0.48
70	-0.86	-0.31	-0.31	-0.31	-0.86	-0.47
71	-0.73	-0.24	-0.3	-0.31	-0.73	-0.38
72	-0.61	-0.24	-0.29	-0.25	-0.62	-0.86
73	-0.51	-0.33	-0.34	-0.34	-0.51	-0.73
74	-0.4	-0.34	-0.34	-0.34	-0.4	-0.61
75	-0.39	-0.34	-0.35	-0.35	-0.4	-0.51
76	-0.34	-0.38	-0.38	-0.38	-0.34	-0.4

Table A 2.18 Pressure coefficient on polyline for 600 mm IM in FB configuration

Perimeter	0°	15°	30°	45°	60°	75°
0	-0.42	-0.31	-0.83	-0.83	-0.68	-0.37
1	-0.42	-0.66	-0.66	-0.66	-0.98	-0.37
2	-0.33	-0.99	-0.64	-0.64	-1	-0.28
3	-0.3	-1.01	-0.39	-0.39	-0.92	-0.26
4	-0.28	-0.93	-0.39	-0.39	-0.44	-0.25
5	-0.29	-0.46	-0.38	-0.38	-0.4	-0.26
6	-0.33	-0.41	-0.34	-0.34	-0.35	-0.3
7	-0.46	-0.35	-0.3	-0.3	-0.29	-0.41
8	-0.49	-0.29	-0.29	-0.29	-0.29	-0.43
9	-0.5	-0.28	-0.29	-0.29	-0.29	-0.44
10	-0.52	-0.28	-0.3	-0.3	-0.31	-0.45
11	-0.48	-0.3	-0.3	-0.3	-0.37	-0.41
12	0.32	-0.36	-0.36	-0.35	-0.41	0.24
13	0.32	-0.42	-0.36	-0.36	-0.46	0.24
14	0.29	-0.48	-0.31	-0.31	-0.56	0.2
15	0.28	-0.6	-0.31	-0.31	-0.51	0.2
16	0.14	-0.55	-0.65	-0.65	-0.46	0.07
17	0.08	-0.49	-0.67	-0.67	0.26	0.02
18	-0.11	0.35	-0.69	-0.69	0.26	-0.11
19	-0.13	0.36	-1.02	-1.02	0.13	-0.12
20	-0.18	0.23	-0.99	-0.99	0.12	-0.17
21	-0.19	0.23	-0.48	-0.48	0.04	-0.19
22	-0.2	0.15	-0.4	-0.4	-0.01	-0.19
23	-0.19	0.08	-0.38	-0.38	-0.1	-0.19
24	-0.19	-0.05	-0.36	-0.36	-0.11	-0.18
25	-0.19	-0.06	-0.31	-0.31	-0.18	-0.17
26	-0.12	-0.15	-0.3	-0.3	-0.18	-0.08
27	-0.12	-0.16	-0.29	-0.29	-0.15	-0.06
28	-0.01	-0.17	-0.3	-0.29	-0.16	0.17
29	0.03	-0.19	-0.31	-0.31	-0.16	0.37
30	0.04	-0.19	-0.41	-0.41	-0.12	0.38
31	0.21	-0.16	-0.58	-0.58	-0.04	0.27
32	0.13	-0.12	-0.59	-0.58	-0.04	0.27
33	0.13	-0.12	-0.59	-0.59	0.13	0.07
34	0	-0.01	-0.02	-0.02	0.26	-0.55
35	-0.41	0.12	0.03	0.03	0.26	-0.63
36	-0.46	0.12	0.02	0.02	0.15	-0.6
37	-0.44	0.04	0.16	0.16	0.14	-0.43

Table A 2.18 (continued)

38	-0.33	0.04	0.15	0.15	0	-0.33
39	-0.26	-0.06	0.06	0.06	-0.63	-0.32
40	-0.26	-0.47	-0.01	-0.01	-0.61	-0.3
41	-0.24	-0.46	-0.01	-0.01	-0.49	-0.3
42	-0.24	-0.39	-0.13	-0.13	-0.43	-0.36
43	-0.28	-0.35	-0.13	-0.13	-0.34	-0.37
44	-0.29	-0.29	-0.13	-0.13	-0.32	-0.48
45	-0.37	-0.27	-0.13	-0.13	-0.32	-0.51
46	-0.39	-0.27	-0.14	-0.14	-0.39	-1.03
47	-0.83	-0.31	-0.11	-0.11	-0.39	-1.06
48	-0.86	-0.31	-0.13	-0.13	-0.53	-1.04
49	-0.84	-0.41	-0.11	-0.11	-0.53	-0.69
50	-0.58	-0.41	-0.07	-0.07	-1.17	-0.36
51	-0.57	-0.94	0	0	-1.2	-0.34
52	-0.31	-0.96	-0.01	-0.01	-0.76	-0.34
53	-0.31	-0.63	0.06	0.06	-0.73	-0.31
54	-0.32	-0.61	0.11	0.11	-0.36	-0.31
55	-0.27	-0.31	0.11	0.11	-0.34	-0.29
56	-0.26	-0.29	0.26	0.26	-0.34	-0.27
57	-0.26	-0.3	0.26	0.26	-0.35	-0.27
58	-0.26	-0.32	-0.51	-0.51	-0.34	-0.27
59	-0.26	-0.31	-0.55	-0.55	-0.29	-0.27
60	-0.27	-0.27	-0.53	-0.53	-0.29	-0.31
61	-0.31	-0.27	-0.49	-0.49	-0.29	-0.32
62	-0.31	-0.27	-0.46	-0.46	-0.3	-0.37
63	-0.31	-0.27	-0.32	-0.32	-0.31	-0.38
64	-0.32	-0.28	-0.29	-0.29	-0.33	-0.39
65	-0.33	-0.29	-0.27	-0.27	-0.36	-0.59
66	-0.64	-0.32	-0.29	-0.29	-0.32	-0.6
67	-0.66	-0.3	-0.32	-0.31	-0.31	-0.82
68	-0.88	-0.29	-0.4	-0.4	-0.33	-0.81
69	-0.65	-0.34	-0.4	-0.4	-0.28	-0.59
70	-0.86	-0.31	-0.62	-0.61	-0.31	-0.47
71	-0.73	-0.24	-0.83	-0.83	-0.24	-0.38
72	-0.61	-0.24	-0.29	-0.25	-0.24	-0.29
73	-0.51	-0.33	-0.34	-0.34	-0.33	-0.34
74	-0.4	-0.34	-0.34	-0.34	-0.34	-0.34
75	-0.39	-0.34	-0.35	-0.35	-0.34	-0.35
76	-0.34	-0.38	-0.38	-0.38	-0.38	-0.38

REFERENCES

[1] Agrawal, N., Mittal, A.K., and Gupta, V.K. (2012). “Along-Wind Interference Effects on Tall Buildings”. In National Conference on Wind Engineering, India. pp. 193–204.

[2] Ahirwar, Ritu. (2012). “Experimental investigation of the effect of cross-sectional shape on wind loads on tall buildings”.

[3] Amin, J.A., Ahuja, A. (2012). “Wind-induced mean interference effects between two closed spaced buildings”. KSCE Journal of civil engineering Eng **16,** 119–131. https://doi.org/10.1007/s12205-012-1163-y

[4] Bhattacharyya, Biswarup & Dalui, Sujit & Ahuja, Ashok. (2014). “Wind Induced Pressure on 'E' Plan Shaped Tall Buildings”. Jordan Journal of Civil Engineering. 8. 120-134.

[5] Carassale L., Freda A., Marrè-Brunenghi M., 2014. “Experimental investigation on the aerodynamic behavior of square cylinders with rounded corners”. Journal of Fluids and Structures, 44, 195-204.

[6] Davenport. “The response of super tall buildings to wind, second century of the skyscraper”, council of tall buildings and urban habitat, 1988, pp. 705-725.

[7] David Malott & Zhizhe Yu, KPF; Dennis Poon & Torsten Gottlebe, Thornton Tomasetti. “Ping An Finance Center: Pioneering China’s Tallest – Efficiencies of Form and Structures”, Sep 2012 – CTBUH 2012 9th World Congress, Shanghai.

[8] Elshaer, A., Bitsuamlak, G.T., El Damatty, A., 2014. “Wind Load Reductions due to Building Corner Modifications”. 22nd Annual Conference of the CFD Society of Canada. Toronto, Canada.

[9] Franke J, Hirsch C, Jensen AG, Krüs HW, Schatzmann M, Westbury PS, Miles SD, Wisse JA, Wright NG (2004) “Recommendations on the use of CFD in wind engineering”. In: Proceedings of the international conference on Urban wind engineering and building aerodynamics: COST C14: impact of wind and storm on city life and built environment. Rhode, Saint-Genèse

[10]Goliya, R. & Samaiya, N. & Sabareesh, G. & Gupta, Abhay. (2013). "Current Status of Interference Effect Studies on Tall Buildings". 68-75. 10.3850/978-981-07-8012-8_250.

[11]Gu, M., and Xie, Z.N. (2011). "Interference Effects of Two and Three Super-Tall Buildings Under Wind Action". Acta Mechanica Sinica, 27(5), pp.687–696.

[12]H. V. Ravindra, Y. T. Krishnegowda, C.J.Gangadara Gowda, Vikram C.K and Manu "Numerical simulation of flow past two square cylinders of different perimeters", International Conference on Emerging Trends in Engineering (ICETE-2011),NMAM Institute of Technology, Nitte, May 4 -5, 2011.

[13]IS-875-(part 3), (1987). Wind Loads Bureau of Indian Standards, Manak Bhawan, New Delhi.

[14]Jamieson, N.j., et al. "Wind Induced External Pressures on a Tall Building with Various Corner Configurations." Journal of Wind Engineering and Industrial Aerodynamics, vol. 15, no. 1-3, 1992, pp. 2401–2412., doi:10.1016/0167-6105(92)90032-6.

[15]Kheyari, Pallab & Dalui, Sujit. (2015). "Estimation of Wind Load on a Tall Building under Interference Effects: A Case Study". 9. 2015

[16]Kawai, H. "Effect of Corner Modifications on Aeroelastic Instabilities of Tall Buildings." Journal of Wind Engineering and Industrial Aerodynamics, vol. 74-76, 1998, pp. 719–729., doi:10.1016/s0167-6105(98)00065-8.

[17]Kwok, Kenny C. S., and Peter A. Bailey. "Aerodynamic Devices for Tall Buildings and Structures." Journal of Engineering Mechanics, vol. 113, no. 3, 1987, pp. 349–365., doi:10.1061/(asce)0733-9399(1987)113:3(349).

[18]Kwok, K.c.s., et al. "Effect of Edge Configuration on Wind-Induced Response of Tall Buildings." Engineering Structures, vol. 10, no. 2, 1988, pp. 135–140., doi:10.1016/0141-0296(88)90039-9.

[19]Kwok, K.C.S. and N. Isyumov. (July 1998), "Aerodynamic Measures to Reduce the Wind-Induced Response of Build-ings and Structures", Proceedings of Structural Engineers World Congress, San Francisco, CD-ROM: T179-6

[20]Lam, Kit & Leung, M.Y. & Zhao, J.G.. (2008). "Interference effects on wind loading of a row of closely spaced tall buildings". Journal of Wind

Engineering and Industrial Aerodynamics 96. 562-583. 10.1016/j.jweia.2008.01.010.

[21]Lee, Y.T. & Boo, S. & Lim, Heechang & Misutani, K.. (2016). “Pressure distribution on rectangular buildings with changes in aspect ratio and wind direction”. 23. 465-483. 10.12989/was.2016.23.5.465.

[22]Lee, B. E. “The Effect of Turbulence on the Surface Pressure Field of a Square Prism.” Journal of Fluid Mechanics, vol. 69, no. 2, 1975, pp. 263–282., doi:10.1017/s0022112075001437.

[23]Li, Yi. (2017). “Aerodynamic treatments for reduction of wind loads on high-rise buildings”. Journal of Wind Engineering and Industrial Aerodynamics. 172. 10.1016/j.jweia.2017.11.006.

[24]Li, Y., Tian, X., Tee, K. F., Li, Q-S., & Li, Y-G. (2018). “Aerodynamic treatments for reduction of wind loads on high-rise buildings”. Journal of Wind Engineering and Industrial Aerodynamics, 172, 107-115. https://doi.org/10.1016/j.jweia.2017.11.006

[25]Mallick, M., Kumar, A. & Patra, K.C. (2019). “Experimental Investigation on the Wind-Induced Pressures on C-Shaped Buildings”. KSCE J Civ Eng **23,** 3535–3546.

[26]Mori, Y., Hishida, K., Maeda, M., (1995). “Buoyancy effect on the wake behind a heated obstacle 619 immersed in a turbulent boundary layer”. International journal of heat and fluid flow 16, 405-416.

[27]Nakamura, Y., et al. “Galloping of Rectangular Cylinders In The Presence of a Splitter Plate.” Journal of Fluids and Structures, vol. 5, no. 5, 1991, pp. 521–549., doi:10.1016/s0889-9746(05)80004-0.

[28]Revuz, Julia & Hargreaves, David & Owen, John. (2012). “On the domain size for the steady-state CFD modeling of a tall building”. Wind and Structures, An International Journal”.15. 313-329. 10.12989/was.2012.15.4.313.

[29]Shirzadi, Mohammadreza & Mirzaei, Parham & Naghashzadegan, Mohammad. (2017). “Improvement of k-epsilon turbulence model for CFD simulation of atmospheric boundary layer around a high-rise building using stochastic optimization and Monte Carlo Sampling technique”. Journal of Wind Engineering and Industrial Aerodynamics. 171. 10.1016/j.jweia.2017.10.005

[30]Stathopoulos, T. (1984). “Adverse Wind Loads on Low Buildings Due to Buffeting”. Journal of Structural Engineering, 110(10), 2374–2392.

[31]T. Tamura, T. Miyagi, “The effect of turbulence on aerodynamic forces on a square cylinder with various corner shapes”, J. Wind Eng. Ind. Aerodyn. 83 (1999) 135–145.

[32]Tang, U.F. & Kwok, K.C.S.. (2004). “Interference excitation mechanisms on a 3DOF aeroelastic CAARC building model”. Journal of Wind Engineering and Industrial Aerodynamic. 92. 1299-1314. 10.1016/j.jweia. 2004.08.004.

[33]Tse K.T., Hitchcock P.A., Kwok K.C.S., Thepmongkorn S., Chan C.M. “Economic perspectives of aerodynamic treatments of square tall buildings”. J Wind Eng Ind Aerodyn 2009;97:455–67.

[34]Virote Boonyapinyo and Pongsakorn Wangkansirikun “Aerodynamic Modifications of High-Rise Buildings for Wind Load and Response Reductions.” The 2016 International Conference on Advances in Wind and Structures (AWAS16)

[35]Vu, H.C ., Ahn, J. & Hwang, J.H. (2016). “Numerical simulation of flow past two circular cylinders in tandem and side-by-side arrangement at low Reynolds numbers”. KSCE Journal of civil engineering 20, 1594–1604

[36]Xie, Z.N., and Gu, M. (2004). “Mean Interference Effects among Tall Buildings”. Engineering Structures, 26(9), pp.1173–1183

[37]Y. Otsuki, K. Fujii, K. Washizu, A. Ohya, Wind tunnel experiments on aerodynamic forces and pressure distribution of rectangular cylinders in a uniform flow, Fifth Symposium on Wind Effects on Structures, 1978, 169-176

[38]Zhai, Zhiqiang & Zhang, Zhao & Zhang, Wei & Chen, Qingyan. (2007). Evaluation of Various Turbulence Models in Predicting Airflow and Turbulence in Enclosed Environments by CFD: Part 1—Summary of Prevalent Turbulence Models.

[39]Zhang, A., Gao, C., and Zhang, L. (2005). “Numerical Simulation of the Wind Field around Different Building Arrangements”. JWEIA, 93(12), pp.891–904.

[40]Zhang, A., and Gu, M. (2008). “Wind Tunnel Tests and Numerical Simulations of Wind Pressures on Buildings in Staggered Arrangement”. JWEIA, 96(10-11), pp.2067–2079.

LIST OF PUBLICATIONS

[1] Effects of Corner Configuration on Tall Buildings under Wind Loads using CFD and Wind Tunnel Technique (ASCE India conference 2020).

[2] Mean Interference Effects on Tall Buildings with Variable Geometry using CFD (Wind and Structures, An International Journal). [In communication]

[3] Aerodynamic mitigation by Corner Modification on Square Model under Wind Loads employing CFD and Wind Tunnel (Sadhana journal). [In communication]